



**HAL**  
open science

## Fast Charging Materials for High Power Applications

Binson Babu, Patrice Simon, Andrea Balducci

► **To cite this version:**

Binson Babu, Patrice Simon, Andrea Balducci. Fast Charging Materials for High Power Applications. Advanced Energy Materials, 2020, 10 (29), pp.2001128. 10.1002/aenm.202001128 . hal-03048814

**HAL Id: hal-03048814**

**<https://hal.science/hal-03048814v1>**

Submitted on 9 Dec 2020

**HAL** is a multi-disciplinary open access archive for the deposit and dissemination of scientific research documents, whether they are published or not. The documents may come from teaching and research institutions in France or abroad, or from public or private research centers.

L'archive ouverte pluridisciplinaire **HAL**, est destinée au dépôt et à la diffusion de documents scientifiques de niveau recherche, publiés ou non, émanant des établissements d'enseignement et de recherche français ou étrangers, des laboratoires publics ou privés.



## Open Archive Toulouse Archive Ouverte

OATAO is an open access repository that collects the work of Toulouse researchers and makes it freely available over the web where possible

This is a publisher's version published in: <https://oatao.univ-toulouse.fr/27021>

### Official URL :

<https://doi.org/10.1002/aenm.202001128>

### To cite this version:

Babu, Binson and Simon, Patrice and Balducci, Andrea *Fast Charging Materials for High Power Applications*. (2020) *Advanced Energy Materials*, 10 (29). 2001128. ISSN 1614-6832

Any correspondence concerning this service should be sent to the repository administrator: [tech-oatao@listes-diff.inp-toulouse.fr](mailto:tech-oatao@listes-diff.inp-toulouse.fr)

# Fast Charging Materials for High Power Applications

Binson Babu, Patrice Simon, and Andrea Balducci\*

An overview of fast charging materials for high power applications is given. The behavior at high current density of several anodic and cathodic materials that have been utilized in lithium-, sodium-, and potassium-ion batteries is considered. Furthermore, the behavior of capacitive and pseudocapacitive materials suitable for electrochemical capacitors and, also, of those that have been utilized for the realization of hybrid-ion capacitors, which are nowadays an interesting reality in the field of high power devices, is discussed. The advantages and limitations of all these materials are critically analyzed with the aim of understanding their impact on real devices. On the basis of this analysis, the most important aspects are identified, which should be addressed in the future for the realization of advanced high power devices.


## 1. Introduction

Rising concerns over the environmental pollution and the increasing use of alternative energy sources is urgently calling for the development of green and sustainable electrochemical energy storage devices.<sup>[1,2]</sup> In the future, it will be necessary to develop a large number of different devices, each of them suited for specific applications. Among them, those suitable for high power application, in which a fast deliver of energy (in the order of minutes or less) is required are presently considered of great importance. These devices are already used in a large number of applications, ranging from portable devices to safety systems, and it has been foreseen that their use will increase significantly

Dr. B. Babu, Prof. A. Balducci  
Institute for Technical Chemistry and Environmental Chemistry  
Center for Energy and Environmental Chemistry Jena (CEEC Jena)  
Friedrich-Schiller-University Jena  
Philosophenweg 7a, Jena 07743, Germany  
E-mail: andrea.balducci@uni-jena.de

Prof. P. Simon  
Centre Interuniversitaire de Recherche et d'Ingénierie des  
Matériaux (CIRIMAT)  
Joint Research Units (UMR) Centre national de la recherche  
scientifique (CNRS)  
Université Paul Sabatier  
118 route de Narbonne, Toulouse Cedex 9 31062, France

Prof. P. Simon  
Réseau sur le Stockage Electrochimique de l'Energie (RS2E)  
FR CNRS 3459  
Amiens Cedex 80039, France

 The ORCID identification number(s) for the author(s) of this article can be found under <https://doi.org/10.1002/aenm.202001128>.

© 2020 The Authors. Published by WILEY-VCH Verlag GmbH & Co. KGaA, Weinheim. This is an open access article under the terms of the Creative Commons Attribution License, which permits use, distribution and reproduction in any medium, provided the original work is properly cited.

DOI: 10.1002/aenm.202001128

in the near future, especially in the transportation field.<sup>[3]</sup> Figure 1 is showing a comparison of the characteristics of high power lithium-ion batteries (LIBs), supercapacitors (SC), and hybrid-ion capacitors (HICs), which are the devices of choice for high power applications.<sup>[4–6]</sup> All these devices are commercially available, and it is foreseen that their market will strong increase in the future.<sup>[7–9]</sup> Among them, high power LIBs, which rely on chemical storage are the systems displaying the higher energy density, but also the lower cycle life. SC, which relay on physical storage, are displaying high power and extremely high cycle life, but limited energy density. The

energy, power, and cycle life of HIC, which rely on both physical and chemical storage, lie in between those of LIB and SC.<sup>[10,11]</sup> Although commercially available, the performance and the safety of high power LIB, SC, and HIC need to be strongly improved in order to match the requirements of all future applications. To realize such an improvement, the selection and the realization of advanced electrode (and electrolyte) materials is essential. These materials should be low cost, ecofriendly, re-usable, and naturally abundant. Furthermore, they should display high reversible capacity and long cycling stability, which is extremely important for high power application.<sup>[12]</sup> The aim of this review paper is to supply an overview about the electrode materials utilized nowadays in high power devices and, at the same time, to identify the most suitable candidates for the realization of the next generation of advanced devices.

### 1.1. Classification of Electrode Materials

Taking into account the mechanism of energy storage, the electrode materials can be classified into three types: faradaic, pseudocapacitive, and non-faradaic (capacitive) (Figure 2).<sup>[13]</sup>

In faradaic materials redox reactions are taking place on the bulk electrode. These reactions involve ions, for example, lithium ions in LIB, of the bulk electrolyte, which can be inserted/extracted from host (electrode) structure, or they can lead to reversible conversion reaction and/or alloying formation. As a result of the faradaic process the host materials undergo phase transformations, which provides a sharp peak in the cyclic voltammetry and a flat plateau during galvanostatic charge–discharge experiments (Figure 2d,g).<sup>[14–17]</sup>

Pseudocapacitive materials are also storing charge thorough faradaic reactions. In these materials, however, the reactions are non-diffusion limited (for instance, taking place on the electrode surface) and they do not lead to crystallographic phase change in the material itself (Figure 2b). Due to this

process, the electrochemical response of these materials are much more similar to that of capacitors (see below) than batteries even though they undergo thorough redox reactions. The cyclic voltammogram of pseudocapacitive materials shows broad redox peaks (quasi-rectangular shapes) and the stored charge ( $Q$ ) depends on the change in potential ( $dE$ ) yielding a pseudocapacitance ( $dQ/dE$ ) which gives a voltage-dependent charge–discharge curve (Figure 2e,h).<sup>[18–20]</sup> In the last years several works tried to elucidated the parameters responsible for the broadening of faradaic peaks and the quasi-rectangular shapes in cyclic voltammograms.<sup>[21]</sup> Conway categorized the pseudocapacitance processes into a) underpotential deposition, b) redox pseudocapacitance (2D), and c) intercalation pseudocapacitance (quasi-2D).<sup>[22,23]</sup> The underpotential deposition pseudocapacitance occurs due to the (monolayer) adsorption of ions at the electrode surface above their redox potential, whereas in redox pseudocapacitance the faradaic charge transfer induced adsorption of ions onto the surface of the material, causing continuous changes in the oxidation state of the active material.<sup>[24]</sup> Intercalation pseudocapacitance involves the fast intercalation of ions into the crystal structure of the active host material resulting in faradaic charge transfer with no crystallographic phase change. Although the processes described above are rather different, the electrochemical response they are generating is very similar. This situation resulted in an open vivid discussion on the scientific communities working on these materials. In this respect, the work of Brousse et al.<sup>[19]</sup> as well as of Dunn<sup>[25]</sup> appears extremely helpful to understand the differences between these materials.

The non-faradaic (capacitive) materials are storing energy through a physical process based on a reversible formation of an electric double layer at the electrode/electrolyte interface. Here, the oxidation state of the materials remains unchanged. This process is extremely fast, and the devices utilizing it are typically indicated as electrical double layer capacitors (EDLCs). Due to the limited amount of charge stored through this process, EDLCs display significantly lower energy than LIB. On the other hand, the power and the cycle life of these latter are much lower than the one of the former. The electrochemical signature of non-faradaic material consists of a triangular charge–discharge profile and a rectangular voltammogram (Figure 2f,i).<sup>[25]</sup>

The charge stored in faradaic materials is typically reported in terms of specific charge capacity ( $\text{mAh g}^{-1}$ ). In the case of non-faradaic materials the specific or gravimetric capacitance ( $\text{F g}^{-1}$  or  $\text{F cm}^{-3}$ ) is mainly utilized. It is important to note that in the case of pseudocapacitive materials this latter value might be misleading, as reported in several works.<sup>[19]</sup> Providing capacity values, for example, expressed in  $\text{C g}^{-1}$ , would be helpful even with materials that show a clear capacitive signature.<sup>[26]</sup>

## 1.2. Electrochemical Signature of High Power Materials

The different charge storage mechanisms existing between the classes of materials discussed above leads to significant differences in their kinetic behavior, which can be analyzed qualitatively as well as quantitatively by using various electrochemical techniques: i) cyclic voltammetry (CV), ii) galvanostatic charge–discharge (GC), iii) electrochemical impedance spectroscopy, etc. As illustrated above in Figure 2, the differentiation between faradic and capacitive type of materials appears



**Binson Babu** received his Ph.D. in physics from the Indian Institute of Science Education and Research-Thiruvananthapuram, India in 2019 and currently pursuing as a postdoctoral research fellow in Prof. Andrea Balducci's group at the Institute for Technical Chemistry and Environmental Chemistry at the Friedrich-Schiller-University, Jena. His research mainly focuses on the development and characterization of novel electrolytes and electrode materials for high power hybrid ion capacitors and metal-ion batteries.

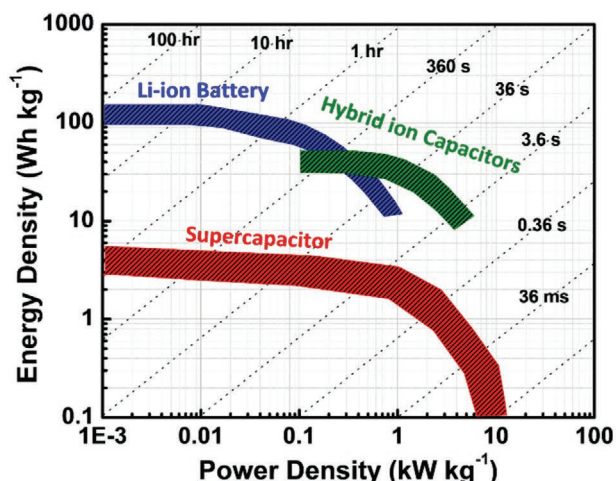


**Patrice Simon** is currently a distinguished professor of materials sciences at Université Paul Sabatier (Toulouse, France) and serves as deputy director of the French network on electrochemical energy storage (RS2E). His research activities are focused on the modification of material/electrolyte interfaces in electrodes for electrochemical energy storage devices, including batteries and electrochemical capacitors.



**Andrea Balducci** is professor of applied electrochemistry at the Institute for Technical Chemistry and Environmental Chemistry and at the Center for Energy and Environmental Chemistry Jena (CEEC Jena) of the Friedrich-Schiller University Jena, Germany. He is working on the development and characterization of novel electrolytes and active/inactive materials suitable for the realization of safe and high performance electrical capacitors, metal-ion batteries, and polymeric batteries.

rather straightforward. On the contrary, differentiating between the faradaic materials and pseudocapacitive materials is more complex, since both undergo redox process, but their electrochemical signature might be very similar to that of capacitive materials. For example, pseudocapacitive materials like hydrous  $\text{RuO}_2$ ,  $\text{MnO}_2$ ,  $\text{T-Nb}_2\text{O}_5$ , are displaying voltammetric profiles very similar to that of capacitive materials although their charge process is implying a (continuous) change of their oxidation state. In the last years several studies have been dedicated to



	Li-ion Battery (LIB)	Supercapacitor (SC)	Hybrid ion capacitor (HIC)
Storage Mechanism	Chemical	Physical	Chemical + Physical
Internal Resistance	High	Low	Medium
Minimum Operating Voltage ( $V_{min}$ )	2.5	0	2.2
Maximum Rated Voltage ( $V_{max}$ )	4.1 – 4.3	2.3 – 3.0	3.8
Specific Energy ( $Wh\ kg^{-1}$ )	75 – 250	2.5 - 15	10 - 100
Specific Power ( $W\ kg^{-1}$ )	150 - 315	500 – 10,000	300 - 5000
Cycle Life	1000 - 10000	100,000 – 1,000,000	10000 – 100,000
Operating Temperature Range	-20 - 60°C	-40 – 70°C	-25 – 85°C
Self-discharge	Very Low (0.1 – 0.3 % Energy/day)	Very High (20 – 40 % Energy/day)	Low
Safety	Safety consideration required	Highly Safety	Highly Safety

**Figure 1.** Ragone plot (left) and table (right) comparing the electrochemical properties of Li-ion battery (LIB), supercapacitor (SC), and hybrid ion capacitor (HIC) (based on the mass of active materials).<sup>[4–6]</sup>

the analysis of the behavior of these materials with the aim of differentiating the diffusion controlled from the non-diffusion controlled (surface controlled) processes.<sup>[18,27,28]</sup>

The level of the reversibility of an electrochemical reactions can be defined based on the voltage difference of the anodic and cathodic redox potential peak ( $\Delta E_{a,c}$ ) in the cyclic voltammogram and the voltage shift of the peaks with respect

to the variation of sweep rate ( $\nu$ ). It has been widely reported that for diffusion limited bulk faradaic processes, an increase in  $\Delta E_{a,c}$  at increased sweep rate ( $\nu$ ) is observed, while in pseudocapacitive materials the  $\Delta E_{a,c}$  is small and varies only a little over a wide range of sweep rate. As a consequence, the (bulk) faradaic materials shows a significant  $\Delta E_{a,c}$  even at low sweep rates, whereas the pseudocapacitive materials shows

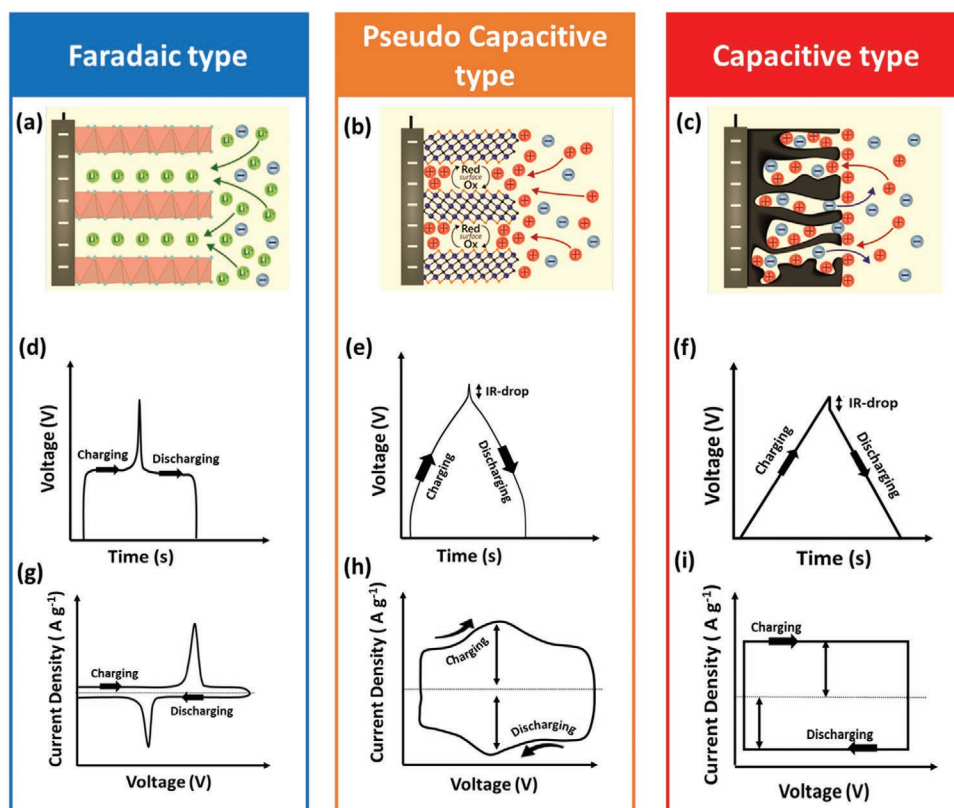


**Figure 2.** Schematic illustration of the electrode processes taking place at a) faradaic, b) pseudocapacitive, and c) capacitive materials. (a–c) Reproduced with permission.<sup>[13]</sup> Copyright 2019, John Wiley and Sons. The figure also reports a schematic representation of a typical galvanostatic charge–discharge and cyclic voltammogram of faradaic d,g) pseudocapacitive, e,h) capacitive, and f,i) materials, respectively.

negligible voltage difference. Utilizing cyclic voltammetry, it is also possible to distinguish between the diffusion and the non-diffusion (surface) controlled processes analyzing curves recorded at different scan rates, and assuming that the current obeys a power-law relationship<sup>[27,29–32]</sup>

$$i = av^b \quad (1)$$

where  $i$  is the measured current,  $v$  is the scan rate,  $a$  and  $b$  (power-law exponent) are the adjustable parameters where  $b$ -value can be obtained from the slope of the linear plot of  $\log i$  versus  $\log v$  for the anodic and cathodic peaks. In addition to the material type, the  $b$ -value highly depends on the potential, sweep rate, interacting ions, and the charge storage mechanism.<sup>[29]</sup> The kinetics of the charge storage mechanisms can be qualitatively determined from the experimental  $b$ -values. The  $b$ -value might be helpful to gain indications about the diffusion and non-diffusion controlled processes (which have theoretical  $b$ -values of 0.5 and 1, respectively) taking place on faradaic, pseudocapacitive, and capacitive materials.<sup>[18,30,33,34]</sup> Nevertheless, it is important to remark that while considering this value it is necessary to carefully take into account the properties, for example, surface area, of the investigated material in order to avoid analysis which are not physically meaningful.

Potentiostatic intermittent titration technique including step potential electrochemical spectroscopy<sup>[35]</sup> and multiple-step chronoamperometry<sup>[36]</sup> have been also utilized to determine the contribution of different charge storage mechanisms, and their use is becoming more and more common to investigate these aspects.

## 2. Materials for High Power Applications: An Overview

All three classes of material discussed above are utilized for the realization of high power devices. In the following, each of these classes will be considered with the aim of understanding their impact on the behavior and performance of metal-ion batteries, supercapacitors, and HIC.

### 2.1. Materials for Metal-Ion Batteries

The reactions taking place in faradaic materials suitable for rechargeable battery can be divided in three main types: a) insertion/extraction reactions, b) alloy reactions, and c) conversion reactions. Alloy reactions typically lead to huge volume expansion, which might cause cracking of the electrodes and rapid capacity declining. On the other hand, conversion reactions typically display large voltage hysteresis in the charge-discharge, which results in a poor efficiency. Because of these limitations, the use of these two classes of materials in high power applications does not appear particularly advantageous.<sup>[37,38]</sup> In this work we will therefore considered only materials relying on insertion/extraction reactions.

The key requirements for the successful implementation of an intercalation material (anode and cathode) in a high power rechargeable battery are:<sup>[39,40]</sup> i) high ionic and electronic conductivity, which are necessary to guarantee a fast charge-discharge process and ii) highly reversibility and minimal or

no change in the host structure during the ion insertion/extraction process, which is necessary to guarantee long life cycles. Furthermore, abundant, inexpensive, environmentally benign, thermally and chemically stable intercalation materials are needed to improve the overall sustainability of the devices in which they are utilized.<sup>[41–43]</sup>

LIBs are nowadays the most widespread energy storage devices in our society. However, there is a strong interest also on the development of alternative metal-ion batteries, based on sodium and potassium, since these two elements are much more abundant than Li.<sup>[44–46]</sup> This interest is clearly reflected on the increasing number of publications about sodium and potassium ion batteries over the last years (Figure 3). It is important to notice that although the working principle of LIB, sodium-ion batteries (NIB), and potassium-ion batteries (KIB) is the same, the materials suitable for high power applications, due to the different properties of these ions, might be significantly different.

#### 2.1.1. Lithium-Ion Batteries

LIBs are presently the devices of choice for a large number of applications, ranging from portable devices to electric vehicles. Although the realization of high energy LIBs is required for several applications, it can be considered as the main focus of large part of the research dedicated to these devices, also the realization of high power systems appears to be of importance. For this reason, in the last years several efforts have been dedicated to the development of materials able to improve the power density of LIBs.<sup>[47]</sup>

*Anodic Materials for LIBs:* Carbon is the cheapest and most abundant element in nature,<sup>[48]</sup> and carbonaceous materials are extensively utilized in energy storage devices, for example, as negative electrode for commercial LIBs.

Carbonaceous materials can be categorized into three types: graphite/graphitized materials, non-graphitizable hard carbon, and graphitizable soft carbon (Figure 4).

The intercalation process of lithium in these materials can be generally described as<sup>[49,50]</sup>



Graphite is one of the stable allotropes of carbon, and is showing reversible Li intercalation at a potential close to that of Li-metal ( $\approx 0.2$  V vs Li/Li<sup>+</sup>). Yazami discovered the usage of graphite as anode material for LIB,<sup>[51]</sup> and it was introduced in commercial devices by Sony Inc. in 1991. Since then, due to their low working potential, high reversible capacity and cycling stability, graphite electrode are the state-of-the-art anode of this technology.<sup>[52]</sup> Graphite is the sequential arrangement of graphene layers separated by a distance of 3.35 Å, and bonded by van der Waals forces in ABAB stacking, in which each graphene layers have a honeycomb structure of hexagonal arrangement of carbon atoms.<sup>[52,53]</sup> The electrochemical activity in graphite happens due to the insertion of Li ion between the graphene layers in 2D manner, and the intercalation occurs through four stages explained by Daumas–Herold model. The theoretical capacity of graphite is  $\approx 372$  mAh g<sup>-1</sup>.<sup>[53–56]</sup> In order to utilize graphite in LIBs, the formation of a passivation layer

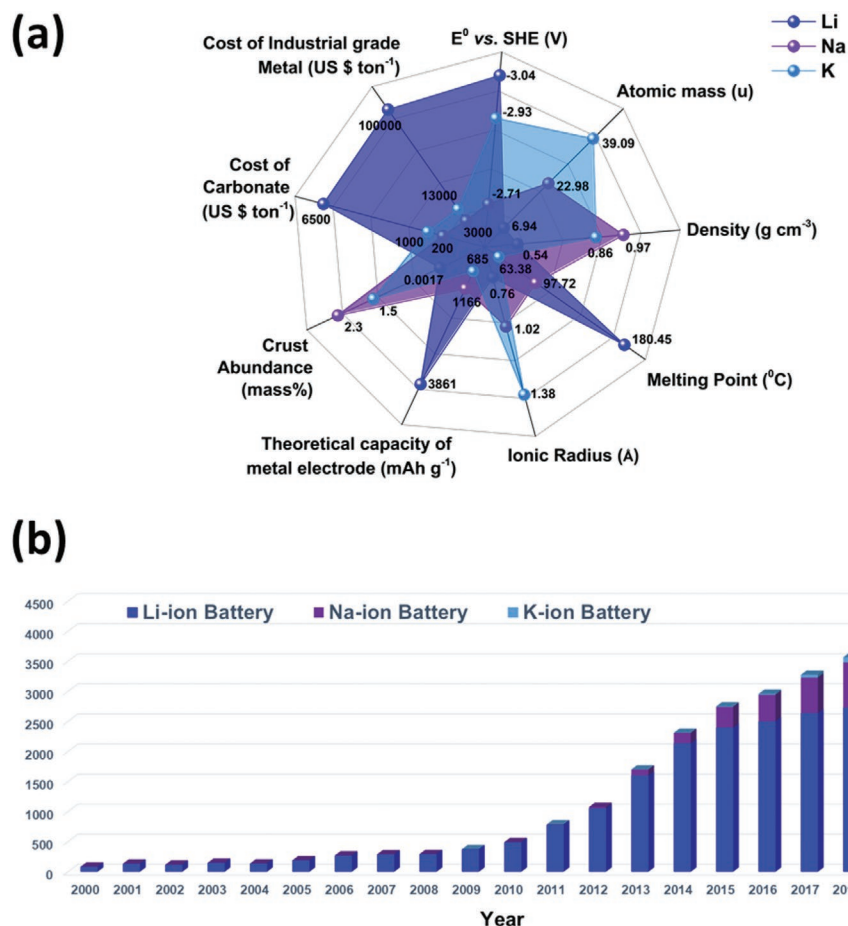


**Figure 3.** a) Comparison of some properties of interest in view of the application in batteries of Li, Na, and K; each axis' values are rescaling independently. b) Number of publications dedicated to lithium, sodium, and potassium batteries; data from Web of Science (February 2020) by searching "metal ion battery" for each battery chemistry (Li, Na, and K).

permeable to lithium ions (solid–electrolyte interface, SEI) on the surface of the graphite electrode is required.<sup>[12,57–59]</sup> The

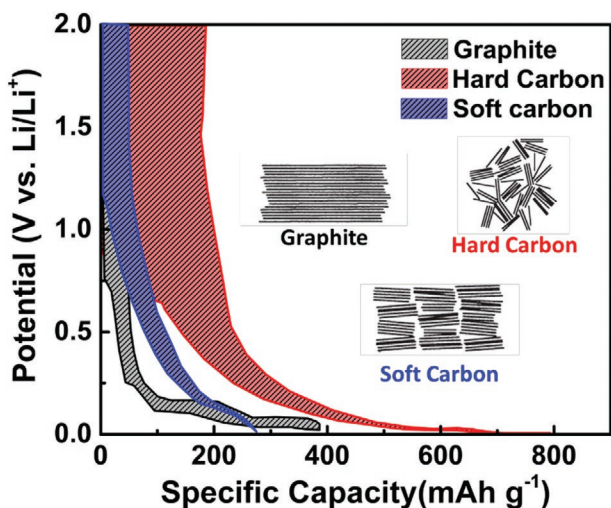


**Figure 4.** Comparison of the voltage profiles of graphite, hard carbon, and soft carbon. Reproduced with permission.<sup>[49]</sup> Copyright 2001, John Wiley and Sons.

formation of the SEI implied an irreversible consumption of lithium ions from the electrolytes and cathodes during the initial cycle of the battery, which causes a reduction of the capacity and an increase of the resistance (and thus impedance) within the cell.<sup>[60–63]</sup> Besides, during fast charging lithium electroplating might occur on the SEI layer. This latter process might create dendrite formation over the cycling, which can eventually destroy the cell, and it might reduce the performance of the materials under high current densities.<sup>[64,65]</sup> Several strategies have been adopted by researchers to improve the electrochemical performances and the rate capabilities of graphite electrodes by changing the loading, coating thickness, and porosity,<sup>[66,67]</sup> modifying the graphite structures and dimensions like ultra-layered graphite,<sup>[68]</sup> highly graphitic carbon nanosheets (HGCNS), etc.<sup>[69]</sup> These materials are able to deliver large capacity at rate higher than 10 C.

Amorphous carbons (hard and soft carbons) have been also investigated as negative electrodes for high performance LIBs. The insertion/de-insertion profile of amorphous carbon are different compared to the graphite (Figure 4). In contrast to graphite voltage profile, the hard carbon and soft carbon undergoes a sloping nature which will decrease the cell voltage and hence limits the energy density. Hard carbons can be seen as a

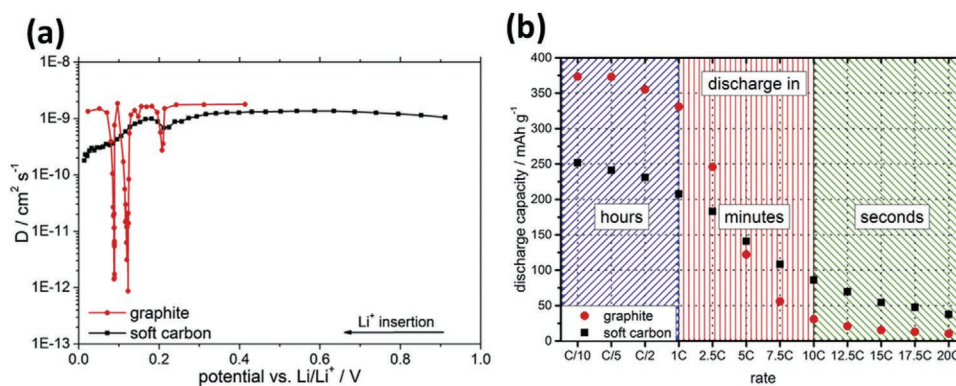


**Figure 5.** a) GITT measurements of graphite and soft carbon based anodes during lithiation and b) C-rate test of graphite and soft carbon based anodes between 0 and 1.5 V versus Li/Li<sup>+</sup>. Reproduced with permission.<sup>[73]</sup> Copyright 2014, Elsevier.

disordered collection of small graphitic grains, which originate in the presence of nanovoids within the material. Due to these latter, hard carbon based electrodes display a reduced volumetric expansion than graphite and, furthermore, these defects provides high gravimetric capacity, which is higher than the theoretical capacity of graphite (372 mAh g<sup>-1</sup>).<sup>[43,53,70]</sup> However, the high fraction of edge sites present in these materials is influencing the SEI formation, reducing the initial coulombic efficiency (due to a large voltage hysteresis), and it is increasing the irreversible capacity loss in full cell device. For these reasons, the use of hard carbon appears less attractive in commercial devices than that of graphite. The graphitizable soft carbon, in contrast to the non-graphitizable hard carbon, is showing higher electronic conductivity, whose interlayer distance and graphitization degrees can be tuned by thermal treatment.<sup>[50,71]</sup> However, as in the case of hard carbon, these materials display an initial irreversible capacity much higher than that of graphite. Graphitizable petroleum coke (PeC), mesocarbon microbeads, ex-mesophase and vapor-grown carbon fibers, etc., are typical soft carbons used for Li-ion insertion.<sup>[72]</sup>

Graphite appears to be the most suitable material for the realization of high energy LIBs. Nevertheless, it has to be noted that for high power application this might not always be the case. As a matter of fact, while in graphite the lithium insertion is hindered every time a new intercalation stage is reached, in soft (and hard) carbon the lithium insertion process does not show significant decrease over the used potential. It has been shown that this difference, which is caused by the different structural and microstructural properties of these carbonaceous materials, has important consequences on the capacity retention of these carbons during the high rates, for example, those typically used in lithium-ion capacitors (LIC). Under these circumstances the use of soft carbon (and also hard carbon) might become more favorable (Figure 5).<sup>[73]</sup>

In order to improve the electrochemical performances of LIBs in terms of rate capabilities, cycle life, etc., also different types of carbon based materials have been developed and considered.<sup>[68,69,74–86]</sup> Dubal et al.<sup>[80]</sup> synthesized nitrogen-doped carbon nanpipes (N-CN Pipes) for high power Li-ion insertion anode material. The kinetic studies of material shows high anodic and cathodic *b*-values and a capacitive contribution of 93.1% at a high scan rate of 10 mV s<sup>-1</sup>, which is attributed to

the pseudocapacitive nature due to the surface redox reactions between Li-ions and N-functional groups on the surface of N-CN Pipes and the disordered carbon structure due to defects induced on the graphene layers.

Titanium based materials have been intensively investigated as alternative to conventional carbon based anodes. The interest on these materials is related to their limited volume strain (<4%) during the lithium insertion/extraction process, which is ensuring a very high reversibility, and thus cycling stability for the devices in which they are used. Furthermore, since the lithium insertion/extraction is taking place at a potential above 1.0 V versus Li/Li<sup>+</sup>, the use of these classes of materials avoids lithium dendrites, ensuring high safety.<sup>[87–89]</sup>

TiO<sub>2</sub> is one of the most abundant, environmentally friendly, and low cost available material, and it shows very interesting electrochemical properties.<sup>[90]</sup>

The general insertion/extraction reaction of lithium ions in TiO<sub>2</sub> can be expressed as:



where *x* depends on the morphology, crystallographic orientation, and the different polymorphs of TiO<sub>2</sub>.<sup>[87]</sup> The reversible accommodation of 1 mole of lithium in TiO<sub>2</sub> crystal structure gives a high theoretical capacity of ≈335 mAh g<sup>-1</sup>. Even though many polymorphs are reported, only anatase, rutile, brookite, and bronze phases have been investigated for LIB applications. Among them, anatase and bronze (TiO<sub>2</sub> (B)) appears as the most promising for high power applications and for this reason they will be considered in the following.

Anatase is the most thermodynamically stable form of TiO<sub>2</sub> polymorphs. It has tetragonal body-centered space group with two TiO<sub>6</sub> octahedra sharing two adjacent edges with other two similar TiO<sub>6</sub> octahedra.<sup>[91–93]</sup> The lithium ion insertion in the anatase framework results in the formation of Li-rich and Li-poor phases, where Li hopping between the two octahedral interstitial sites can take place. The lithium ion diffusion has been estimated in the range of ≈10<sup>-17</sup> cm<sup>2</sup> s<sup>-1</sup>.<sup>[32,94]</sup> It has been shown that the use of nanosized anatase TiO<sub>2</sub> particles is leading to an improvement of capacity and to a change of the storage process, in which a solid solution reaction is more prominent than



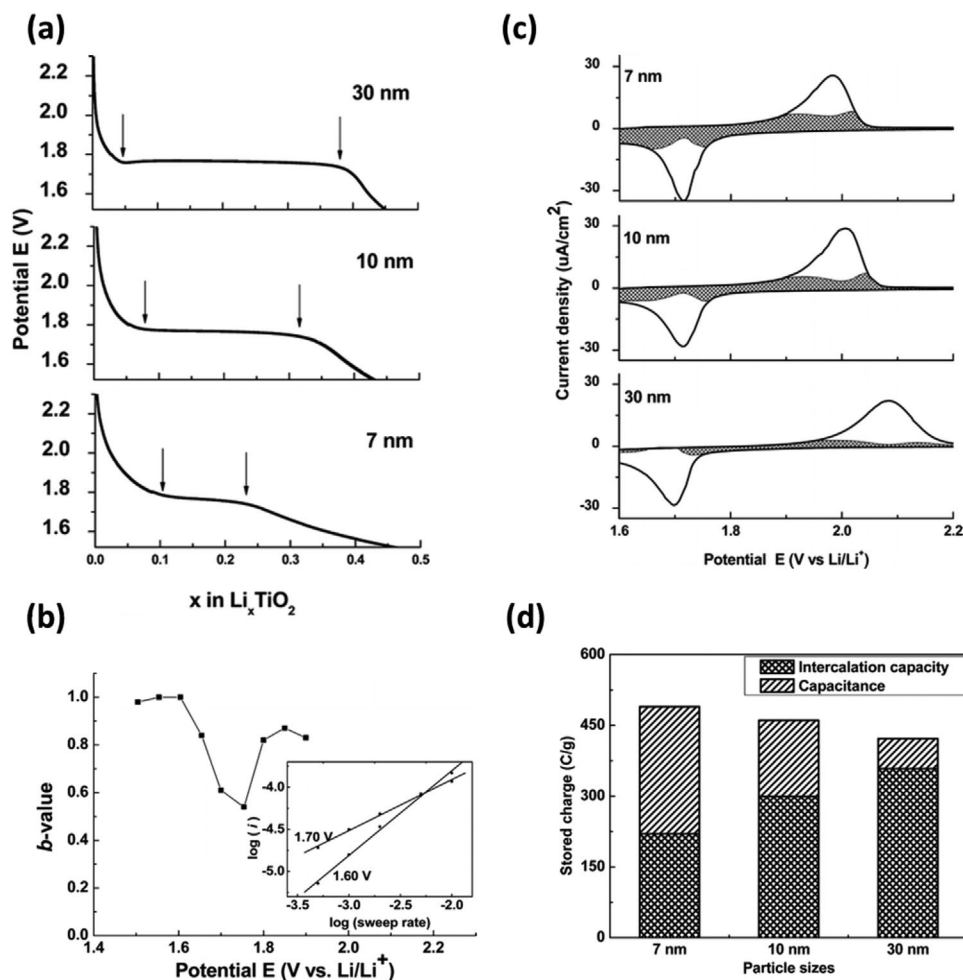


**Figure 6.** a) Galvanostatic discharge curves for nanocrystalline  $\text{TiO}_2$  films at a rate of  $\approx 1$  C for films at different dimensions, b)  $b$ -values for the 10 nm film plotted as a function of potential for cathodic sweeps ( $\text{Li}^+$  insertion). Inset: power law dependence of current on sweep rate (at 1.60 V,  $b = 1.0$ , and at 1.70 V,  $b = 0.55$ ), c) cyclic voltammetry ( $0.5 \text{ mV s}^{-1}$ ) showing the capacitive contribution for the three  $\text{TiO}_2$  films, and d) the histogram compares the quantitatively differentiated lithium intercalation and capacitive contributions for  $\text{TiO}_2$  nanoparticle films at sweep rate of  $0.5 \text{ mV s}^{-1}$ . Reproduced with permission.<sup>[27]</sup> Copyright 2007, American Chemical Society.

the two-phase equilibrium reaction typically of not nano-sized materials.<sup>[95]</sup> This behavior has been well described by Wagemaker et al.<sup>[96]</sup> which utilizing neutron diffraction could show the particle size dependence of anatase to the Li composition. Dunn et al.<sup>[27]</sup> revealed the pseudocapacitive behavior of nanosized  $\text{TiO}_2$  anatase. They investigated in detail the variation of  $b$ -value of  $\text{TiO}_2$  nanocrystals at different potentials and they showed that the low  $b$ -value (0.55) at 1.70 V versus  $\text{Li}/\text{Li}^+$  can be associated with faradaic current, while the high  $b$ -value (0.8–1.0) at higher and lower peak potentials indicates the occurrence of non-diffusion-limited processes of capacitive current. They were able to differentiate the capacitive and faradaic contributions in  $\text{TiO}_2$  nanocrystals having different thicknesses, and they show that an increase of the capacitive contribution is taking place when the particle size is decreasing (Figure 6). As a consequence, the nanosized anatase  $\text{TiO}_2$  is displaying improved behavior during test carried out at high current density, making these nanomaterials appealing for high power applications.

$\text{TiO}_2$  (B) is another interesting  $\text{TiO}_2$  polymorph, which displays properties similar to anatase, but with the advantage of a reduced irreversible capacity during cycling.<sup>[41,97,98]</sup> Marchand and co-workers discovered  $\text{TiO}_2$  (B) in 1980, showing that this polymorph features an open perovskite-like layered crystal structure and low density compared to other polymorphs.<sup>[88]</sup> It has been shown that the lithium insertion process in  $\text{TiO}_2$  (B) is taking place through a two-phase reaction,<sup>[99]</sup> and Zukalova and co-workers<sup>[100]</sup> investigated the pseudocapacitive behavior of this material.

As in the case of anatase, the use of nanosized  $\text{TiO}_2$  (B) particles, which are shortening the lithium diffusion path ways on the material, is favorable in view of high power applications. Armstrong et al.<sup>[101,102]</sup> synthesized  $\text{TiO}_2$  (B) nanowires with diameters in the range of 40–60 nm and lengths up to several micrometers. They showed that these materials display high capacity ( $305 \text{ mA h g}^{-1}$ ) and excellent capacity retention over prolonged cycling. The same group has also synthesized  $\text{TiO}_2$  (B) nanotubes, showing that these materials display high specific capacity ( $338 \text{ mAh g}^{-1}$ ) and they are able to deliver very

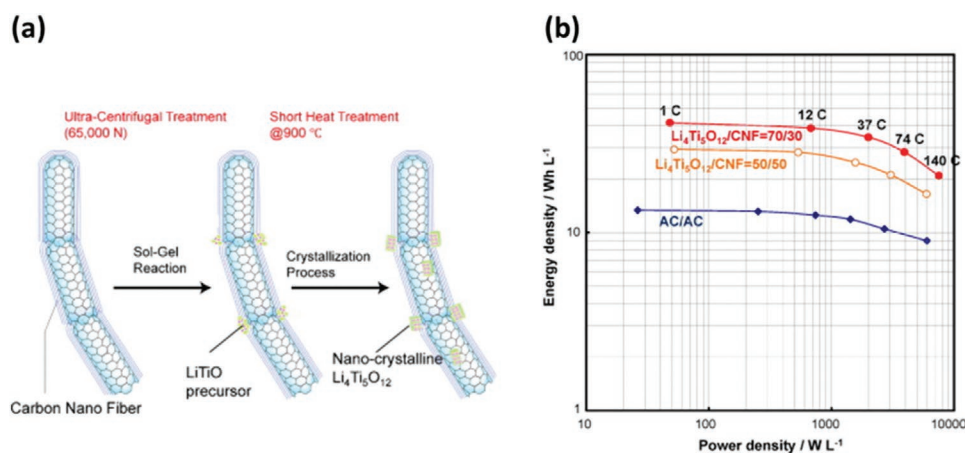


**Figure 7.** a) Schematic illustration for the two-step formation procedure of the nc- $\text{Li}_4\text{Ti}_5\text{O}_{12}/\text{CNF}$  composite, b) Ragone plots of hybrid capacitor systems ((nc- $\text{Li}_4\text{Ti}_5\text{O}_{12}/\text{CNF}$ )/AC), assembled using two types of the composites with weight ratio of  $\text{Li}_4\text{Ti}_5\text{O}_{12}/\text{CNF} = 50/50$  or  $70/30$  and conventional EDLC system (AC/AC). Reproduced with permission.<sup>[113]</sup> Copyright 2010, Elsevier.

good capacity also at high current densities ( $95 \text{ mAh g}^{-1}$  at  $2000 \text{ mA g}^{-1}$ , corresponding to  $21 \text{ C}$ ).<sup>[103]</sup>

The spinel framework materials described by the general formula  $\text{AB}_2\text{O}_4$ , provides robust crystalline structure with 3D diffusion pathways, and for these favorable features they have been largely investigated as electrode materials for energy storage devices. The spinel structure ( $\text{Li}_4\text{Ti}_5\text{O}_{12}$ ) (LTO), undergoes a reversible two-phase reaction from spinel ( $\text{Li}_4\text{Ti}_5\text{O}_{12}$ ) to rock salt structure ( $\text{Li}_7\text{Ti}_5\text{O}_{12}$ ) by reducing  $\text{Ti}^{4+}$  to  $\text{Ti}^{3+}$ , that is resulting in a theoretical capacity of  $175 \text{ mAh g}^{-1}$ . The volume change associated to this reversible reaction, which take place at  $1.55 \text{ V}$  versus  $\text{Li}/\text{Li}^+$ , is extremely low ( $\approx 0.2\%$ ), and for this reason LTO is considered a “zero strain” anodic material.<sup>[104]</sup> Due to these positive features, its low cost and environmental friendliness, LTO is considered as one of the most promising anodic material for practical application.<sup>[105]</sup> One of main drawback of LTO is its insulating nature. For this reason, in the last years tremendous efforts have been made to enhance the electronic mobility and the ionic diffusion of this material, with the goal to realize LTO based electrodes able to display high performance.<sup>[106–115]</sup> Kim et al.<sup>[112]</sup> developed LTO nanowires able to deliver high capacity at low C-rate ( $165 \text{ mAh g}^{-1}$  at  $0.1 \text{ C}$ ) and, at the same time, to retain large part of this capacity ( $>90\%$ ) also at high C-rate. In 2009 Naoi et al.,<sup>[113]</sup> developed a high rate LTO based electrode featuring a unique nanostructure in which nanocrystalline LTO ( $\approx 5\text{--}20 \text{ nm}$ ) were grafted onto carbon nanofiber anchors (nc- $\text{Li}_4\text{Ti}_5\text{O}_{12}/\text{CNF}$ ). This innovative material was obtained utilizing a sol-gel synthesis under ultra-centrifugal force (Figure 7). The group showed that nc- $\text{Li}_4\text{Ti}_5\text{O}_{12}/\text{CNF}$  can deliver a very high capacity at very high C-rate ( $158 \text{ mAh g}^{-1}$  at  $300 \text{ C}$ , which corresponds to  $95\%$  of the capacity delivered by the electrode at  $1 \text{ C}$ -rate).

$\text{TiNb}_2\text{O}_7$  (TNO) is a mixture of titanium-niobium based binary metal oxides, which was proposed by John B. Goodenough's group as an alternative anode material for Li-ion battery.<sup>[116]</sup> The theoretical capacity of TNO is  $388 \text{ mAh g}^{-1}$  (which results from a 5-electron transfer reaction involving the redox couples  $\text{Ti}^{4+}/\text{Ti}^{3+}$ ,  $\text{Nb}^{5+}/\text{Nb}^{4+}$ , and  $\text{Nb}^{4+}/\text{Nb}^{3+}$ ) and the lithium-ion insertion within its structure is taking place at a potential higher than  $1 \text{ V}$  versus  $\text{Li}/\text{Li}^+$ . These properties, together with

its 2D structure, are making TNO an attractive alternative to lithium titanate.<sup>[34,117,118]</sup> As other titanates, TNO displays intrinsic poor electronic and ionic conductivities, which are limiting its use in high power applications.<sup>[116]</sup> In the last years many efforts have been dedicated toward the realization of designed TNO, for example, nanostructures,<sup>[119–125]</sup> microspheres,<sup>[123,126]</sup> nanospheres,<sup>[127]</sup> nanofibers,<sup>[128]</sup> carbon composites,<sup>[129–132]</sup> doping with hetero atoms.<sup>[133,134]</sup> Guo et al.<sup>[135]</sup> reported about the use of nanoporous TNO synthesized via a sol-gel synthesis, showing that this material was able to deliver a stable capacity of  $128 \text{ mAh g}^{-1}$  at  $50 \text{ C}$ . Song et al.<sup>[134]</sup> proposed the use of TNO doped with  $\text{Mo}^{6+}$  ions (Mo-TNO), and they showed that these materials exhibit high capacity at high C-rate ( $184 \text{ mAh g}^{-1}$  at  $100 \text{ C}$ ). Utilizing TNO nanospheres, Cheng et al.<sup>[127]</sup> realized systems displaying high capacity and high stability ( $160 \text{ mAh g}^{-1}$  after  $10\,000$  cycles at  $5 \text{ C}$ ).

Table 1 compares some properties of importance for high power applications of selected anodic materials belonging to the families discussed above.

The variation of the specific capacities at different current densities of the materials considered in Table 1 is compared in Figure 8. As shown, the anodic materials of LIBs are able to deliver high specific capacity up to current densities of  $10\text{--}50 \text{ A g}^{-1}$ . Above these values their performance starts to decline quite significantly. To date, graphite still appears as the carbonaceous material able to display the best set of properties for the realization of high power LIBs. Titanium base anodes are also displaying very promising performance at high current densities, but their use might reduce the cell voltage (and thus the energy) of the devices limiting the range of application of LIBs based on these materials.

**Cathodic Materials for LIBs:** The cathodic materials utilized in commercial LIB consist of transition metal oxides and/or layered compound. In the following session, the high power behavior of some of these compounds will be considered.<sup>[15,40,136]</sup>

Layered transition metal oxide having a general formula of  $\text{LiMeO}_2$  (Me = transition metal elements such as Co, Ni, and Mn) have been largely utilized as cathodic materials for LIBs.  $\text{LiCoO}_2$  (LCO) was proposed by Goodenough and it is the first

**Table 1.** Properties of selected high power anodic materials for LIBs.

Anode material	Maximum capacity [mAh g <sup>-1</sup> ]	Capacity @ high rate/mAh g <sup>-1</sup>	Capacity retention	Reference
Ultrafine layered graphite (2 mm)	395.55 (0.1 C-rate)	139.17 (10 C-rate)	86.2% after 800 cycles (@ 3 C-rate)	[68]
Microporous polymer-derived porous hard carbon (CMP-PHC)	408 (0.2 C-rate)	136.2 (60 C-rate)	94.3% after 1800 cycles (@ 5 C-rate)	[74]
N-doped carbon nanopipes (N-CNPipes)	982 (0.1 A g <sup>-1</sup> )	150 (20.0 A g <sup>-1</sup> )	345 after 1000 cycles (@ 0.5 A g <sup>-1</sup> )	[80]
Peanut shells-derived porous hard carbons (PSDHC-600A)	1230 (0.05 A g <sup>-1</sup> )	230 (8.0 A g <sup>-1</sup> )	310 mAhg <sup>-1</sup> after 10 000 cycles (@ 5.0 A g <sup>-1</sup> )	[85]
Mesoporous anatase with an ordered 3D pore structure	322 (0.09 C-rate) (1 C = 0.336 A g <sup>-1</sup> )	85 (107.0 C-rate)	81 mA h g <sup>-1</sup> after 50 cycles (@ 36.0 A g <sup>-1</sup> )	[125]
CNT-threaded TiO <sub>2</sub>	265 (1.0 C-rate) (1 C = 0.170 A g <sup>-1</sup> )	150 (100.0 C-rate)	87% after 1000 cycles (@ 20 C)	[132]
Carbon-supported stacked TiO <sub>2</sub> nanosheets (CTNSs)	191 (2.0 C-rate) (1 C = 0.170 A g <sup>-1</sup> )	109 (50.0 C-rate)	155 mA h g <sup>-1</sup> after 150 cycles (@ 10 C)	[89]
Mesoporous TiO <sub>2</sub> -B microspheres	256 (0.1 C-rate) (1 C = 0.335 A g <sup>-1</sup> )	115 (60.0 C-rate)	90.0% (149 mAh g <sup>-1</sup> ) after 5000 cycles (@ 10 C)	[98]
Nanoparticulate TiO <sub>2</sub> (B)	230 (0.16 A g <sup>-1</sup> )	122 (18.0 A g <sup>-1</sup> )		[46]
LTO nanocrystals (LTO-nc)	170 (0.5 C-rate) (1 C = 0.175 A g <sup>-1</sup> )	70 (100.0 C-rate)	95.0% (133 mAh g <sup>-1</sup> ) after 100 cycles (@ 10 C)	[106]
Nanosized Li <sub>4</sub> Ti <sub>5</sub> O <sub>12</sub> /carbon (N-LTO/C)	161 (0.2 C-rate) (1 C = 0.175 A g <sup>-1</sup> )	85.33 (90.0 C-rate)	95.0% (131 mAh g <sup>-1</sup> ) after 1000 cycles (@ 10 C)	[115]
nc- Li <sub>4</sub> Ti <sub>5</sub> O <sub>12</sub> /CNF	167 (1.0 C-rate) (1 C = 0.175 A g <sup>-1</sup> )	158 (300.0 C-rate)	90.0% after 9000 cycles (@ 20 C)	[113]
Porous TiNb <sub>2</sub> O <sub>7</sub> nanospheres (PTNO NSs)	285 (1.0 C-rate) (1 C = 0.387 A g <sup>-1</sup> )	167 (50.0 C-rate)	(160 mAh g <sup>-1</sup> ) after 10 000 cycles (@ 5 C)	[127]
Porous TiNb <sub>2</sub> O <sub>7</sub> microspheres (PTNO MSs)	265 (0.1 C-rate) (1 C = 0.387 A g <sup>-1</sup> )	143 (100.0 C-rate)	90% (190 mAh g <sup>-1</sup> ) after 1000 cycles (@ 5 C)	[126]
TiNb <sub>2</sub> O <sub>7</sub> nanotubes (TNO NTs)	294 (0.1 C-rate) (1 C = 0.387 A g <sup>-1</sup> )	180 (100.0 C-rate)	80% (170 mAh g <sup>-1</sup> ) after 700 cycles (@ 1 C)	[123]

transition metal oxide cathode material which has been successfully introduced in commercial devices.<sup>[137]</sup> LCO displays a cubic close-packed arrangement “O3-type structure.”<sup>[40,138]</sup> It has a theoretical capacity of 274 mAh g<sup>-1</sup> and a high volumetric capacity of 1363 mAh cm<sup>-3</sup>. It features a flat plateau around 3.8 V versus Li/Li<sup>+</sup>. The major disadvantage of this material is its low thermal stability and its high cost and toxicity, due to the presence of Co, and the fact that its structure is very dependent on the amount lithium ions that are extracted during the charge process. For this reason, only 50% of its theoretical capacity can be safely utilized and its practical capacity is ≈140 mAh g<sup>-1</sup>.<sup>[139–142]</sup> Okubo et al.<sup>[143]</sup> reported about the dependency of the electrochemical property of LCO on the particle size, showing the disappearance of the typical discharge potential plateau of this material in the case LCO particles with size lower than 10 nm.

It has been shown that nanocrystalline LCO (17 nm) might display high rate capability (retention of 65% of the initial capacity at 100 C).

LiNi<sub>0.8</sub>Co<sub>0.15</sub>Al<sub>0.05</sub>O<sub>2</sub> (NCA) is a widely used commercial cathodic material, for example, in Panasonic batteries for Tesla EVs, which shows high discharge capacity and calendar life comparable to that of LCO cathode.<sup>[144]</sup> In the last years considerable efforts have been made to synthesize nanosized materials having different morphologies, for example, microrods (NCA-MRs),<sup>[145]</sup> yolk-shell NCA microspheres (NCA Ms),<sup>[146]</sup> hierarchical plates of NCA (HP-NCA),<sup>[147]</sup> able to display high performance also at high C-rates. The hierarchical NC plates (NCA- HP) synthesized by Wang et al.<sup>[147]</sup> exhibits a high specific capacity of 207 mAh g<sup>-1</sup> (0.1 C-rate) and maintains a capacity of 124 mAh g<sup>-1</sup> even at a higher rate of 10.0 C-rate,

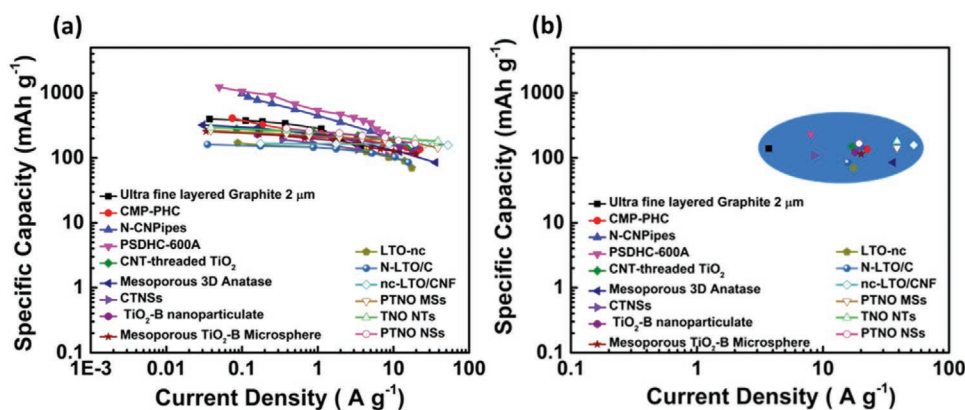


**Figure 8.** Comparison of a) rate capability at different current densities and b) achieved specific capacity at maximum current density of different anodic materials for LIB (the marked area is giving a visual indication about the range of capacities and current densities achievable by these materials).

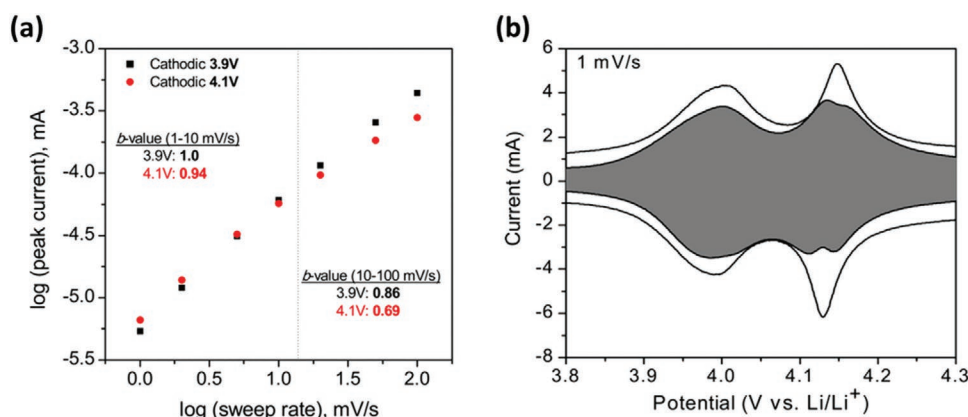


**Figure 9.** a) Plots of  $\log(\text{peak current})$  versus  $\log(\text{sweep rate})$  and b) capacitive contributions to the total current for nanoporous  $\text{Li}_x\text{Mn}_2\text{O}_4$  ( $1 < x < 2$ ) at  $1 \text{ mV s}^{-1}$ . Reproduced with permission.<sup>[150]</sup> Copyright 2016, ACS Nano.

which is attributed to its microstructure which facilitates the rapid insertion/extraction of lithium ions.

Spinel  $\text{LiMn}_2\text{O}_4$  displays several promising features such as high thermal stability, low cost, abundance, and environmental friendliness, but it has a lower capacity compared to LCO.<sup>[148,149]</sup> Lesel et al.<sup>[150]</sup> investigated nanostructured LMO and showed that these materials are displaying high anodic and cathodic  $b$ -values and exhibit a significant capacitive contribution (72% at  $1.0 \text{ mV s}^{-1}$ ) (Figure 9). These Nanoporous LMO can deliver a capacity of  $\approx 44 \text{ mAh g}^{-1}$  at 50 C.

In 1997, Goodenough group proposed the use of phospholivine structure  $\text{LiFePO}_4$  (LFP) as cathode material for LIB. LFP is a cheap, non-toxic, and ecofriendly material displaying excellent thermal stability. LFP has a theoretical capacity of  $170 \text{ mAh g}^{-1}$  and a flat charge–discharge plateau around 3.4 V versus  $\text{Li}/\text{Li}^+$ . In the last years a large amount of studies have been dedicated to this material, and many efforts have been made to improve its low electronic conductivity ( $\sigma_e < 10^{-9} \text{ S cm}^{-1}$ ) as well as the lithium diffusion coefficient ( $D \approx 10^{-14} \text{ cm}^2 \text{ s}^{-1}$ ).<sup>[138,151–153]</sup> Among the various LFP reported in the literature, the nanostructured core–shell LFP/graphitic carbon composite proposed by Naoi et al.<sup>[153]</sup> appears as one of the most promising materials for high power application as it is able to deliver capacity of  $60 \text{ mAh g}^{-1}$  at 100 C (Figure 10).

Monoclinic  $\text{Li}_3\text{V}_2(\text{PO}_4)_3$  (LVP) exhibits high energy and power density, thermal stability, high safety, low costs, and a large theoretical specific capacity of  $197 \text{ mA h g}^{-1}$  when charged up to 4.8 V versus  $\text{Li}/\text{Li}^+$ .<sup>[154]</sup> It also features a high average operating potential of around 4 V versus  $\text{Li}/\text{Li}^+$  ( $\sim 0.6 \text{ V}$  higher than that of LFP). LVP has 3D pathways for  $\text{Li}^+$  insertion/extraction, which facilitate fast migration of the  $\text{Li}^+$  ions inside its structure.<sup>[154,155]</sup> However, LVP suffers from intrinsically low electronic conductivity, which limits its high rate performance. Furthermore, the capacity of LVP usually drops rapidly during the process of  $\text{Li}^+$  insertion/deinsertion due to side reactions between the active material and commonly used organic electrolytes at such a high potential (4.8 V vs  $\text{Li}/\text{Li}^+$ ). In the last years several efforts have been dedicated to improve the rate performance as well as the stability at high potential of LVP.<sup>[154–158]</sup> Among the proposed strategies, the use of ionic liquids assisted synthesis appears very interesting. Zhang et al.<sup>[159]</sup> showed that is

possible to use protic ionic liquids (PILs) as soft template and carbon source for the synthesis of carbon-coated LVP nanocrystals embedded in a micrometer-sized carbon matrix. LVP/PIL based electrodes exhibit high performance and stable  $\text{Li}^+$  ion storage performance due to the fast  $\text{Li}^+$  diffusivity, high electronic conductivity, and favorable nanoarchitecture of the material. Very high specific capacities of  $100 \text{ mAh g}^{-1}$  at 100 C in the potential range of 3.0–4.3 V and  $120 \text{ mAh g}^{-1}$  at 50 C in the potential range of 3.0–4.8 V were obtained. Furthermore, excellent cycling stability during 10 000 cycles at 50 C (3.0–4.8 V) could be demonstrated (Figure 11).

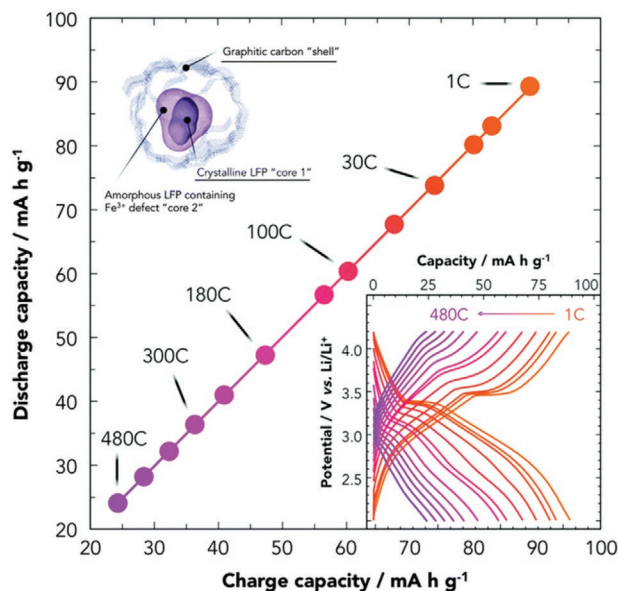


**Figure 10.** Plots of discharge capacity versus charge capacity of a half-cell consisting of  $\text{Li}/1 \text{ M LiPF}_6 \text{ EC} + \text{DEC}/(\text{LFP}/\text{graphitic carbon})$  composite as a function of C-rate. (Inset below right: Charge–discharge profiles at different charge C-rates from 1 to 480 C. Inset top left: Schematic illustration of the core–shell nanostructure of the LFP/graphitic carbon composite, representing a minute structure consisting of an amorphous outer sphere of an LFP containing  $\text{Fe}^{3+}$  defects and an inner sphere of crystalline LFP.) Reproduced with permission<sup>[153]</sup> Copyright 2016, Royal Society of Chemistry.

**Table 2.** Properties of selected high power cathodic materials for LIBs.

Cathode material	Maximum capacity [mAh g <sup>-1</sup> ]	Capacity @ high c-rate/mAh g <sup>-1</sup>	Capacity retention	Reference
Carbon-coated LCO (C-LCO)	130 (0.1 C-rate) (1 C = 0.140 A g <sup>-1</sup> )	123 (1.0 C-rate)		[140]
Al <sub>2</sub> O <sub>3</sub> -coated LiCoO <sub>2</sub>	174 (0.1 C-rate) (1 C = 0.140 A g <sup>-1</sup> )	140 (3.0 C-rate)	94% (163 mAh g <sup>-1</sup> ) after 50 cycles (@ 0.5 C)	[141]
Nanocrystalline LiCoO <sub>2</sub>	120 (1.0 C-rate) (1 C = 0.137 A g <sup>-1</sup> )	75 (100.0 C-rate)	75% after 20 cycles (@ 10.0 C)	[143]
LiMnO <sub>2</sub> nanorods	200 (0.02 A g <sup>-1</sup> )	140 (0.1 A g <sup>-1</sup> )	180 mAh g <sup>-1</sup> after 30 cycles (@ 0.02 A g <sup>-1</sup> )	[160]
SS-Li(Ni <sub>0.5</sub> Mn <sub>0.5</sub> )O <sub>2</sub>	235 (0.05 C-rate) (1 C = 0.280 A g <sup>-1</sup> )	183 (6.0 C-rate)		[161]
Yolk-shell NCA microspheres (NCA Ms)	225.9 (0.1 C-rate) (1 C = 0.180 A g <sup>-1</sup> )	129.7 (1.0 C-rate)	89.38% (185.9 mAh g <sup>-1</sup> ) after 49 cycles (@ 0.2 C)	[146]
NCA-MRs	218 (0.1 C-rate) (1 C = 0.180 A g <sup>-1</sup> )	115 (10.0 C-rate)	93% (168 mAh g <sup>-1</sup> ) after 100 cycles (@ 1.0 C)	[145]
NCA-HP	207 (0.1 C-rate) (1 C = 0.180 A g <sup>-1</sup> )	124 (10.0 C-rate)	92.1% (152 mAh g <sup>-1</sup> ) after 50 cycles (@ 1.0 C)	[147]
LiMn <sub>2</sub> O <sub>4</sub> hollow nanofibers	119 (1.0 C-rate) (1 C = 0.150 A g <sup>-1</sup> )	56 (16.0 C-rate)	87% (103 mAh g <sup>-1</sup> ) after 1250 cycles (@ 1.0 C)	[162]
Mesoporous Li <sub>x</sub> Mn <sub>2</sub> O <sub>4</sub>	44 (50.0 C-rate) (1 C = 0.065 A g <sup>-1</sup> )	20 (1000.0 C-rate)	90% after 265 cycles (@ 32.0 C)	[150]
LiFePO <sub>4</sub> /graphitic carbon	89 (1.0 C-rate) (1 C = 0.170 A g <sup>-1</sup> )	24 (480.0 C-rate)	96% after 2000 cycles (@ 240.0 C)	[153]
LVP/CA	110 (0.5 C-rate) (1 C = 0.133 A g <sup>-1</sup> )	100 (10.0 C-rate)	94.7% after 100 cycles (@ 1.0 C)	[163]
LVP/PIL	158 (1.0 C-rate) (1 C = 0.197 A g <sup>-1</sup> )	126 (50.0 C-rate)	70% after 10 000 cycles (@ 50.0 C)	[159]

**Table 2** compares some properties of importance for high power applications of selected cathodic materials belonging to the families discussed above.<sup>[160–163]</sup>

The variation of the specific capacities at different current densities of the materials considered in Table 2 is compared in **Figure 12**. As shown, the cathodic materials of LIBs are able to deliver high specific capacity up to current densities of 50–100 A g<sup>-1</sup>. Presently, phosphate based cathodes, for example, LFP and LVP, appears as very promising candidates for high power LIBs. The overall high power behavior of high voltage cathodes should be further improved.

### 2.1.2. Sodium-Ion Batteries

As discussed above, the interest in NIB increased continuously in the last years. Sodium is very abundant and cheap, and sodium salts display good solubility in organic solvent.<sup>[164,165]</sup>

Since metallic sodium and lithium display rather comparable potential plating ( $E_{\text{Na}^+/\text{Na}} = -2.71$  V vs SHE and  $E_{\text{Li}^+/\text{Li}} = -3.04$  V vs SHE), the use of this metal allows the realization of systems having operative voltage comparable to LIBs. Furthermore, since sodium is not forming alloys with aluminum at low potential, its use makes possible the utilization of aluminum current collectors in both, the cathode and the anode. These properties are obviously making NIBs very attractive systems, and nowadays they are considered as one of the most promising alternative to LIBs.<sup>[166–169]</sup>

**Anodic Materials for NIBs:** The intercalation process of lithium and sodium ions into graphite is not following a similar behavior, and the use of this material appears much more challenging for NIB than for LIBs, also in the case of high power applications.<sup>[170–172]</sup> Theoretical studies indicated that the limited thermodynamic stability of sodium binary graphite intercalation compounds (b-GICs) is affecting the solubility of Na-ions in graphite, preventing Na intercalation into the graphite.<sup>[173–177]</sup>

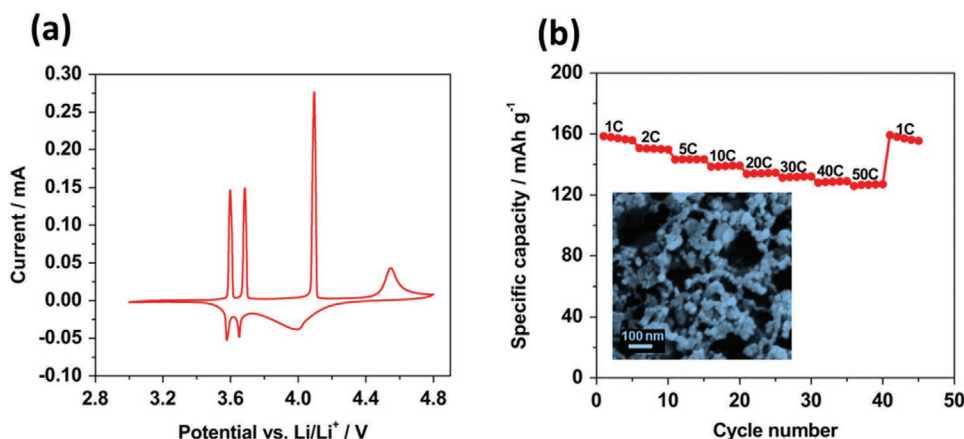


**Figure 11.** a) Cyclic voltammety of LVP electrodes in the potential range of 3.0–4.8 V versus Li/Li<sup>+</sup> at a scan rate of 0.05 mV s<sup>-1</sup> and b) specific discharge capacity of LVP electrodes when charged/discharged at various discharge current densities in the range of 1–50 C (inset shows the SEM image of LVP/PIL nanoparticles). Reproduced with permission.<sup>[159]</sup> Copyright 2015, Elsevier.

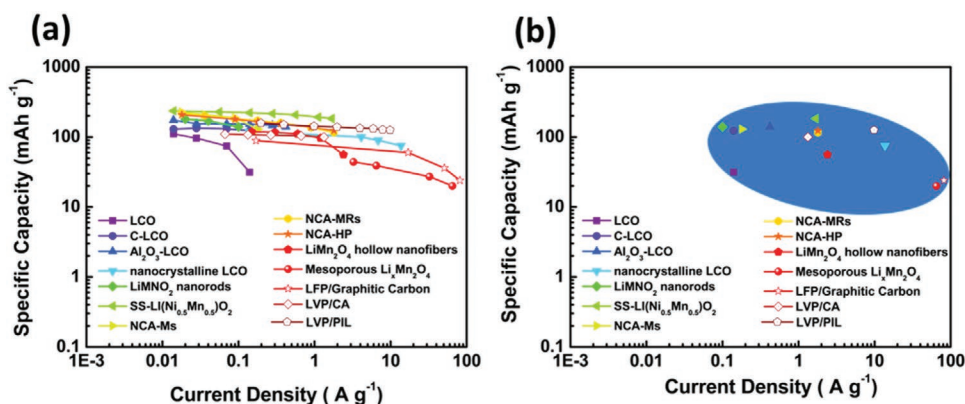


**Figure 12.** Comparison of a) rate capability at different current densities and b) achieved specific capacity at maximum current density of different cathodic materials for LIB (the marked area is giving a visual indication about the range of capacities and current densities achievable by these materials).

Yoon et al.<sup>[174]</sup> systematically investigated the graphite intercalation behavior of various alkali metals (AM = Li, Na, K, Rb, Cs) and demonstrated that the instability of Na-GIC is due to the unfavorable local Na-graphene interaction ( $\approx 0.5$  eV) compared with those for other AMs. This work suggested that an effective strategy to increase the Na-ion accommodation in the graphite host is to screen the Na-ions with solvent molecules in order to mitigate the direct local interactions between the Na-ions and the graphene layers.

Jache et al.<sup>[178]</sup> reported about an improved Na-ion intercalation inside the graphite realized by co-intercalation mechanism involving ether based electrolytes and sodium. They showed that utilizing sodium triflate (NaOTf) in diglyme it is possible to achieve capacities in the order of  $100 \text{ mAh g}^{-1}$ , which can be maintained for a high number of charge-discharge cycles. Utilizing a similar approach, Kim et al.<sup>[179]</sup> reported that graphite electrode can deliver in the electrolyte NaPF<sub>6</sub> in diethylene glycol dimethyl ether (DEGDME) capacity of  $\approx 150 \text{ mAh g}^{-1}$  at low current density, which are decreased to more than  $75 \text{ mAh g}^{-1}$  at  $10 \text{ A g}^{-1}$ . Furthermore, they demonstrated the partial pseudocapacitive behavior Na<sup>+</sup>-solvent co-intercalation in graphite and estimated the capacitive and intercalation contributions of Na storage quantitatively (Figure 13).

By a process of oxidation and partial reduction of graphite, Wen et al.<sup>[180]</sup> prepared expanded graphite (EG) with a long-range-ordered layered structure having an enlarged interlayer lattice spacing of  $4.3 \text{ \AA}$  able to deliver reversible capacity of  $284 \text{ mAh g}^{-1}$  at a current density of  $20 \text{ mA g}^{-1}$ .

The feasibility of Na-ion intercalation in non-graphitizable hard carbon was first demonstrated by Stevens and Dahn.<sup>[171]</sup> The hard carbon based electrode display a high capacity of  $\approx 300 \text{ mAh g}^{-1}$  (tenfold that of graphite), but also a low initial coulombic efficiency. Although this low efficiency is a barrier for practical utilization, this material in nowadays the anode of choice for commercial NIB.<sup>[181,182]</sup> There are various models proposed to explain the mechanism of Na storage in hard carbon.<sup>[183,184]</sup> The first model was the card-house model proposed by Stevens et al.<sup>[171]</sup> which consider two distinct Na-storage mechanisms. Subsequently, Mitlin's group showed that nanopore filling is not responsible for the dominant Na-ion charge storage mechanism at lower voltage plateau regions<sup>[185,186]</sup> and Bommier et al.<sup>[187]</sup> proposed a three-part storage mechanism, by utilizing the ex situ XRD, and Na-plating experiments, indicating that the Na-ion intercalation between graphene sheets and minor Na-ion adsorption on pore surfaces are responsible for the low voltage plateau region. Later studies based on

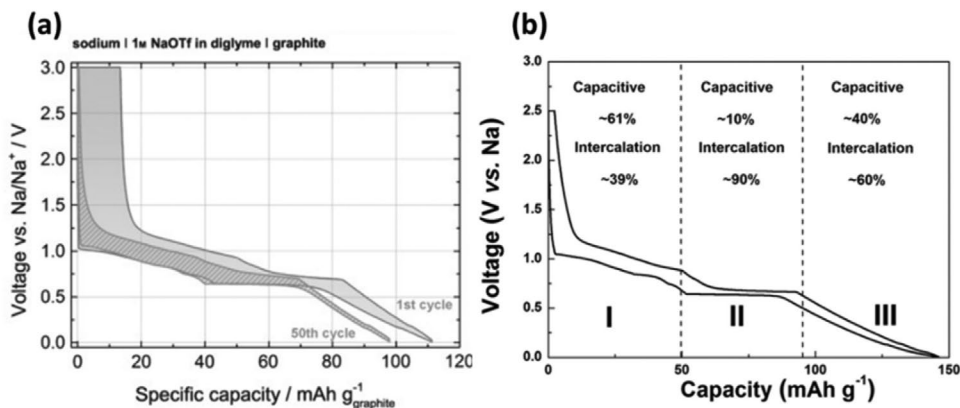


**Figure 13.** a) Voltage profile (1st and 50th cycle) of graphite in a sodium triflate (NaOTf) diglyme electrolyte. Reproduced with permission.<sup>[178]</sup> Copyright 2014, John Wiley and Sons. b) Quantitative contributions of capacitive and intercalation of Na-ions in graphite electrode in NaPF<sub>6</sub> in DEGDME electrolyte. Reproduced with permission.<sup>[179]</sup> Copyright 2014, John Wiley and Sons.

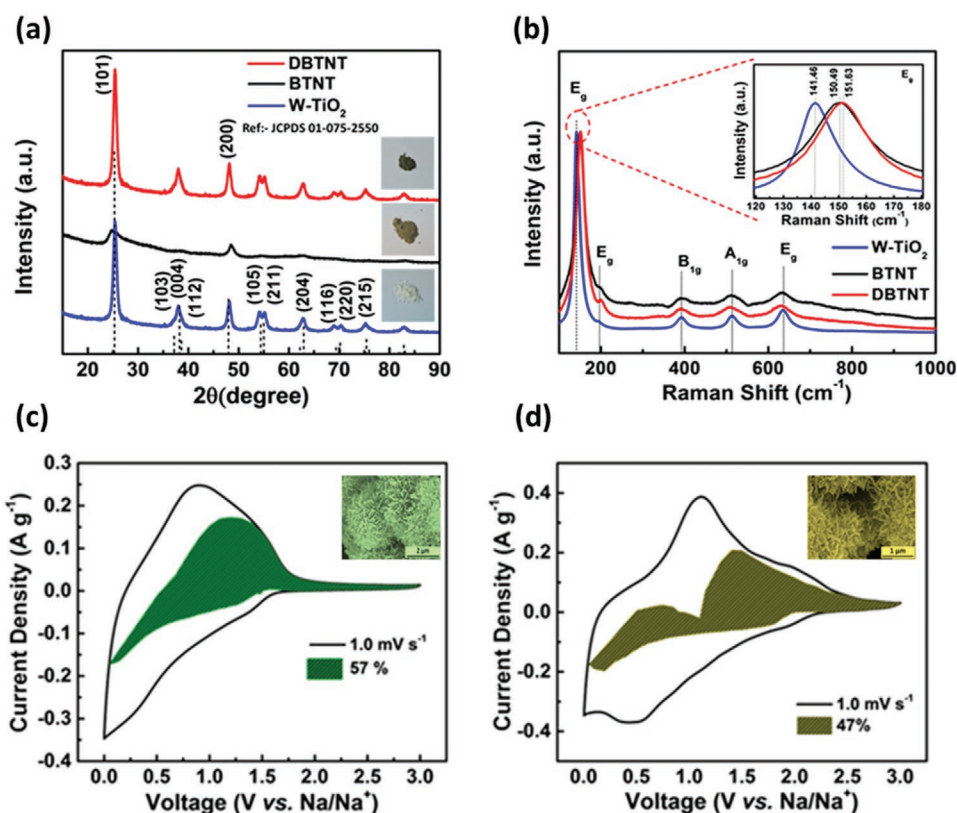


**Figure 14.** Comparison of a) powder XRD pattern, b) Raman spectra of BTNT and DBTNT, with commercial pristine white anatase  $\text{TiO}_2$ , capacitive contribution (shaded region) of c) BTNT and d) DBTNT. Reproduced with permission.<sup>[205]</sup> Copyright 2018, American Chemical Society.

binding energies shows the two stages “adsorption-pore-filling sodium storage mechanism” in hard carbons.<sup>[188]</sup> Various studies showed that the more amorphous nature of non-graphitizable hard carbon (compared to graphite) is favorable also in view of high power application.<sup>[189,190]</sup> Ding et al.<sup>[191]</sup> investigated the Na-ion intercalation in air activated peanut shell ordered carbon (PSOC-A), showing that these materials can deliver a capacity of  $107 \text{ mAh g}^{-1}$  at a higher current density of  $3.2 \text{ A g}^{-1}$  ( $\approx 10 \text{ C}$ ), and retain 75% of their initial capacity after 10 000 cycles. Qie et al.<sup>[192]</sup> proposed the use of sulfur-doped carbon and showed that these material deliver a capacity of  $120 \text{ mAh g}^{-1}$  at  $5 \text{ A g}^{-1}$ .

Also graphitizable soft carbons have been considered as anodic materials for the SIB anode.<sup>[71,193,194]</sup> Yao et al.<sup>[195]</sup> showed the use of microporous soft carbon nanosheets (CNSs) make the realization of electrode able to deliver high capacity ( $232 \text{ mAh g}^{-1}$  at  $20 \text{ mA g}^{-1}$ ) and high performance at high current densities ( $103 \text{ mAh g}^{-1}$  at  $1.0 \text{ A g}^{-1}$ ) possible. This high performance is attributed to the extra sodium-ion storage sites and the high kinetics of Na-ions at the micropores, and edge defects in the nanosheets.<sup>[44]</sup>

Titanium based anodes have been widely investigated also for NIBs. It has been shown that apart from the crystal structure, the electrochemical performance of  $\text{TiO}_2$  anodes for NIBs is also depending on the textural as well as microstructural features, stability of SEI, etc.<sup>[196–200]</sup> As in the case of graphite, the larger size of Na-ions compared to Li-ions is affecting the use of these materials in NIB.<sup>[201,202]</sup> The electrochemical performance of  $\text{TiO}_2$  anodes can be enhanced by nanocrystallization, which

shortens the diffusion pathway. Coating and doping also helps to improve its electronic conductivity as well as mechanical stability.<sup>[203–205]</sup>

Mitlin and co-workers<sup>[206]</sup> investigated the behavior of mesoporous anatase  $\text{TiO}_2$  nanocrystals electrodes, showing that these electrodes exhibits a highly stable reversible capacity ( $\approx 150 \text{ mA h g}^{-1}$ ) and good rate capability. Passerini and co-workers<sup>[207]</sup> showed that in contrast with the pure two phase intercalation reaction of Li-ions in anatase  $\text{TiO}_2$ , the Na-ions undergo a different reaction mechanism involving the formation of intermediate sodium titanate phase, and the formation of an amorphous sodium titanate phase able to provide a reversible specific capacity of about  $140 \text{ mAh g}^{-1}$ . Chen et al.,<sup>[208]</sup> showed the fast  $\text{Na}^+$  pseudocapacitive intercalation behavior of  $\text{TiO}_2/\text{graphene}$  nanocomposites (capacity contribution of 78.2% at a scan rate of  $5 \text{ mV s}^{-1}$ ) and reported that nanostructured black anatase titania can deliver a specific capacity of  $208 \text{ mAh g}^{-1}$  at  $0.2 \text{ C}$  and deliver high capacity also at higher C-rate. Babu et al.<sup>[205]</sup> made a comparative study of the semicrystalline (BTNT) and crystalline brown  $\text{TiO}_2$  (DBTNT) nanotubes, aggregates in a flower-like morphology, containing  $\text{Ti}^{3+}$  induced by hydrothermal method. The kinetic study reported in this work reveals that the crystalline  $\text{TiO}_2$  displays higher capacity compared to the brown  $\text{TiO}_2$  (57% vs 47%) and the former can be utilized as high power anode material (Figure 14).

Yang et al.<sup>[209]</sup> fabricated nitrogen-doped  $\text{TiO}_2(\text{B})$  nanorods which exhibit a specific capacity of  $225 \text{ mA h g}^{-1}$ , good rate

**Table 3.** Properties of selected high power anodic materials for NIBs.

Anode material	Maximum capacity [mAh g <sup>-1</sup> ]	Capacity @ high c-rate/mAh g <sup>-1</sup>	Capacity retention	Reference
Natural graphite	150 (0.1 A g <sup>-1</sup> )	75 (10.0 A g <sup>-1</sup> )	80.0% after 2500 cycles (@ 0.5 A g <sup>-1</sup> )	[179]
Hollow carbon nanospheres (HC-NS)	200 (0.05 A g <sup>-1</sup> )	50 (10.0 A g <sup>-1</sup> )	160 mAh g <sup>-1</sup> after 100 cycles (@ 0.05 A g <sup>-1</sup> )	[217]
Microporous soft carbon nanosheets (SC-NS)	232.2 (0.02 A g <sup>-1</sup> )	103.8 (1.0 A g <sup>-1</sup> )	93.0% (128.7 mAh g <sup>-1</sup> ) after 3500 cycles (@ 0.8 A g <sup>-1</sup> )	[195]
Carbon-coated anatase TiO <sub>2</sub> (c-TiO <sub>2</sub> )	165 (0.5 C-rate) (1 C = 0.330 A g <sup>-1</sup> )	53 (100.0 C-rate)	90.7% (91 mAh g <sup>-1</sup> ) after 50 cycles (@ 5.0 C)	[218]
G-TiO <sub>2</sub>	265 (0.05 A g <sup>-1</sup> ) (1 C = 0.330 A g <sup>-1</sup> )	90 (12.0 A g <sup>-1</sup> )	120 mAh g <sup>-1</sup> after 4000 cycles (@ 2.0 C)	[208]
Mesoporous single-crystal-like TiO <sub>2</sub> -Graphene ( MWTOG)	268 (0.1 C-rate) (1 C = 0.335 A g <sup>-1</sup> )	104 (20.0 C-rate)	126 mAh g <sup>-1</sup> after 18 000 cycles (@ 10.0 C)	[219]
BTNT	109 (0.1 A g <sup>-1</sup> )	48 (1.0 A g <sup>-1</sup> )	68 mAh g <sup>-1</sup> after 300 cycles (@ 0.1 A g <sup>-1</sup> )	[205]
Carbon-coated anatase TiO <sub>2</sub> hollow spheres (CCAnTHSs)	204.8 (0.5 C-rate) (1 C = 0.335 A g <sup>-1</sup> )	84.9 (25.0 C-rate)	92.3% (140.4 mAh g <sup>-1</sup> ) after 500 cycles (@ 5.0 C)	[220]
Black anatase titania (Black TiO <sub>2</sub> )	207.6 (0.2 C-rate) (1 C = 0.335 A g <sup>-1</sup> )	91.2 (20.0 C-rate)	99.1% (185.1 mAh g <sup>-1</sup> ) after 500 cycles (@ 1.0 C)	[221]
Rutile TiO <sub>2</sub> mesocrystals (C-TiO <sub>2</sub> -MR)	280 (0.1 A g <sup>-1</sup> )	152 (2.0 A g <sup>-1</sup> )	99.1% (138 mAh g <sup>-1</sup> ) after 200 cycles (@ 0.5 A g <sup>-1</sup> )	[222]
Graphene-rich wrapped petal-like rutile TiO <sub>2</sub> (G/P-RTiO <sub>2</sub> )	202.4 (0.25 C-rate) (1 C = 0.335 A g <sup>-1</sup> )	59.8 (12.5 C-rate)	94.4% (74.6 mAh g <sup>-1</sup> ) after 4000 cycles (@ 10.0 C)	[223]
Nitrogen-doped TiO <sub>2</sub> (B) (N-TiO <sub>2</sub> (B))	231.5 (0.1 C-rate) (1 C = 0.167 A g <sup>-1</sup> )	110 (20 C-rate)	93.4% after 200 cycles (@ 2.0 C)	[209]
NTO nanotubes (ST-NTO)	287 (0.2 C-rate) (1 C = 0.177 A g <sup>-1</sup> )	84 (10 C-rate)	100% (78 mAh g <sup>-1</sup> ) after 10 000 cycles (@ 10.0 C)	[224]
Na <sub>2</sub> Ti <sub>7</sub> O <sub>15</sub> nanotubes	258 (0.05 A g <sup>-1</sup> )	108 (1.5 A g <sup>-1</sup> )	96% (130.6 mAh g <sup>-1</sup> ) after 200 cycles (@ 1.0 A g <sup>-1</sup> )	[215]
Na <sub>2</sub> Ti <sub>9</sub> O <sub>19</sub>	140 (0.02 A g <sup>-1</sup> )	25 (5 A g <sup>-1</sup> )	96% (117 mAh g <sup>-1</sup> ) after 100 cycles (@ 0.02 A g <sup>-1</sup> )	[225]

performance, and a good cycling stability (capacity retention of 93.4% ratio after 200 cycles at 2 C). The open structural framework of sodium titanates host matrixes can easily accommodate larger alkali ions without any structural degradation.<sup>[210–212]</sup> Senguttuvan et al.<sup>[213]</sup> reported that layered structured Na<sub>2</sub>Ti<sub>3</sub>O<sub>7</sub>, which can reversibly uptake two Na-ions per formula unit at an average potential of 0.3 V versus Na/Na<sup>+</sup>, provides a capacity of 200 mAh g<sup>-1</sup>. Ko et al.<sup>[214]</sup> reported that the exfoliated Na<sub>2</sub>Ti<sub>3</sub>O<sub>7</sub> nanoplatelets and nanosheets (Na<sub>2</sub>Ti<sub>3</sub>O<sub>7</sub> NP-NS) display high capacities in the range of 100–150 mA h g<sup>-1</sup> at higher rates and also exhibits a capacitive contribution of 84% at 10 mV s<sup>-1</sup>. Li et al.<sup>[215]</sup> developed Na<sub>2</sub>Ti<sub>7</sub>O<sub>15</sub> nanotubes on a Ti net substrate used directly as a binder-free anode for Na-ion batteries, showing that these materials deliver high reversible capacity

(258 mA h g<sup>-1</sup> at 50 mA g<sup>-1</sup>) and exhibit 96% capacity retention over 200 cycles at 1.0 A g<sup>-1</sup>.

**Table 3** compares some properties of importance for high power applications of selected anodic materials belonging to the families discussed above.<sup>[216–225]</sup>

The variation of the specific capacities at different current densities of the materials considered in Table 3 is compared in **Figure 15**. As shown, the anodic material of NIBs are able to deliver high specific capacity up to current densities of 10 A g<sup>-1</sup>. Above these values their performance starts to decline. To date, hard carbon, due to their low cost and higher capacity appears as the most promising carbonaceous anodes. However, their irreversible capacity during the first cycles needs to be decreased in the future. An interesting alternative for high

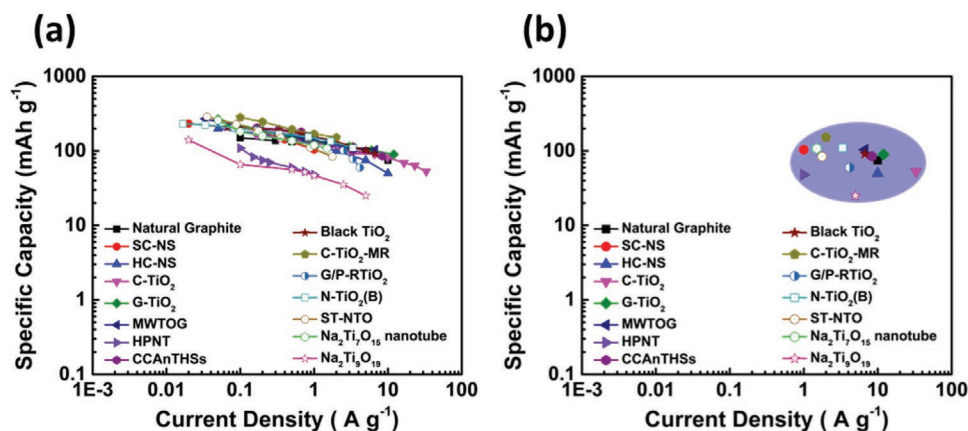


**Figure 15.** Comparison of a) rate capability at different current densities and b) achieved specific capacity at maximum current density of different anodic materials for NIB (the marked area is giving a visual indication about the range of capacities and current densities achievable by these materials).



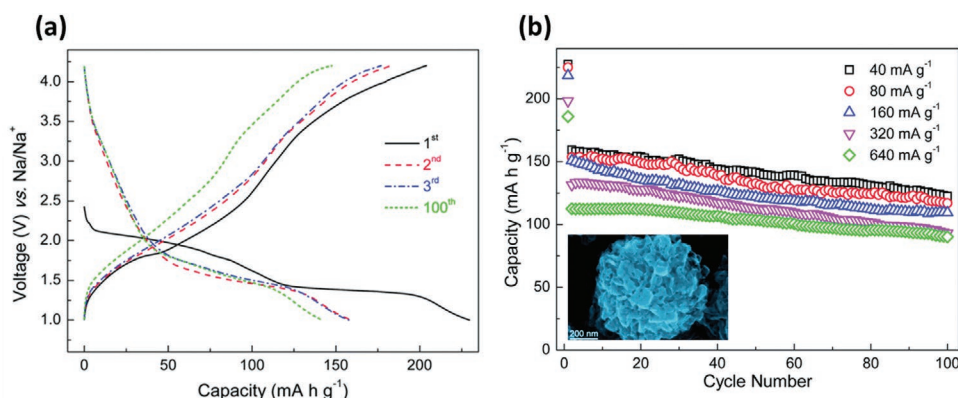


**Figure 16.** a) Galvanostatic charge–discharge profile of  $V_2O_5$  hollow nanospheres at a current density of  $20 \text{ mA g}^{-1}$  and b) specific capacity versus cycle number at different current densities. Reproduced with permission.<sup>[236]</sup> Copyright 2014, Royal Society of Chemistry.

power applications are titanium based materials although their use is limiting the cell voltage.

**Cathodic Materials for NIBs:** The properties of the cathode of NIB are strongly influencing the operative voltage as well as the power output of the devices.<sup>[226,227]</sup>

Transition metal oxide can be categorized as sodium-free metal oxides  $MO_x$  ( $M = V, Mn, Mo$ ) and sodium-inserted metal oxides ( $Na_xMO_2$ ,  $0 < x \leq 1$ ;  $M = Fe, Mn, Ni, Co, Cr, Ti, V$ , and their combinations).<sup>[227–229]</sup> Vanadium oxide ( $VO_2$ ) has been long regarded as an interesting cathode for NIBs due to its theoretical capacity ( $323 \text{ mA h g}^{-1}$ ) satisfactory capacity, structural flexibility, low cost, and large availability. During the initial Na-insertion process, the  $VO_2$  spontaneously changes to the stable  $NaVO_2$  phase and then the reversible reaction occurs between  $Na_{0.3}VO_2$  and  $NaVO_2$  during charging and discharging.<sup>[230–232]</sup> Vanadium pentoxide ( $V_2O_5$ ), which can be divided in orthorhombic and bilayered  $V_2O_5$ , has been also considered as cathodic material for NIBs.<sup>[233,234]</sup> The electrochemical performance of orthorhombic  $V_2O_5$  is improved by various processes such as nanoporous carbon encapsulation,<sup>[235]</sup> by engineering hollow nanoarchitecture, etc. Wang's group<sup>[236]</sup> synthesized  $V_2O_5$  hollow nanospheres, which shows a high specific discharge capacity of  $\approx 150 \text{ mA h g}^{-1}$  corresponding to the formation of  $NaV_2O_5$ , and maintains a capacity of  $112.4 \text{ mA h g}^{-1}$  at a high current density

of  $640 \text{ mA g}^{-1}$ . It should be noted, however, that Vanadium is expensive and therefore materials based on this element might not be the most suitable for large-scale production (Figure 16).

The sodium-inserted metal oxides ( $Na_xMO_2$ ,  $0 < x \leq 1$ ;  $M = Fe, Mn, Ni, Co, Cr, Ti, V$ , and their combinations) can be divided on the basis of their structure in two main types: a) tunnel structure and b) layered structure. These materials have been largely investigated and used in NIBs. Among the various compounds,  $Na_{0.44}MnO_2$  that has a theoretical capacity of  $121 \text{ mA h g}^{-1}$ , is probably the most extensively investigated.<sup>[237–239]</sup> The 1D ultralong and continuous fibrous network structure of  $Na_{0.44}MnO_2$  nanofibers developed by Fu et al.<sup>[239]</sup> exhibits a superior rate performance with a reversible specific capacity of  $69.5 \text{ mAh g}^{-1}$  at  $10 \text{ C}$ .

The layer structured sodium-inserted metal oxide  $Na_xMO_2$  can be categorized into P2 and O3 phases based on the Na environment and the number of oxygen stacking sequences.<sup>[240]</sup> The chemical environment of the Na-ions (host sites) at the prismatic and octahedral sites can be represented by “P” and “O,” whereas the numbers “2” and “3” indicate the quantity of repeated transition  $MeO_2$ -metal layer in a unit cell.<sup>[164]</sup> The P2- $Na_{0.7}CoO_2$  microspheres (s-NCO) developed by Fang et al.<sup>[241]</sup> exhibits a high specific capacity of  $125 \text{ mAh g}^{-1}$  at  $5 \text{ mA g}^{-1}$ , excellent rate capability of  $64 \text{ mAh g}^{-1}$  at a higher rate of  $16 \text{ C}$  and long-term cycling stability (86% retention in capacity over 300 cycles) (Figure 17).

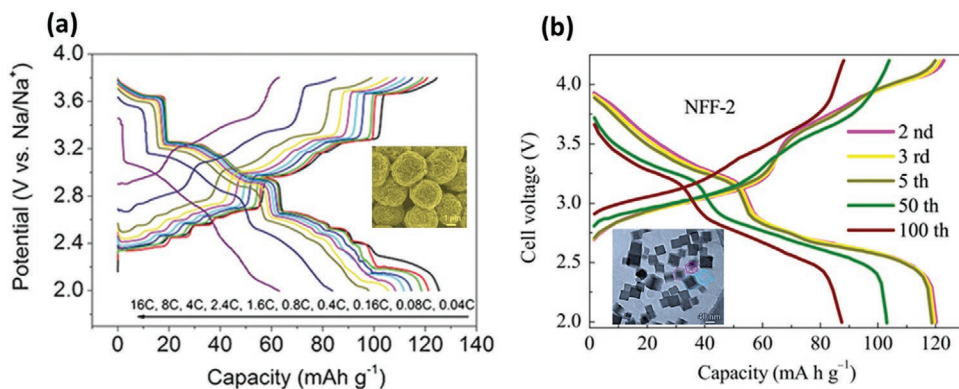


**Figure 17.** a) Charge/discharge voltage profiles of the s-NCO electrode at various current rates (inset shows the FESEM image of P2- $Na_{0.7}CoO_2$  microspheres). Reproduced with permission.<sup>[241]</sup> Copyright 2017, John Wiley and Sons. b) Charge and discharge curves at  $200 \text{ mA g}^{-1}$  (inset: TEM image) of  $Na_xFeFe(CN)_6$  nanocubes (NEF-2). Reproduced with permission.<sup>[242]</sup> Copyright 2015, Elsevier.

**Table 4.** Properties of selected high power cathodic materials for NIBs.

Cathode material	Maximum capacity [mAh g <sup>-1</sup> ]	Capacity @ high c-rate/mAh g <sup>-1</sup>	Capacity retention	Reference
Carbon quantum dot-coated VO <sub>2</sub> (C-VOCQD)	321 (0.3 C-rate) (1 C = 0.320 A g <sup>-1</sup> )	133 (60.0 C-rate)	81% after 200 cycles (@ 60.0 C)	[231]
Graphene quantum dots (GQDs) are coated onto the VO <sub>2</sub> (GVG)	306 (0.33 C-rate) (1 C = 0.300 A g <sup>-1</sup> )	93 (120.0 C-rate)	88% (111 mAh g <sup>-1</sup> ) after 1500 cycles (@ 60.0 C)	[232]
Single-crystalline bilayered V <sub>2</sub> O <sub>5</sub> nanobelts	235.7 (0.040 A g <sup>-1</sup> )	134 (0.640 A g <sup>-1</sup> )	170 mAh g <sup>-1</sup> after 100 cycles (@ 0.080 A g <sup>-1</sup> )	[233]
Orthorhombic V <sub>2</sub> O <sub>5</sub> hollow nanospheres	159.3 (0.040 A g <sup>-1</sup> )	112.4 (0.640 A g <sup>-1</sup> )	88% (109.5 mAh g <sup>-1</sup> ) after 100 cycles (@ 0.160 A g <sup>-1</sup> )	[234]
Nanoporous carbon-coated orthorhombic V <sub>2</sub> O <sub>5</sub> (V <sub>2</sub> O <sub>5</sub> -RFC)	170 (0.040 A g <sup>-1</sup> )	92 (0.640 A g <sup>-1</sup> )	140 mAh g <sup>-1</sup> after 70 cycles (@ 0.040 A g <sup>-1</sup> )	[235]
Rod-like Na <sub>0.44</sub> MnO <sub>2</sub>	124 (0.10 C-rate) (1 C = 0.120 A g <sup>-1</sup> )	80 (20.0 C-rate)	86% after 500 cycles (@ 20.0 C)	[237]
Na <sub>0.44</sub> MnO <sub>2</sub> nanoplates	112 (0.10 C-rate) (1 C = 0.120 A g <sup>-1</sup> )	96 (10.0 C-rate)	97.8% after 100 cycles (@ 0.5 C)	[239]
Na <sub>0.44</sub> MnO <sub>2</sub> nanofibers	128 (0.20 C-rate) (1 C = 0.121 A g <sup>-1</sup> )	70 (10.0 C-rate)	80 mAh g <sup>-1</sup> after 140 cycles (@ 0.42 C)	[239]
P2-Na <sub>0.7</sub> CoO <sub>2</sub> microspheres	125 (0.04 C-rate) (1 C = 0.125 A g <sup>-1</sup> )	64 (16.0 C-rate)	86% after 300 cycles (@ 0.4 C)	[241]
Na <sub>0.61</sub> Fe[Fe(CN) <sub>6</sub> ] <sub>0.94-0.06</sub> (HQ-NaFe)	170 (0.025 A g <sup>-1</sup> )	70 (0.600 A g <sup>-1</sup> )	170 mAh g <sup>-1</sup> after 150 cycles (@ 0.025 A g <sup>-1</sup> )	[251]
Na <sub>x</sub> FeFe(CN) <sub>6</sub> nanocubes	120.7 (0.2 A g <sup>-1</sup> )	73.6 (1.2 A g <sup>-1</sup> )	87.4 mAh g <sup>-1</sup> after 100 cycles (@ 0.2 A g <sup>-1</sup> )	[242]
Na <sub>1.72</sub> Mn[Fe(CN) <sub>6</sub> ] <sub>0.99</sub> ·2.0H <sub>2</sub> O (NMHFCs)	117 (0.1 C-rate) (1 C = 0.120 A g <sup>-1</sup> )	45 (40.0 C-rate)	121 mAh g <sup>-1</sup> after 30 cycles (@ 0.05 C)	[252]
Carbon-coated olivine NaFePO <sub>4</sub> (C-NaFePO <sub>4</sub> )	306 (0.33 C-rate) (1 C = 0.154 A g <sup>-1</sup> )	93 (120.0 C-rate)	90% after 100 cycles (@ 0.1 C)	[249]

Prussian blue analogues (PBAs, Na<sub>x</sub>M[Fe(CN)<sub>6</sub>]<sub>y</sub>·zH<sub>2</sub>O, M = Fe, Co, Mn, Ni, Cu, etc.; 0 < x < 2; 0 < y < 1) are a large family of transition metal hexacyanoferrates, and they are attracting an increasing interest as cathode materials for NIBs because of their high theoretical capacity, low cost, and ease of synthesis, as well as because of their (rigid) open framework, rich redox active, and structural stability. The 3D-diffusion channels and the weak interaction with the diffusing ions facilitates the transport of these latter through the material. Liu et al.<sup>[242]</sup> reported about an Na-rich Na<sub>x</sub>FeFe(CN)<sub>6</sub> nanocubes (NEF-2) able to deliver a capacity of 120 mA h g<sup>-1</sup> at a current density of 200 and 74 mA h g<sup>-1</sup> when the current density is increased to 1200 mA g<sup>-1</sup>. One of the main drawback of these materials is their limited thermal stability, which is hindering practical application.<sup>[226,229,243–245]</sup>

Polyanion-type compounds having robust 3D framework consist of a series of strongly covalently bonded polyanion units (XO<sub>4</sub>)<sup>n-</sup> (X = S, P, Si, etc.). Due to their structural stability, high safety, suitable high operating voltages, high thermal-abuse tolerance, and small volume change upon cycling are considered as interesting cathodic materials for NIBs.<sup>[227,246–248]</sup> Iron, vanadium, and manganese based polyanions are the commonly investigated cathodes for NIBs.

Olivine-type-structured NaMPO<sub>4</sub> (M = Fe, Mn) and NASICON-structured Na<sub>x</sub>M<sub>2</sub>(PO<sub>4</sub>)<sub>3</sub> (M = V, Ti) are the compounds that got greater attention as Na-ion battery cathode materials due to their good electrochemical properties. Zhu et al.<sup>[249]</sup> reported about carbon-coated triphylite NaFePO<sub>4</sub> showing improved electrochemical performance comparable to C-LiFePO<sub>4</sub>. Several works showed that Na<sub>3</sub>V<sub>2</sub>(PO<sub>4</sub>)<sub>3</sub>F<sub>2</sub> also is a promising cathode for NIBs.<sup>[227,247]</sup>

**Table 4** compares some properties of importance for high power applications of selected cathodic materials belonging to the families discussed above.<sup>[250–252]</sup>

The variation of the specific capacities at different current densities of the materials considered in Table 4 is compared in **Figure 18**. As shown, the cathodic materials of NIBs are able to deliver high specific capacity up to current densities which almost reach 50 A g<sup>-1</sup>. Presently, metal oxides appears more suited for high energy than for high power applications. Olivine-type structure, on the other hand, display a set of properties which make them very promising materials in view of the realization of high power NIBs. PBA also display interesting properties, but further investigation is needed to assess the use in real systems.

### 2.1.3. Potassium-Ion Batteries

As shown in Figure 3, the interest in KIBs increased considerably in the last 5 years. Potassium is very abundant, and it displays a low standard reduction potential ( $E_{K^+/K} = -2.93$  V vs SHE), which is allowing the realization of high voltage devices. As in the case of NIB, KIB also can be realized utilizing Al current collectors for both the cathode and the anode. Furthermore, it has been shown that K based electrolytes might display high conductivities which might be even higher than those of lithium and sodium electrolytes, for example, in the case of imide based salts. These properties are making potassium based systems very interesting in view of the realization of high power devices.<sup>[253–264]</sup>

**Anodic Materials for KIBs:** A wide variety of carbonaceous materials such as graphite, hard carbon, graphitizable soft carbon, doped carbons, carbon nanotube, have been considered and tested as negative electrodes for KIBs.

The insertion of potassium ions in graphite leads to the formation of KC<sub>8</sub>, corresponding to a theoretical capacity of

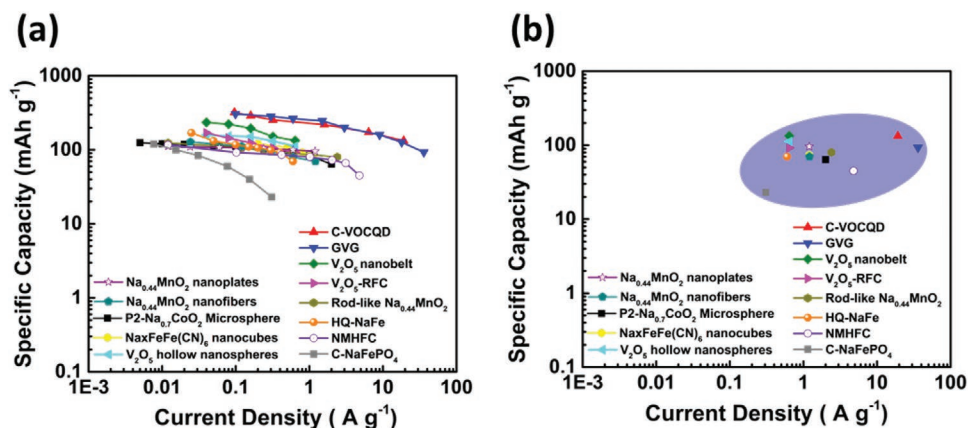


**Figure 18.** Comparison of a) rate capability at different current densities and b) achieved specific capacity at maximum current density of different cathodic materials for NIB (the marked area is giving a visual indication about the range of capacities and current densities achievable by these materials).

279 mAh g<sup>-1</sup> (assuming the full formation of KC<sub>8</sub>). Some studies indicated that the formation enthalpies of KC<sub>8</sub> (-16.5 kJ mol<sup>-1</sup>) is even more favorable than that of LiC<sub>6</sub> (-27.5 kJ mol<sup>-1</sup>).<sup>[265,266]</sup> Taking this point into account, the utilization of graphite in KIBs appears certainly less challenging than in NIBs. The potassium ion insertion in graphite in non-aqueous electrolyte was first demonstrated by Jian et al.,<sup>[259]</sup> which showed that graphite has a high reversible capacity of 273 mAh g<sup>-1</sup>.<sup>[257,267,268]</sup> More recently Cao et al.<sup>[269]</sup> showed that an HGCNC displays capacity of 175 mAh g<sup>-1</sup> at 35 C and shows promising cyclability (92% capacity retention after 100 cycles) (Figure 19).

Non-graphitizable hard carbon has been also considered as anode material for KIBs. Jian et al.<sup>[270]</sup> compared the electrochemical reaction of Na<sup>+</sup> and K<sup>+</sup> with hard carbon microsphere electrodes derived from sucrose. They showed that, thanks to the higher diffusion coefficient of K ions (compared to that of Na-ions) within its structure, this material is allowing a better high rate performance for KIBs than for NIBs. The same group also investigated hard-soft composite carbon, showing that this composite electrodes display capacity (80 mAh g<sup>-1</sup> at 10 C), higher rate capability, and very stable long-term cycling (93% of capacity retention after 200 cycles).<sup>[271]</sup> Ji's group<sup>[259]</sup>

investigated the use of soft carbon based electrode, and they showed that the use of this material allows significantly higher performance than graphite at high current density. As illustrate in Figure 20, during test carried out at 5 C the soft carbon electrode was able to deliver a capacity of more than 150 mAh g<sup>-1</sup>, while the graphite electrode was not able to display any significant capacity.<sup>[269,272]</sup>

Apart from the carbonaceous materials, potassium titanate (K<sub>2</sub>Ti<sub>4</sub>O<sub>9</sub>, K<sub>2</sub>Ti<sub>6</sub>O<sub>13</sub>, and K<sub>2</sub>Ti<sub>8</sub>O<sub>17</sub>) has been recently investigated as anodic materials for KIBs. Kishore et al.<sup>[273]</sup> reported for the first time the behavior of potassium tetratitanate (K<sub>2</sub>Ti<sub>4</sub>O<sub>9</sub>), synthesized by the solid state method using K<sub>2</sub>CO<sub>3</sub> and TiO<sub>2</sub>, showing that this material displays an initial capacity of 97 mAh g<sup>-1</sup> (theoretical capacity 129 mA h g<sup>-1</sup>). Dong et al.<sup>[274]</sup> reported the use of K<sub>2</sub>Ti<sub>6</sub>O<sub>13</sub> microscaffolds, demonstrating that this material displays excellent rate capability (57 mAh g<sup>-1</sup> at 1.0 A g<sup>-1</sup>). Han et al.,<sup>[275]</sup> showed that K<sub>2</sub>Ti<sub>8</sub>O<sub>17</sub> nanorods display a stable capacity exceeding 115 mAh g<sup>-1</sup> for 50 cycles.

Table 5 compares some properties of importance for high power applications of selected anodic materials belonging to the families discussed above.<sup>[276,277]</sup>

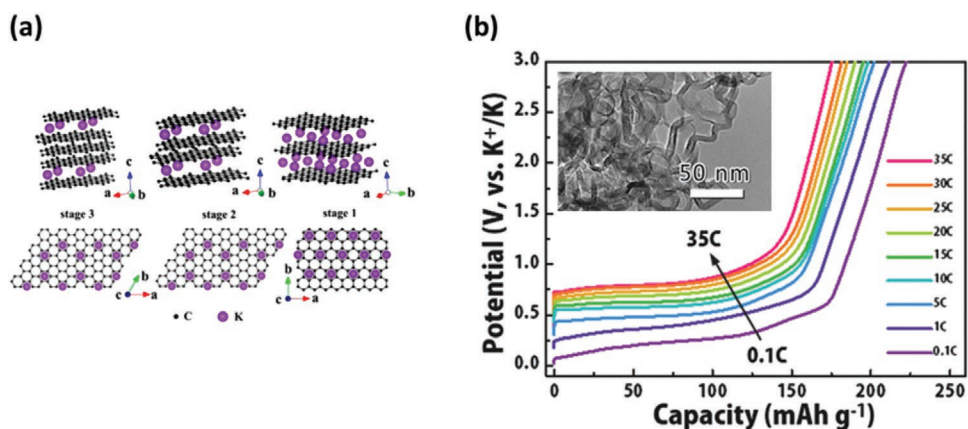


**Figure 19.** a) Structure diagrams of different K-GICs, side view (top row) and top view (bottom row). Reproduced with permission.<sup>[259]</sup> Copyright 2015, American Chemical Society. b) Voltage profiles at different depotassiation rates of CNC electrode (inset: HRTEM image of CNC electrode after depotassiation at the high rate of 35 C). Reproduced with permission.<sup>[269]</sup> Copyright 2018, John Wiley and Sons.

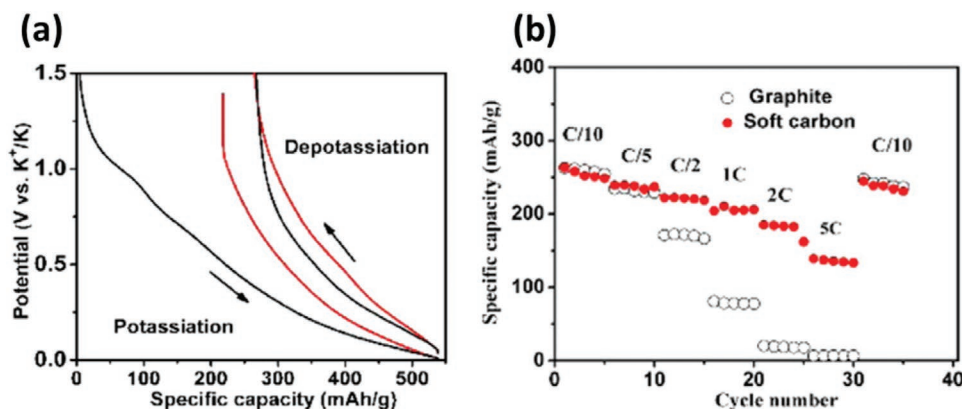


**Figure 20.** a) Voltage profiles in the potential range between 0.01 and 1.5 V at C/40 and b) capacity retention at different C-rates of soft carbon electrodes. Reproduced with permission.<sup>[259]</sup> Copyright 2015, American Chemical Society.

The variation of the specific capacities at different current densities of the materials considered in Table 5 is compared in Figure 21. As shown, the anodic material of KIBs are able to deliver high specific capacity up to current densities of maximum 10 A g<sup>-1</sup>. Similarly to NIBs, in KIBs also hard carbon and titanium based anodes appears as promising candidates. However, for both anodic materials further efforts appears necessary in order to achieve the stability required for high power applications.

**Cathodic Materials for KIBs:** In the last years many efforts have been dedicated toward the development of high performance cathodes for KIB. Layer-type structures have been one of the most investigated class of materials.<sup>[256]</sup> The typical layered oxide materials can be represented as K<sub>x</sub>MO<sub>2</sub> (M = Mn, Fe, and Co) and it is important to notice that, in contrast to the Li and Na systems, the voltage curves of the K-layered compounds (e.g., K<sub>x</sub>MO<sub>2</sub>) are steeper due to the large K<sup>+</sup>-ion size.<sup>[278,279]</sup> Vaalma et al.<sup>[280]</sup> demonstrated the K-ion storage property of a layered birnessite K<sub>0.3</sub>MnO<sub>2</sub>, and showed that this material can deliver a reversible capacities of ≈70 mA h g<sup>-1</sup> in the voltage range of 1.5–3.5 V. Wang et al.<sup>[281]</sup> synthesized K<sub>0.7</sub>Mn<sub>0.5</sub>Fe<sub>0.5</sub>O<sub>2</sub> nanowire, showing that these cathodic materials exhibit a high specific capacity (114 mA h g<sup>-1</sup> at 100 mA g<sup>-1</sup>) in the voltage range of 1.5–4.0 V versus K/K<sup>+</sup>.

Prussian blue analogues (PBAs) having the composition of K<sub>x</sub>M<sub>A</sub>[M<sub>B</sub>(CN)<sub>6</sub>]<sub>1-δ</sub>·nH<sub>2</sub>O, (0 ≤ x ≤ 2) received considerable attention as K-ion intercalation cathode material due to their long cycle life, scalability, easiness of synthesis, etc.<sup>[282,283]</sup> Eftekhari et al.<sup>[284]</sup> reported the first use of KFe[Fe(CN)<sub>6</sub>] as cathode of KIBs utilizing a non-aqueous electrolyte (1 M KBF<sub>4</sub> in 3:7 EC/EMC). Afterward, several studies explored the use of PBAs as cathodic materials for KIBs. Bie et al.<sup>[285]</sup> reported the use of K<sub>1.75</sub>Mn[FeII(CN)<sub>6</sub>]<sub>0.93</sub>·0.16H<sub>2</sub>O (K-MnHCFE) showing that this material delivers a capacity of 141 mA h g<sup>-1</sup> (with an average operating potential of 3.8 V vs K/K<sup>+</sup>) and it is able to maintain a capacity of 108 mAh g<sup>-1</sup> during tests at 1 A g<sup>-1</sup> (Figure 22).

Polyanionic compounds such as phosphates, pyrophosphates, fluorophosphates, sulfates have been also considered as potential cathodic materials for KIBs.<sup>[286–288]</sup> The K<sub>3</sub>V<sub>2</sub>(PO<sub>4</sub>)<sub>2</sub>F<sub>3</sub> developed by Lin et al.<sup>[289]</sup> delivered a capacity of 104 mA h g<sup>-1</sup> at 10 mA g<sup>-1</sup> and maintains a higher capacity of 50 mA h g<sup>-1</sup> at higher rate of 500 mA g<sup>-1</sup>. It also shows a good stability of 95% (90 mA h g<sup>-1</sup>) after 180 cycles at 0.02 A g<sup>-1</sup> (Figure 23).

Also organic compounds have been considered as cathodic materials for KIB due to their flexible structures and low cost.<sup>[286]</sup> Xing et al.<sup>[290]</sup> reported for the first time reported the use of the organic compounds 3,4,9,10-perylene-tetracarboxylic

**Table 5.** Properties of selected high power anodic materials for KIBs.

Anode material	Maximum capacity [mAh g <sup>-1</sup> ]	Capacity @ high c-rate/mAh g <sup>-1</sup>	Capacity retention	Reference
Expanded graphite	263 (0.01 A g <sup>-1</sup> )	175 (0.2 A g <sup>-1</sup> )	174 mA h g <sup>-1</sup> after 500 cycles (@ 0.02 A g <sup>-1</sup> )	[268]
Hard carbon microspheres (HCS)	262 (0.1 C-rate) (1 C = 0.279 A g <sup>-1</sup> )	136 (5.0 C-rate)	83% (216 mA h g <sup>-1</sup> ) after 100 cycles (@ 0.1 C)	[270]
Hard–soft composite carbon (HCS-SC)	260 (0.1 C-rate) (1 C = 0.279 A g <sup>-1</sup> )	81 (10.0 C-rate)	93% (200 mA h g <sup>-1</sup> ) after 200 cycles (@ 1.0 C)	[271]
Nitrogen-doped carbon nanofibers (NCNF-650)	238 (0.1 A g <sup>-1</sup> )	101 (20 A g <sup>-1</sup> )	146 mA h g <sup>-1</sup> after 4000 cycles (@ 2.0 A g <sup>-1</sup> )	[272]
Graphitic carbon nanocage (CNC)	221 (0.1 C-rate) (1 C = 0.279 A g <sup>-1</sup> )	40 (5.0 C-rate)	92% (195 mA h g <sup>-1</sup> ) after 100 cycles (@ 0.2 C)	[269]
Nitrogen-doped carbon nanotubes (NCNTs)	282 (0.02 A g <sup>-1</sup> )	102 (2.0 A g <sup>-1</sup> )	77.86% (102 mA h g <sup>-1</sup> ) after 500 cycles (@ 2.0 A g <sup>-1</sup> )	[277]
K <sub>2</sub> Ti <sub>4</sub> O <sub>9</sub>	97 (0.03 A g <sup>-1</sup> )	20 (2.0 A g <sup>-1</sup> )	80 mA h g <sup>-1</sup> after 10 cycles (@ 0.03 A g <sup>-1</sup> )	[273]
Potassium titanate (M-KTO, K <sub>2</sub> Ti <sub>4</sub> O <sub>9</sub> )	150 (0.02 A g <sup>-1</sup> )	81 (0.3 A g <sup>-1</sup> )	61% after 100 cycles (@ 0.05 A g <sup>-1</sup> )	[276]
K <sub>2</sub> Ti <sub>6</sub> O <sub>13</sub> microscaffolds	95 (0.02 A g <sup>-1</sup> )	64 (0.5 A g <sup>-1</sup> )	85% (59 mA h g <sup>-1</sup> ) after 1000 cycles (@ 0.5 A g <sup>-1</sup> )	[274]
K <sub>2</sub> Ti <sub>8</sub> O <sub>17</sub> nanorods	181.5 (0.02 A g <sup>-1</sup> )	44.2 (0.5 A g <sup>-1</sup> )	110.7 mA h g <sup>-1</sup> after 50 cycles (@ 0.02 A g <sup>-1</sup> )	[275]

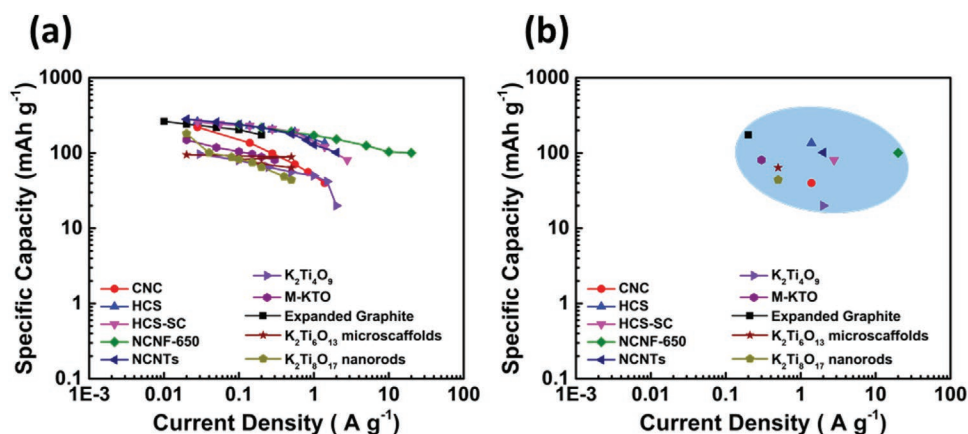


**Figure 21.** Comparison of a) rate capability at different current densities and b) achieved specific capacity at maximum current density of different anodic materials for KIB (the marked area is giving a visual indication about the range of capacities and current densities achievable by these materials).

acid-dianhydride (PTCDA), and showed that this material can deliver a capacity of 122 mAh g<sup>-1</sup> at 20 mA g<sup>-1</sup> and exhibits acceptable cycling stability.

**Table 6** compares some properties of importance for high power applications of selected cathodic materials belonging to the families discussed above.<sup>[291–293]</sup>

The variation of the specific capacities at different current densities of the materials considered in **Table 6** is compared in **Figure 24**. As shown, the cathodic materials of KIBs are able to deliver high specific capacity up to current densities of maximum 5 A g<sup>-1</sup>. So far, PBAs and polyanionic compounds appear as the most promising cathodic materials, but further efforts are certainly needed to improve their performance, especially in terms of cyclic stability.

## 2.2. Comparison of the High Power Performance of Materials for LIBs, NIBs, and KIBs

**Figure 25** compares the achieved specific capacity of the anodic (a) and cathodic (b) materials of LIB, NIB, and KIB, at maximum current density, which have been considered in the previous sessions.

As shown, the anodic materials of LIBs can be efficiently utilized with current densities reaching 50 A g<sup>-1</sup>. These

values of currents are presently higher than those possible for NIBs and, especially, for KIBs. Overall, carbonaceous materials appear as the most promising for high power applications. While graphite seems to be promising for KIBs, its use in high power NIBs seems to be more problematic. On the other hand, hard carbons appear at the moment as the most performing anodic materials for these types of metal-ion batteries. Titanium based anode are also very interesting for high power LIBs and NIBs. Their use in KIBs, although promising, need to be further investigated. The lower operative voltage of the devices containing these anodes, however, might have a negative impact on their overall energy and power.

In the case of cathodic materials the situation appears different. As show in **Figure 25b**, the high power performance of the materials suitable for LIBs and NIBs appears rather comparable, and they can be efficiently utilized up to 50 A g<sup>-1</sup>. The performance of the materials suitable for KIBs still need to be improved, as at the moment the power output of these materials is much lower (of the order of 1–2 A g<sup>-1</sup>). Among the investigated materials, nanosized iron and vanadium phosphate within a carbon matrix appears as promising for the realization of MIBs.

Taking this result into account, the high power performance of the materials for NIBs and KIBs can be considered overall

**Table 6.** Properties of selected high power cathodic materials for KIBs.

Cathode material	Maximum capacity [mAh g <sup>-1</sup> ]	Capacity @ high c-rate/mAh g <sup>-1</sup>	Capacity retention	Reference
K <sub>0.3</sub> MnO <sub>2</sub>	70 (0.1 C-rate) (1 C = 0.279 A g <sup>-1</sup> )	≈42 (5.0 C-rate)	68% after 620 cycles (@ 0.1 C)	[280]
K <sub>0.7</sub> Mn <sub>0.5</sub> Fe <sub>0.5</sub> O <sub>2</sub> nanowire	114 (0.1 A g <sup>-1</sup> )	57 (1.0 A g <sup>-1</sup> )	≈87% after 450 cycles (@ 1.0 A g <sup>-1</sup> )	[281]
P2-type K <sub>0.6</sub> CoO <sub>2</sub>	78 (0.002 A g <sup>-1</sup> )	43 (0.15 A g <sup>-1</sup> )	≈60% after 120 cycles (@ 0.1 A g <sup>-1</sup> )	[291]
K <sub>0.220</sub> Fe[Fe(CN) <sub>6</sub> ] <sub>0.805</sub> ·4.01H <sub>2</sub> O nanoparticles	74.5 (0.05 A g <sup>-1</sup> )	36 (0.4 A g <sup>-1</sup> )	44.7 mAh g <sup>-1</sup> after 150 cycles (@ 0.3 A g <sup>-1</sup> )	[292]
K <sub>1.75</sub> Mn[FeI(CN) <sub>6</sub> ] <sub>0.93</sub> ·0.16H <sub>2</sub> O (K-MnHCFe)	137 (0.03 A g <sup>-1</sup> )	108 (1.0 A g <sup>-1</sup> )	≈130 mAh g <sup>-1</sup> after 100 cycles (@ 0.03 A g <sup>-1</sup> )	[285]
K <sub>3</sub> V <sub>2</sub> (PO <sub>4</sub> ) <sub>3</sub> /C	54 (0.02 A g <sup>-1</sup> )	23 (0.2 A g <sup>-1</sup> )	52 mAh g <sup>-1</sup> after 100 cycles (@ 0.02 A g <sup>-1</sup> )	[293]
K <sub>3</sub> V <sub>2</sub> (PO <sub>4</sub> ) <sub>2</sub> F <sub>3</sub>	104 (0.01 A g <sup>-1</sup> )	20 (0.5 A g <sup>-1</sup> )	95% (90 mAh g <sup>-1</sup> ) after 180 cycles (@ 0.02 A g <sup>-1</sup> )	[289]
PTCDA	122 (0.02 A g <sup>-1</sup> )	56 (0.2 A g <sup>-1</sup> )	63 mAh g <sup>-1</sup> after 300 cycles (@ 0.01 A g <sup>-1</sup> )	[290]

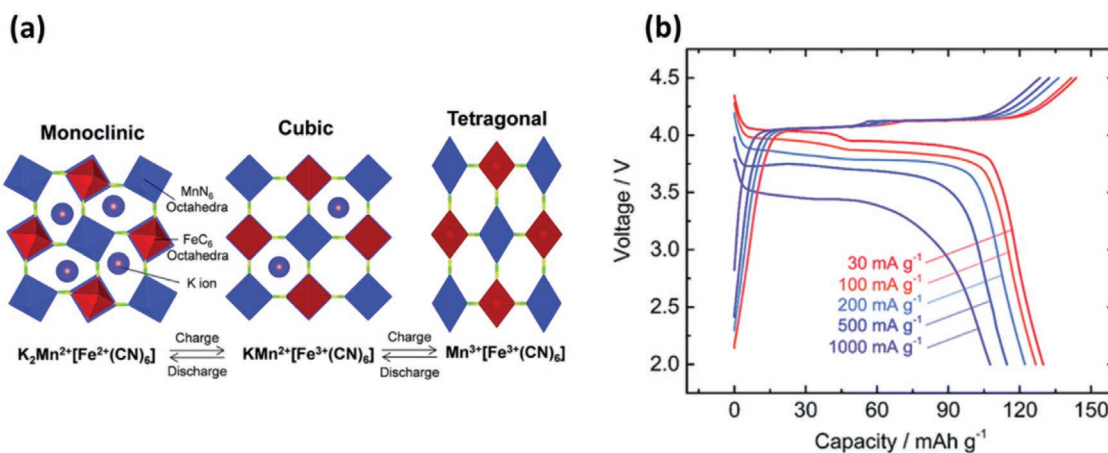


**Figure 22.** a) Crystal structures and phase transition observed by electrochemical potassium extraction (charging) and insertion (discharging) and b) discharge rate capability of K-MnHCFe in a K half-cell at current densities from 30 to 1000 mA g<sup>-1</sup> after the electrodes are charged at a low current rate of 30 mA g<sup>-1</sup>. Reproduced with permission.<sup>[285]</sup> Copyright 2017, Royal Society of Chemistry.

already promising. Since these technologies are younger compared to LIBs, it is reasonable to suppose that this performance will further improve in the near future.

### 2.3. Materials for Electrochemical Capacitors

Electrochemical capacitors are the devices of selection for a large number of high power applications. These devices are commercially available and their market, although smaller than that of LIBs, increased continuously in the last years.<sup>[3]</sup> It has been forecast that this trend will continue also in the next years.

#### 2.3.1. Carbonaceous Materials for Capacitive Storage

Carbonaceous materials are the most utilized materials for the realization of energy storage devices relying on physical storage process. Activated carbon (AC) are the state-of-the-art active materials for EDLCs, but in the last years several other carbonaceous materials, for example, graphene, have been widely investigated.<sup>[294,295]</sup> Table 7 compares several properties of

interest for high performance for some selected carbonaceous materials in aqueous and organic electrolytes. It is important to remark that the capacity of these materials depends on the voltage excursion at which they are subjected to during their use in energy storage devices. Typically, the capacity of an AC is estimated to be of the order of 30 mAh g<sup>-1</sup>.<sup>[296]</sup>

The variation of the specific capacities at different current densities of the materials considered in Table 7 is compared in Figure 26.<sup>[297–302]</sup> As shown, these are able to deliver a constant specific capacity up to current densities exceeding 100 A g<sup>-1</sup>, indicating that these materials are perfectly suited for high power application.

#### 2.3.2. Pseudocapacitive Materials

Pseudocapacitive materials exhibiting linear or almost linear charge/discharge profile with no prominent flat plateau and shows nearly overlapped and broad redox peaks in cyclic voltammogram. The pseudocapacitive property was first observed in RuO<sub>2</sub> material by Trasatti group in 1970s.<sup>[303]</sup> In the following years, a very large amount of studies have been dedicated to these kinds of materials. Depending on their nature and their structure, the pseudocapacitive materials can be classified into

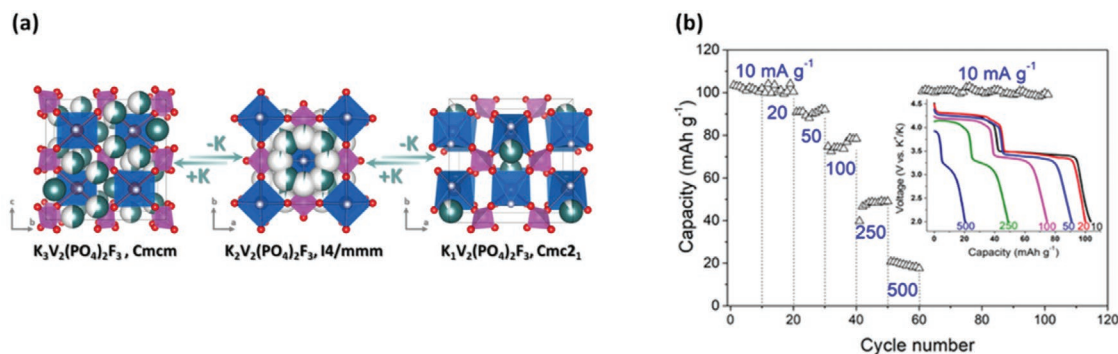


**Figure 23.** a) Phase transformation during K ion insertion and extraction in K<sub>3</sub>V<sub>2</sub>(PO<sub>4</sub>)<sub>2</sub>F<sub>3</sub> and b) rate capability study at different current densities. Reproduced with permission.<sup>[289]</sup> Copyright 2019, Elsevier.

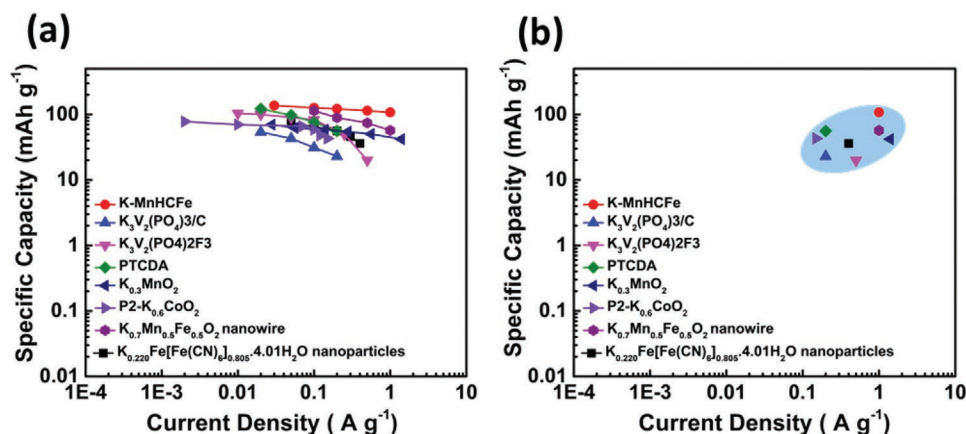


**Figure 24.** Comparison of a) rate capability at different current densities and b) achieved specific capacity at maximum current density, of different cathode materials for KIB (the marked area is giving a visual indication about the range of capacities and current densities achievable by these materials).

two groups: i) intrinsic pseudocapacitors and ii) extrinsic pseudocapacitors.<sup>[33]</sup> In the last years several efforts have been dedicated to understanding of the faradaic and capacitive contributions of pseudocapacitive materials, and it has been shown that the entity of these two contributions depend on several parameters related to the electrode materials, for example, crystallinity and morphology, and on the nature of the electrolyte.<sup>[27,304–308]</sup>

Intrinsic pseudocapacitor materials display the typical characteristics of capacitive charge storage in a wide range of particle dimension and morphology regardless of their crystalline property. Two of the most investigated materials within this class are  $\text{MnO}_2$  and  $\text{Nb}_2\text{O}_5$ . In the last 10–25 years a very large number of studies have been dedicated to the influence of the structural and morphological properties of  $\text{MnO}_2$  on its electrochemical performance.<sup>[309]</sup> Among them, those of Brousse and Belanger appears nowadays as a reference for the community working on this material.<sup>[310–319]</sup> The interest in  $\text{Nb}_2\text{O}_5$  has increased after Dunn’s group has showed that orthorhombic T- $\text{Nb}_2\text{O}_5$  undergoes fast faradaic intercalation pseudocapacitance even in the bulk electrode showing very high rate performance (40  $\text{mAh g}^{-1}$  at 1000 C-rates).<sup>[18,28,33,320–324]</sup> After this, pioneering works have been dedicated to further improve the electrochemical behavior of this type of materials.<sup>[325–327]</sup>

MXenes are a novel family of 2D early transition metal carbides and carbonitrides, which are produced by selective etching of the A element from MAX phases.<sup>[328–331]</sup> MXenes display excellent electronic conductivity and, thanks to their tunable 2D structure, they also guarantee a fast ion transport and high surface accessibility to electrolyte ion. Additionally, the presence of an active redox metallic center (M) made MXene promising electrode materials for energy storage devices.<sup>[332–343]</sup>

**Figure 27** compares the number of publications dedicated to the use of this new class of materials in supercapacitors with that dealing with AC. As shown, MXenes are nowadays one of the most investigated class of materials for supercapacitors.

These works showed that MXenes display excellent performance, in terms of capacitance and capacitance retention, in aqueous electrolytes.<sup>[332,344–346]</sup> It has been reported, for example, that macroporous  $\text{Ti}_3\text{C}_2\text{T}_x$  MXene film exhibits a capacitance of  $210 \text{ F g}^{-1}$  at a very high scan rate of  $10 \text{ V s}^{-1}$  in an aqueous  $\text{H}_2\text{SO}_4$  electrolyte, and that MXene hydrogel electrodes reach to record values of  $1500 \text{ F cm}^{-3}$ .<sup>[346]</sup> Their use in non-aqueous electrolytes appears, however, more difficult. Although encouraging results have been recently obtained, the use of MXenes based electrode in these electrolytes appears therefore as the main challenge related to the use of this new class of materials in high power

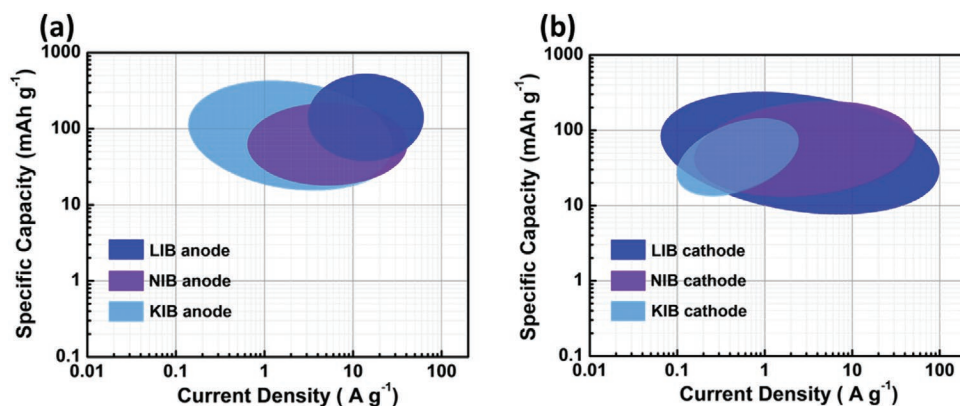


**Figure 25.** Comparison of the achieved specific capacity of a) anodic and b) cathodic materials of LIBs, NIBs, and KIBs at maximum current density (the marked area is giving a visual indication about the range of capacities and current densities achievable by these materials).

**Table 7.** Properties of selected capacitive materials for supercapacitors.

Material	Maximum capacity [mAh g <sup>-1</sup> ]	Capacity @ high c-rate/mAh g <sup>-1</sup>	Capacity retention	Reference
Aqueous electrolytes				
3D interconnected porous carbons (IPCs) from MOF-5 (IPC <sub>3-M</sub> )	≈30 (0.05 A g <sup>-1</sup> )	≈25 (20.0 A g <sup>-1</sup> )	95.9% after 1000 cycles	[297]
CFAC-800-5.5K	≈32 (0.1 A g <sup>-1</sup> ) (288 F g <sup>-1</sup> )	≈29 (30.0 A g <sup>-1</sup> ) (260 F g <sup>-1</sup> )	98.5% after 10 000 cycles (@ 1.0 A g <sup>-1</sup> )	[298]
N-doped porous CNF (N-CNFs-900)	≈28 (1.0 A g <sup>-1</sup> ) (202 F g <sup>-1</sup> )	≈23 (30.0 A g <sup>-1</sup> ) (164.5 F g <sup>-1</sup> )	97% (195.9 F g <sup>-1</sup> ) after 3000 cycles (@ 1.0 A g <sup>-1</sup> )	[299]
Hierarchical porous carbon (HPC)	≈26 (0.05 A g <sup>-1</sup> ) (185 F g <sup>-1</sup> )	≈18 (100.0 A g <sup>-1</sup> ) (130 F g <sup>-1</sup> )		[300]
Non-aqueous electrolytes				
Nitrogen-doped and activated CNTs (NA-CNTs)	≈48 (1.0 A g <sup>-1</sup> ) (98 F g <sup>-1</sup> )	≈21 (30.0 A g <sup>-1</sup> ) (42 F g <sup>-1</sup> )	91% after 10 000 cycles (@ 3.0 A g <sup>-1</sup> )	[301]
Oligomer-derived carbon (ODC)	≈37 (1.0 A g <sup>-1</sup> ) (105 F g <sup>-1</sup> )	≈21 (10.0 A g <sup>-1</sup> ) (60 F g <sup>-1</sup> )	90% after 5000 cycles (@ 4.0 A g <sup>-1</sup> )	[302]

devices. Very recently it has been shown that the redox-controlled A-site etching of MAX phases in Lewis acidic melts can be a successful strategy to overcome this challenge and to fully exploit the capacity of these materials on non-aqueous electrolytes.<sup>[347]</sup>

Extrinsic pseudocapacitors materials varies their pseudocapacitive nature depending on the particle size and morphology. These materials undergo phase transformation in their bulk state during ion storage, and gradually changes to capacitive storage while bringing down to the nanometer dimension.<sup>[348]</sup> Due to the increased surface area and the decrease in diffusion distances at the nanometer scale, these materials, for example, V<sub>2</sub>O<sub>5</sub>, exhibit high rate capability.<sup>[30]</sup>

**Table 8** compares some properties of importance of high power applications for selected pseudocapacitive materials belonging to the families discussed above.

The variation of the specific capacities at different current densities of the materials considered in Table 8 is compared in **Figure 28**.<sup>[349–359]</sup> As shown, these are able to deliver a constant specific capacity up to current densities exceeding 100 A g<sup>-1</sup>, indicating that pseudocapacitive materials are perfectly applicable in high power devices.

## 2.4. Materials for Hybrid Systems

In order to overcome the limitations of metal-ion batteries (in terms of power) and supercapacitors (in terms of energy) the

realization of hybrid devices, in which faradaic and non-faradaic storage process are simultaneously utilized, is a viable strategy.<sup>[360]</sup> The first LIC were developed by Amatucci et al.<sup>[361]</sup> by combining an LTO as negative electrode with an AC positive electrode working in a conventional electrolyte for LIBs. After this pioneering study, a large number of works have been dedicated to these hybrid devices.<sup>[362]</sup> **Figure 29** shows the number of publications dedicated to metal-ion capacitors over the last 15 years (from 2005 till 2020).

The HICs can be classified into type I and type II based on their cell configurations. In type I HIC, a battery type anode (negative electrode) is combined with a capacitive electrode (positive electrode) (e.g., graphite/activated carbon) (**Figure 30a**). During charging, the cations from the electrolyte intercalate into the active material of the negative electrode whereas the anions adsorb on the surface of a highly porous carbon positive electrode. Since the battery material operates (via intercalation/deintercalation) at the low potential, a typical signature of flat potential plateau (blue curve) can be seen in the charge–discharge profile (**Figure 30c**) and the voltage profile (**Figure 30e**). The capacitive carbon undergoes anion adsorption/desorption during charging/discharging, showing the typical signature of triangular curve (red curve) varies in a potential range of E<sub>c1</sub> to E<sub>c2</sub>. The upper potential of the carbon material is limited due to the oxidative decomposition of the electrolyte (**Figure 30e**). Due to the flat stable potential of the negative electrode and the triangular potential profile at the positive electrode, the HIC behaves in a supercapacitor manner

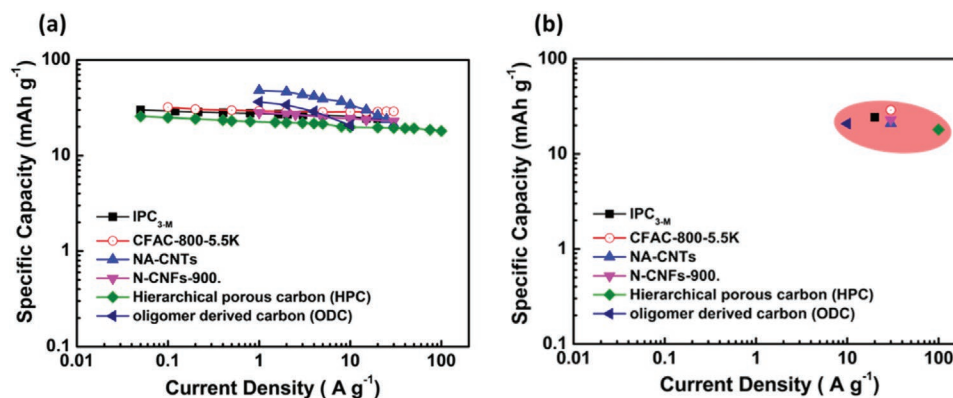


**Figure 26.** Comparison of a) rate capability at different current densities and b) achieved specific capacity at maximum current density, of different double layer capacitive materials (the marked area is giving a visual indication about the range of capacities and current densities achievable by these materials).



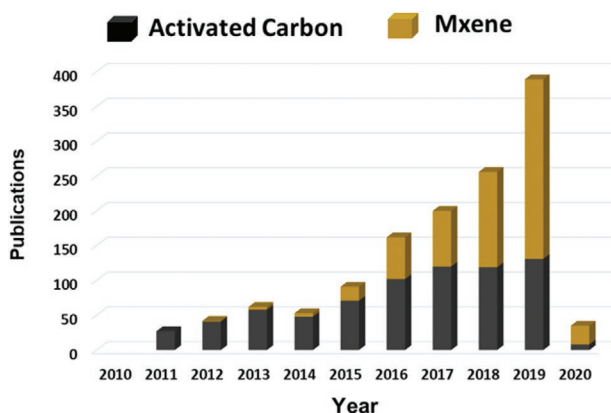


**Figure 27.** Number of publications dedicated to MXene and activated carbon from 2010 to 2020, data from Web of Science (February 2020).

where the potential varies in a triangular way between the lowest cell voltage of  $E_{c1}-E_b$  and highest cell voltage of  $E_{c2}-E_b$ .

Type II HIC consists on the combination of a capacitive negative electrode with a battery cathode (positive electrode) (e.g., activated Carbon/LFP) (Figure 30b). In this case, during the charging process the cations deintercalate from the positive electrode into the electrolyte, whereas simultaneous cation adsorption happens at the surface of the negative electrode. An idealized schematic charge–discharge profile of the battery cathode with flat potential (blue curve) and capacitive negative electrode having the typical triangular potential profile (red curve) is shown in Figure 30d.

In both types of HICs, the capacitive carbon electrode (positive electrode in type I and negative electrode in type II) is the limiting factor determining the operative voltage and hence the

energy density of the device. Since the electrodes are connected in series, the overall capacity is limited by the less capacitive carbon material, and a correct mass balancing is absolutely needed to maximize the energy density.

#### 2.4.1. Materials for Lithium-Ion Capacitors

The most investigated LIC relies on the combination of a negative electrode based on graphite with a positive electrode based on AC. This electrode combination allows the realization of devices with operative voltage of 4 V. In the last years several works have been dedicated to these devices. The Beguin's group extensively investigated the influence of operating potential and mass loading of the electrodes in AC/graphite. They showed that a maximum energy density of  $140 \text{ Wh kg}^{-1}$  (at  $64 \text{ W kg}^{-1}$  at the lab scale level, considering only the electrode material) can be obtained in a wide potential window of 1.5–5.0 V. However this high operative voltage is limiting the cycling stability, which can be improved by cycling the system at maximum 4.5 V.<sup>[363]</sup> Sivakumar and Pandolfo<sup>[364]</sup> showed the importance and the impact of prelithiation process on the graphite electrode, which is needed to introduce lithium into the device and to generate a uniform SEI layer on the surface of the negative electrode of LIC.

Due to the fact that lithium ions are inserted in graphite through a multistage process, the use of this carbonaceous material might impact the performance at high current density of LIC.<sup>[73]</sup> For this reason hard and soft carbons have been widely investigated as alternative to graphite. Cao et al.<sup>[365]</sup> fabricated LIC by using the stabilized lithium metal powders over the surface of the hard carbon electrodes (without prelithiation of the negative electrodes) in combination with AC positive electrode

**Table 8.** Properties of selected pseudocapacitive materials for supercapacitors.

Anode material	Maximum capacity [mAh g <sup>-1</sup> ]	Capacity @ high c-rate/mAh g <sup>-1</sup>	Capacity retention	Ref.
Non-aqueous electrolytes				
T-Nb <sub>2</sub> O <sub>5</sub>	140 (1.0 C-rate) (1 C = 0.201 A g <sup>-1</sup> )	40 (1000.0 C-rate)	100% after 1000 cycles	[18]
Mesoporous Nb <sub>2</sub> O <sub>5</sub> /carbon (m-Nb <sub>2</sub> O <sub>5</sub> @C)	184 (0.01 A g <sup>-1</sup> )	115.1 (5.0 A g <sup>-1</sup> )	80% (195 mAh g <sup>-1</sup> ) after 4000 cycles (@ 2.0 A g <sup>-1</sup> )	[327]
Nb <sub>2</sub> O <sub>5</sub> @carbon core–shell nanocrystals (TNb <sub>2</sub> O <sub>5</sub> @CNCs)	180 (0.05 A g <sup>-1</sup> )	90 (5.0 A g <sup>-1</sup> )		[349]
Nb <sub>2</sub> O <sub>5</sub> /HGF	184 (1.0 C-rate) (1 C = 0.201 A g <sup>-1</sup> )	85 (100.0 C-rate)	90% (125 mAh g <sup>-1</sup> ) after 10 000 cycles (@ 10 C-rate)	[325]
Porous TiO <sub>2</sub> (B) nanosheets (TiO <sub>2</sub> (B)-BH)	278 (0.25 C-rate) (1 C = 0.335 A g <sup>-1</sup> )	159 (20.0 C-rate)	100% (186.8 mAh g <sup>-1</sup> ) after 1000 cycles (@ 5 C-rate)	[350]
H <sub>2</sub> Ti <sub>3</sub> O <sub>7</sub> nanowires	≈190 (1.0 A g <sup>-1</sup> )	≈100 (40.0 A g <sup>-1</sup> )	100 mAh g <sup>-1</sup> after 200 cycles (@ 40.0 A g <sup>-1</sup> )	[351]
V <sub>2</sub> O <sub>5</sub> /mesoporous carbon (V <sub>2</sub> O <sub>5</sub> /mc)	184 (0.10 A g <sup>-1</sup> )	68 (5.0 A g <sup>-1</sup> )	60% (163 mAh g <sup>-1</sup> ) after 100 cycles (@ 0.5 A g <sup>-1</sup> )	[352]
Nanocrystalline LiCoO <sub>2</sub>	120 (1.0 C-rate) (1 C = 0.137 A g <sup>-1</sup> )	75 (100.0 C-rate)	75% after 20 cycles (@ 10.0 C)	[143]
MoS <sub>2</sub> nanoparticles	182 (1.0 C-rate) (1 C = 0.167 A g <sup>-1</sup> )	91 (100.0 C-rate)	70% after 3000 cycles (@ 20 C-rate)	[353]
R-MoO <sub>3-x</sub>	270 (1 mVs <sup>-1</sup> )	150 (100 mVs <sup>-1</sup> )	95% after 50 cycles (@ 10 mV s <sup>-1</sup> )	[354]
Aqueous electrolytes				
RuO <sub>2</sub> /G	≈157 (0.1 A g <sup>-1</sup> ) (565 F g <sup>-1</sup> )	≈126 (20.0 A g <sup>-1</sup> ) (455 F g <sup>-1</sup> )	80% after 5000 cycles (@ 1.0 A g <sup>-1</sup> )	[355]
K <sup>+</sup> -inserted α-MnO <sub>2</sub> (or K <sub>x</sub> MnO <sub>2</sub> ) nanorod arrays	≈87 (1.0 A g <sup>-1</sup> ) (260 F g <sup>-1</sup> )	≈38 (20.0 A g <sup>-1</sup> ) (115 F g <sup>-1</sup> )	95% after 5000 cycles (@ 4.0 A g <sup>-1</sup> )	[356]
MnO <sub>2</sub> /CNTs	≈50 (1.0 A g <sup>-1</sup> ) (201 F g <sup>-1</sup> )	≈35 (20.0 A g <sup>-1</sup> ) (140 F g <sup>-1</sup> )	100% after 10 000 cycles (@ 1.0 A g <sup>-1</sup> )	[357]
Ti <sub>3</sub> C <sub>2</sub> T <sub>x</sub>	110 (2 mVs <sup>-1</sup> )	63 (1000 mVs <sup>-1</sup> )	98% after 10 000 cycles (@ 1.0 A g <sup>-1</sup> )	[358]
LaMnO <sub>3-x</sub>	200 (1 mVs <sup>-1</sup> )	127 (100 mVs <sup>-1</sup> )		[359]

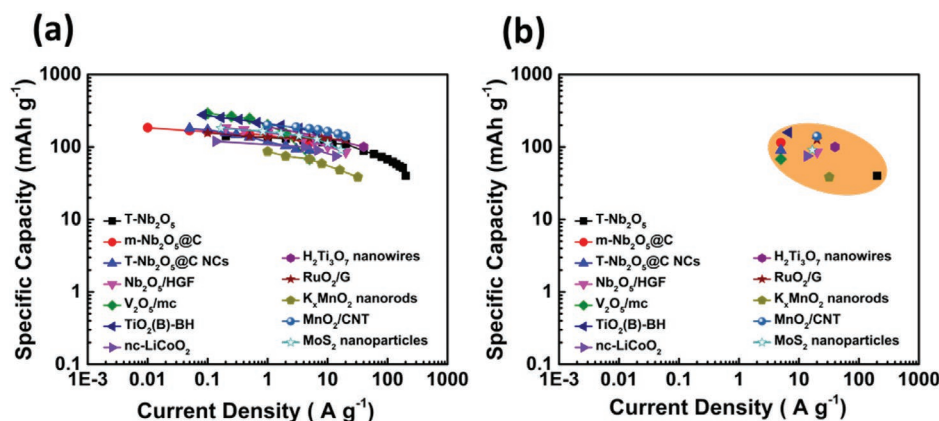


**Figure 28.** Comparison of a) rate capability at different current densities and b) achieved specific capacity at maximum current density of different pseudocapacitive materials (the marked area is giving a visual indication about the range of capacities and current densities achievable by these materials).

showing that these devices can deliver high energy density ( $\approx 80 \text{ Wh kg}^{-1}$  in lab cell) and retaining 60% of their maximum energy at a high discharge C-rate of 44 C. Schroeder et al.<sup>[366]</sup> investigated the use of soft carbon (PeC), as negative electrode for LIC. They showed that PeC based LICs deliver a specific energy and power of  $48 \text{ Wh kg}^{-1}$  and  $9 \text{ kW kg}^{-1}$ , respectively, at a high current density of  $4.5 \text{ A g}^{-1}$  (corresponding to 30 C) in a potential range of 0–4.0 V and maintains a high stability of 50 000 cycles.

On the other hand, research activities have been directed toward the improvement of the positive electrode of this kind of LIC. Lee et al.<sup>[367]</sup> fabricated LIC utilizing positive electrodes based on urea-reduced graphene oxide (URGO) in combination with graphite, showing that this electrode combination allows the realization of devices able to deliver high energy and power densities ( $106 \text{ Wh kg}_{\text{total}}^{-1}$  of  $84 \text{ W kg}^{-1}$ , respectively). Recently Wang et al.<sup>[368]</sup> investigated a LIC containing a 3D porous nitrogen-doped graphene sheet (N-GS) as negative electrode combined with a 3D porous activated nitrogen-doped graphene sheet (A-N-GS) as positive electrode, working at 4.5 V. They showed that this system delivers an energy density of  $188 \text{ Wh kg}^{-1}$  and promising cycling stability.

In parallel to carbonaceous materials, the use of titanium based materials in LIC has also been extensively

investigated.<sup>[87,110,369]</sup> Cai et al.<sup>[370]</sup> fabricated LIC containing mesoporous anatase  $\text{TiO}_2$  microspheres and commercial AC, showing that these devices can display maximum energy density of  $\approx 80 \text{ Wh kg}^{-1}$  with 98% capacitive retention after 1000 cycles. As mentioned above, Amatuucci et al.<sup>[361]</sup> proposed the first LIC, which was based on LTO and AC. This device showed a maximum energy density of  $\approx 18 \text{ Wh kg}^{-1}$  with good cycling stability. Babu et al.<sup>[371]</sup> investigate LIC containing nanoporous AC (RHDPC-KOH) in combination with LTO, showing that devices realized with these materials exhibit maximum energy density of  $\approx 61 \text{ Wh kg}^{-1}$ . The Naoi's group<sup>[360,372]</sup> utilized nanoscale lithium titanate crystals hyperdispersed and entangled within a nanocarbon matrix ( $\text{Li}_4\text{Ti}_5\text{O}_{12}$  (LTO)/CNF) as negative electrode coupled with an AC positive electrode. This device exhibits maximum energy density as high as  $40 \text{ Wh L}^{-1}$  ( $55 \text{ Wh kg}^{-1}$ ) (see **Figure 31**).<sup>[113,373]</sup>

Aravindan et al.<sup>[128]</sup> were the first to report about a LIC containing  $\text{TiNb}_2\text{O}_7$  as negative electrode in combination with an AC positive electrode, showing that utilizing this electrode combination is possible to realize devices able to deliver high energy and power densities ( $43 \text{ Wh kg}^{-1}$  and  $3 \text{ kW kg}^{-1}$ , respectively) with a good cyclability. Böckenfeld et al.<sup>[163]</sup> showed the use of monoclinic lithium vanadium phosphate ( $\text{Li}_3\text{V}_2(\text{PO}_4)_3$ , LVP) as anode material for Li-ion capacitor. The fabricated LVP/CA//AC

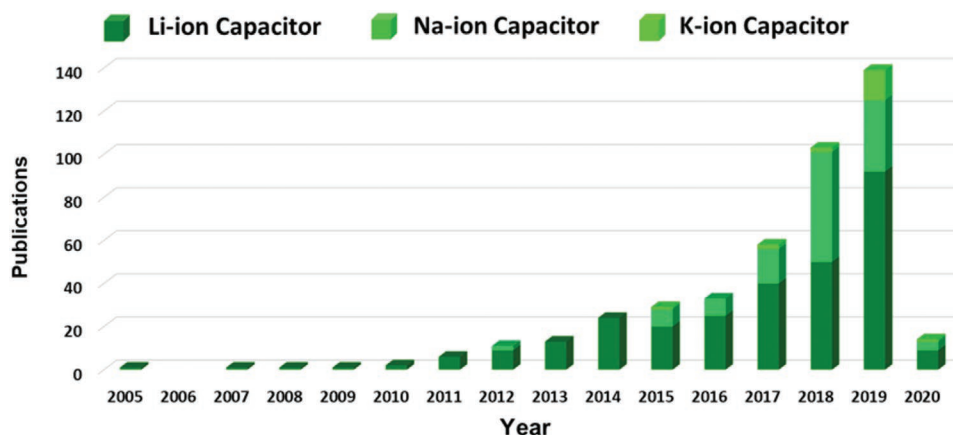


**Figure 29.** Number of publications dedicated to metal-ion capacitors over the last 15 years (from 2005 till 2020), data from Web of Science (February 2020).

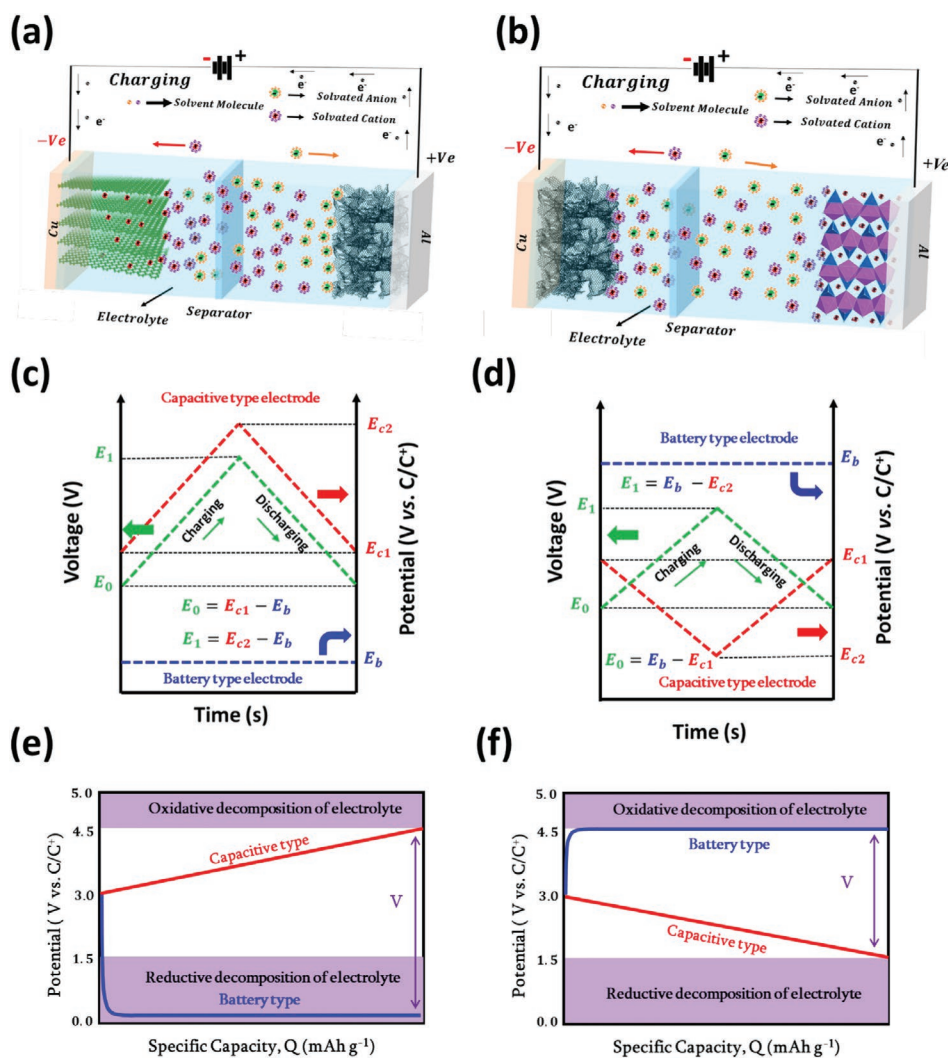


**Figure 30.** Schematic representation of a) type I and b) type II hybrid ion capacitor. Illustration of galvanostatic charge/discharge and voltage profile of c,e) type I and d,f) type II hybrid ion capacitors.

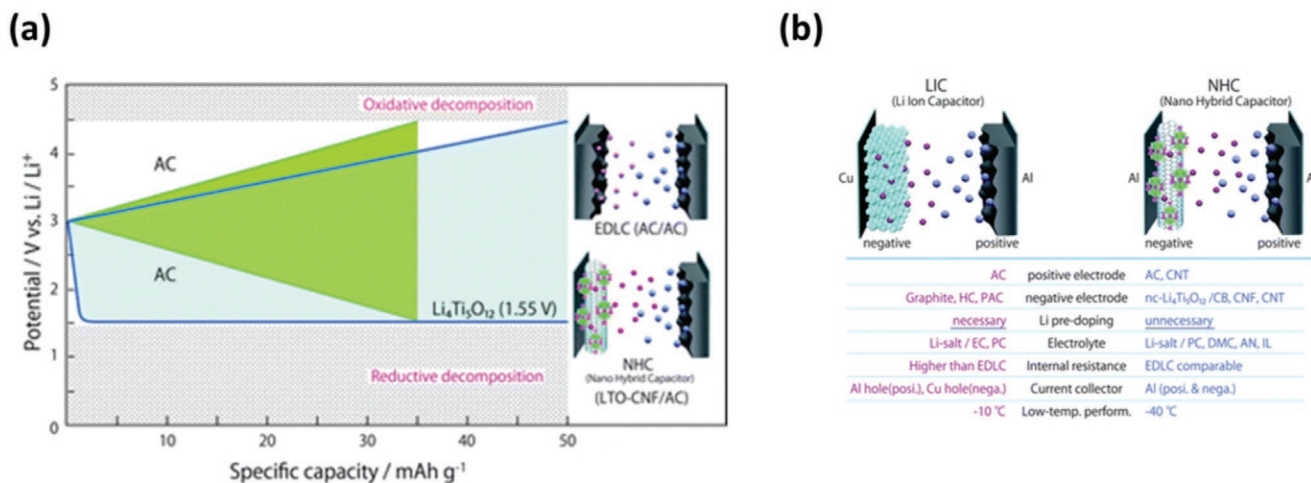


**Figure 31.** a) Illustration of a nanohybrid capacitor consisting of Li<sub>4</sub>Ti<sub>5</sub>O<sub>12</sub> (LTO)/CNF nanocomposite negative electrode combined with an activated carbon (AC) positive electrode. b) Comparative study of carbonaceous anode based LIC with nanohybrid capacitor. Reproduced with permission.<sup>[360]</sup> Copyright 2012, Royal Society of Chemistry.

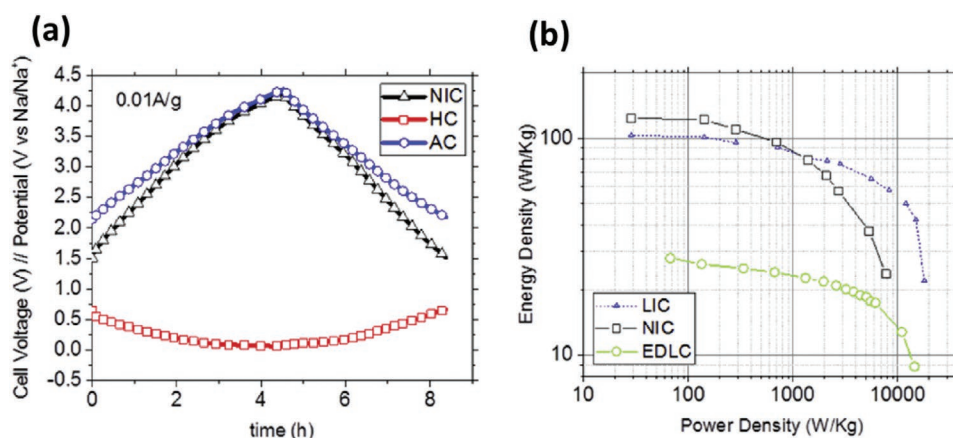


**Figure 32.** a) NIC fabricated with olive pit based HC as anode and AC as cathode in 1 M NaFP<sub>6</sub> EC:PC and b) Ragone plot comparing the NIC versus EDLC and LIC technologies with olive pit based electrode materials. Reproduced with permission.<sup>[381]</sup> Copyright 2017, Elsevier.

device cycled in a potential range of 0.0–4.0 V exhibits a capacity of 55 mAh g<sup>-1</sup> at 1 C and at very high C-rate of 100 C it delivers a specific capacity of 16 mAh g<sup>-1</sup> and good cycling stability.

Also pseudocapacitive materials have been utilized as active materials for the negative electrode of LIC. The Dunn's group<sup>[28]</sup> fabricated an LIC containing a negative electrode based on T-Nb<sub>2</sub>O<sub>5</sub> and a commercial AC positive electrode, which was cycled in a potential window of 1.0–3.0 V. An energy density of 40 Wh kg<sup>-1</sup> and 27 Wh kg<sup>-1</sup> were measured at a power density of 300 W kg<sup>-1</sup> (9 min) and 1500 W kg<sup>-1</sup> (1 min), respectively, based on the total active material. The hybrid device runs about 1000 cycles at a charge/discharge rate of 3000 W kg<sup>-1</sup> (22 s) without any substantial energy loss. Chen et al.<sup>[374]</sup> explored the use of V<sub>2</sub>O<sub>5</sub> as negative electrode for LICs. Utilizing this material with carbon nanotube, they realized a device able to display a maximum energy and power density of 40 Wh kg<sup>-1</sup> and 6.3 kW kg<sup>-1</sup>, respectively, and exhibits high cyclability (80% capacity retention after 10 000 cycles).

Taking these results into account, the combination of non-graphitizate negative electrode with AC positive electrode appears as a reliable solution for the realization of high performance system. In the future it will be important to improve the capacity as well as the operative potential of the positive electrode in order to further increase the energy of these devices. To reach this goal, the development of novel electrolytes appears essential. The use of non-carbonaceous materials as well as that of pseudocapacitive materials is certainly promising. Nevertheless, the cycling stability as well as the aging processes taking place in these devices need to be further investigated. Additionally, their feasibility for large production should also be considered.

Also the type II LIC has been investigated. Ma et al.<sup>[375]</sup> first reported the application of LiMn<sub>2</sub>O<sub>4</sub> as cathode for Li-ion capacitor along with Birnessite-type manganese dioxide (MnO<sub>2</sub>)/MWCNT (37%) as composite anode. The (MnO<sub>2</sub>)/MWCNT//LiMn<sub>2</sub>O<sub>4</sub> Li-ion capacitor cycled in a potential between 0 and 2.5 V delivered maximum energy and power density of 56 Wh kg<sup>-1</sup> and 2.4 kW kg<sup>-1</sup>, respectively. The LiMn<sub>2</sub>O<sub>4</sub>/AC Li-HEC system fabricated by Cericola et al.<sup>[376]</sup> delivered a higher energy (≈45 Wh kg<sup>-1</sup>) density and a power density of ≈1.2 kW kg<sup>-1</sup>. Sathish et al.<sup>[377]</sup> investigated an LIC using carbon-coated LVP as positive electrode

with activated carbon as negative electrode. The AC // LVP-C device shows a maximum energy density of 25 Wh kg<sup>-1</sup> and a cycling stability of 66% after 1000 cycles (0.5 A g<sup>-1</sup>).

Overall, the electrochemical performance of type II LIC appear lower than that of type I. The selection of suitable pseudocapacitive materials (for the negative electrode) and the use of high voltage cathodes (for the positive electrode) will be therefore crucial for the development of these systems.

#### 2.4.2. Materials for Sodium-Ion Capacitors

The investigation dedicated to NIC started in the last decade. Yin et al.<sup>[378]</sup> were to first to report about an NIC based on sodium titanate nanotubes and porous carbon, working in a potential window of 0–3.0 V, and delivering a maximum energy and power density of 34 Wh kg<sup>-1</sup> and 889 W kg<sup>-1</sup>, respectively. Kuratani et al.<sup>[379]</sup> used a pre-sodiated hard carbon as the negative electrode and AC as the positive electrode to fabricate NIC and compared the performance of this device with those of an LIC. They showed that the rate capability displayed by the NIC was comparable to that of LIC, and that the systems were displaying a good stability (91% capacity retention after 1000 cycles). After this work, several studies have been dedicated to NIC, and great attention has been dedicated to use of hard carbon on this devices. Ding et al.<sup>[191]</sup> reported about an NIC containing hard carbon (as negative electrode) and porous carbon (as positive electrode) derived from peanut shell precursor, operating in a potential window of 1.5–4.2 V, and showing energy and power of 201 Wh kg<sup>-1</sup> and 285 W kg<sup>-1</sup>, respectively. Wang et al.<sup>[380]</sup> investigated a quasi-solid state NIC containing nanoporous disordered carbon as negative and macroporous graphene as the positive electrodes, and an Na-ion conducting gel polymer electrolyte. This device, which displayed an operative voltage of 4.2 V delivered an energy density of 168 Wh kg<sup>-1</sup>. Ajuria et al.<sup>[381]</sup> investigated NICs containing hard carbon and AC, which were both synthesized from recycled olive pit bio-waste, and they showed that NIC containing these materials display a maximum energy and power density of 100 Wh Kg<sup>-1</sup> and 7 kW kg<sup>-1</sup>, respectively (see Figure 32).

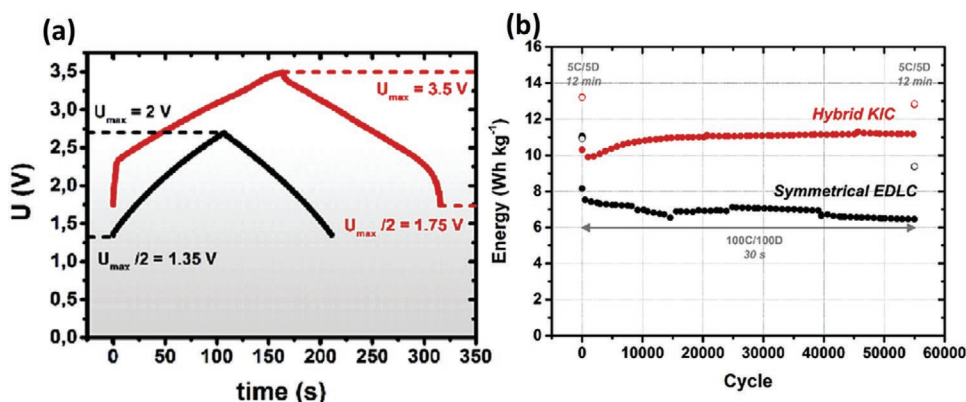


**Figure 33.** Comparison of a) galvanostatic charge–discharge and b) long-term cycling of hybrid KIC and EDLC symmetric capacitor. Reproduced with permission.<sup>[388]</sup> Copyright 2017, Elsevier.

Han et al.<sup>[382]</sup> assembled an NIC utilizing the graphitic meso-carbon microbead in combination with AC and using a diglyme based electrolyte. They reported that this kind of NIC delivers an energy density of 93.5 and power density of 573 W kg<sup>-1</sup> at 4 C. Yang et al.<sup>[383]</sup> realized an NIC combining a 3D framework soft carbon (3DFC) with a 3DFC-derived nanoporous. They showed that this device delivers energy density of 111 Wh kg<sup>-1</sup> (@ 200 W kg<sup>-1</sup>) and, at a power density of 20 kW kg<sup>-1</sup>, it displays energy density of 67 Wh kg<sup>-1</sup>.

Also non-carbonaceous materials have been used for the realization of NICs. For example, Le et al.<sup>[219]</sup> synthesized single-crystal-like TiO<sub>2</sub> anchored on graphene. The NIC realized utilizing this material in combination with an AC show an energy density of 64.2 W h kg<sup>-1</sup> and high power density of 1357 W kg<sup>-1</sup>, as well as 90% of capacitance retention after 10 000 cycles. Babu et al.<sup>[205]</sup> investigated the use of semicrystalline and crystalline brown TiO<sub>2</sub> as negative electrode for NICs and realized an NIC containing Na<sub>2</sub>Ti<sub>2</sub>O<sub>4</sub>(OH)<sub>2</sub> as negative and porous carbon as positive electrode. This device, which was working at 4.0 V, delivered an energy density of ≈65 Wh kg<sup>-1</sup> (at 500 W kg<sup>-1</sup>, 0.20 A g<sup>-1</sup>).<sup>[384]</sup> Dall’Agnese et al.<sup>[388]</sup> demonstrated the usage of 2D vanadium carbide, V<sub>2</sub>CT<sub>x</sub>, from the MXene family, as positive electrode for NICs, showing the possibility of using this new family of materials also in NIC. Recently, Feng et al.<sup>[385]</sup> demonstrated a high-energy-density NIC (200 Wh kg<sup>-1</sup>) by utilizing the pseudocapacitive nature of interface-engineered dual-phase hierarchical TiO<sub>2</sub> nanosheets.

Wasiński et al.<sup>[386]</sup> showed the first proof of concept of a type II NICs in organic electrolytes by using the Na<sub>0.4</sub>MnO<sub>2</sub> as battery-type positive electrode in combination with an AC negative electrode. Later Kaliyappan et al.<sup>[387]</sup> fabricated an NIC containing Al<sub>2</sub>O<sub>3</sub>-coated NMNC (NMNC-Al) and AC, showing that this device delivers a maximum energy density of 75 Wh kg<sup>-1</sup>, a power density of 2.23 kW kg<sup>-1</sup> and a good cycling stability (98% capacity retention after 10 000 cycles).

Taking these results into account, NICs appears already as very interesting high power devices, able to almost match the performance of LICs. In the future the stability of these devices should be further improved and, as in the case of LIB, the introduction of novel electrolytes will be of great importance.

#### 2.4.3. Materials for Potassium-Ion Capacitors

As shown in Figure 29, the interest in KIC also increased constantly in the last years. The first prototype of KIC was reported by Comte et al.<sup>[388]</sup> which utilized graphite as negative electrode and AC as positive electrode and an electrolyte based on 0.8 mol L<sup>-1</sup> KPF<sub>6</sub> in acetonitrile (ACN), and showed that this device displays high cycling stability (Figure 33).

Chen et al.<sup>[389]</sup> investigated a KIC containing a negative electrode based on oxygen-rich CNSs and a positive electrode based on activated carbon showing that this device displays an energy density of 149 Wh kg<sup>-1</sup> with an encouraging cycling stability (80% capacity retention after 5000 cycles). Yang et al.<sup>[390]</sup> considered KIC containing (3D) nitrogen-doped framework carbon (3DNFC) 3D nitrogen-doped framework activated carbon (3DNFAC) as negative and positive electrodes, respectively. They showed that these devices, which are operating in the voltage window 0–4.2 V, can display high performance (164 Wh kg<sup>-1</sup> and 210 W kg<sup>-1</sup>) and high cycling stability (92% capacity retention after 10 000 cycles at 2.0 A g<sup>-1</sup>).

Also non-carbonaceous materials have been considered as negative electrodes for KICs. Dong et al.<sup>[274]</sup> combined K<sub>2</sub>Ti<sub>6</sub>O<sub>13</sub> (KTO) microscaffolds with an N-doped nanoporous carbon, showing that KIC containing these materials can display a maximum energy density of 58.2 Wh kg<sup>-1</sup> and a maximum power density of 7.2 kW kg<sup>-1</sup>, with good cycling stability over 5000 cycles. Recently Chen’s group<sup>[391]</sup> reported a hybrid KIC delivering energy density of 101 Wh kg<sup>-1</sup> and a maximum power density ≈2.2 kW kg<sup>-1</sup> with promising cycling stability.

Ramasamy et al.<sup>[392]</sup> fabricated type II KIC with P3-type layered K<sub>0.45</sub>Mn<sub>0.5</sub>Co<sub>0.5</sub>O<sub>2</sub> as cathode and commercial activated carbon (AC) as anode in 0.8 M KPF<sub>6</sub> dissolved in EC: DEC (1:1 v/v) electrolyte. The fabricated device exhibits a very high energy density of 43 Wh kg<sup>-1</sup> and attains a maximum power density of 30 kW kg<sup>-1</sup> and retains 88% of its energy density up to 30 000 cycles at 10 A g<sup>-1</sup>.

The research on KIC (types I and II) is on its initial stage and further investigation are needed to assess the behavior of high power devices based on potassium. Presently, the main challenge for the realization of these devices appears to be

the introduction of a carbonaceous K-ion intercalation materials able to guarantee high voltage and high stability to these devices.

### 3. Conclusions

The development of advanced high power devices requires the use of materials able to display very favorable ionic and electronic conductivities and, at the same time, high structural stability. These properties are necessary to guarantee high performance at high current densities and long cycling stability. In this review we reported an overview about the electrochemical performance of several faradaic, pseudocapacitive, and capacitive materials which have been proposed and investigated in the last years. We analyzed the use of these materials in high power metal-ion batteries, in electrochemical capacitors and in metal-ion capacitor hybrid devices. From this analysis it is possible to come to some important conclusions about the materials and, also, about the considered devices.

Regarding the materials (anodic and cathodic) suitable for metal-ion batteries, we showed that those developed for LIBs are presently displaying the best performance at high current densities, and that they can be efficiently utilized up to 50 A g<sup>-1</sup>. In the case of anodic materials, the gap between those suitable for LIBs and those suitable for NIBs and KIBs is rather large. Among the considered anodic materials, hard carbons are presently one of the most promising and, at the same, the one that can be successfully used in all metal-ion batteries technologies. Nevertheless, the initial irreversible capacity displayed by these materials need to be reduced. Titanium based anode are also very interesting for high power applications as they can guarantee high capacity at higher current densities. However, the use of this latter materials is typically leading to the realization of devices with lower operative voltage compared to the systems containing hard carbons.

In the case of cathodic materials, the situation appears different. Here, the performance of materials suitable for LIBs and NIBs appears rather comparable, and both of them can be efficiently utilized up to 50 A g<sup>-1</sup>. These current densities, at the moment, appear too high for the cathodic materials developed for KIBs, which are able to efficiently work up to 1–2 A g<sup>-1</sup>. Overall, nanosized iron and vanadium phosphate dispersed in a carbon matrix appears as cathodic materials that are able to guarantee the best performance in terms of capacity at high current density and cycling stability.

Currently, LIBs are the best devices for applications which require charge–discharge times in the order of (several) tens of minutes. Nevertheless, the performance of NIBs appears already very promising and close to that of LIB. Although these latter batteries display higher energy density, their use on NIBs in high power application could be interesting, especially taking into account their fast charging, their cost, and the abundance of sodium. The performance of KIBs need to be further improved. Taking into account the fact that NIBs and KIBs are younger technologies compared to LIBs, it is reasonable to expect a significant improvement in the high power performance of these devices in the coming years.

Regarding the materials suitable for electrochemical capacitors, we showed that ACs are allowing the realization of high power EDLC in combination with both aqueous and organic electrolytes. The practical capacity of these materials is of the order of 30 mAh g<sup>-1</sup>, and it can be maintained at current densities exceeding 100 A g<sup>-1</sup>. EDLCs are appearing the best devices for applications which require charge–discharge time in the order of few minutes–seconds. The use of pseudocapacitive materials, such as MXenes and Nb<sub>2</sub>O<sub>5</sub>, makes a substantial increment of capacity compared to AC possible, maintaining high performance at current densities exceeding 100 A g<sup>-1</sup>. Nevertheless, they can be mainly used as negative electrodes and their operative voltage, at the moment, is not significantly different from that of AC and, also, that of anodic materials based on titanium, for example, TiO<sub>2</sub>. The enlargement of the potential window of use of these materials appears therefore crucial for their successful introduction in real devices.

The combination of faradic and capacitive materials in hybrid devices such as LICs, NICs, and KICs is a very interesting strategy for the realization of devices able to display high performance in a timeframe comprise between few minutes and seconds. The type I LICs shows very promising values of energy and power. This high performance is strongly related to the high operative voltage which characterize these devices. The same is true for NICs and KICs and, considering the points discussed before, it is reasonable to suppose that the performance of these two latter systems might increase significantly in the near future. To realized such an increase, however, it will be necessary to work in two main directions: 1) to introduce positive electrodes displaying higher capacity of AC, for example, based on innovative pseudocapacitive materials and 2) to introduce innovative electrolytes, which can guarantee high stability for AC (and/or pseudocapacitive materials) at maximum operative voltage of the order of 4.5–5.0 V. The use of type II hybrid devices systems appears presently not particularly advantageous due to the lower operative voltage of these devices compared the one of type I. In this case, the combination of pseudocapacitive materials, for example, MXenes, with high power–high voltage cathodes could give a new impulse toward the development of this type of hybrid systems.

To conclude, the development of fast charging materials can be certainly considered as a topic of great relevance in the field of energy storage. In the future, it will necessary to intensify the research in materials suitable for sodium and potassium based systems, as they appear promising in view of the realization of advanced high power device. In parallel, it will be necessary to further extend the operational window of pseudocapacitive materials, for example, MXenes, and to develop pseudocapacitive materials which can be used as positive electrodes. Finally, it will be necessary to design innovative electrolytes stable at high potential and with favorable transport properties in order to fully exploit capacity of the novel materials which will be realized.

### Acknowledgements

A.B. and B.B. wish to thank the Thüringer Ministerium für Wirtschaft, Wissenschaft und Digitale Gesellschaft (TMWWDG), and the Thüringer Aufbau Bank (TAB) within the project LiNaKon (2018 FGR 0092)

for the financial support. A.B. and P.S. wish to thank the Deutsche Forschungsgemeinschaft (DFG) and the Agence Nationale de la Recherche (ANR) for the financial support of the project “New Electrolytes for Capacitive Electrochemical Storage (NECES)”. P.S. also wish to thank ANR for the support with the LABEX Stire EX. A.B. and P.S. also wish to thank the Alistore-ERI Consortium for the fruitful and stimulating discussion about high power materials.

## Conflict of Interest

The authors declare no conflict of interest.

## Keywords

electrochemical capacitors, high power materials, hybrid systems, metal-ion batteries

Received: March 30, 2020

Revised: May 20, 2020

Published online: June 22, 2020

- 
- [1] M. Armand, J. M. Tarascon, *Nature* **2008**, 451, 652.  
 [2] M. Winter, B. Barnett, K. Xu, *Chem. Rev.* **2018**, 118, 11433.  
 [3] C. Schütter, S. Pohlmann, A. Balducci, *Adv. Energy Mater.* **2019**, 9, 1900334.  
 [4] V. F. Pires, E. Romero-Cadaval, D. Vinnikov, I. Roasto, J. F. Martins, *Energy Convers. Manage.* **2014**, 86, 453.  
 [5] <https://www.avnet.com/wps/portal/abacus/resources/engineers-insight/article/hybrid-capacitors-combine-supercapacitor-and-li-on-technology/> (accessed: November 2019).  
 [6] [https://www.yuden.co.jp/ut/solutions/lithium\\_ion/property/](https://www.yuden.co.jp/ut/solutions/lithium_ion/property/) (accessed: November 2019).  
 [7] Y. Liu, Y. Zhu, Y. Cui, *Nat. Energy* **2019**, 4, 540.  
 [8] G. Martin, L. Rentsch, M. Höck, M. Bertau, *Energy Storage Mater.* **2017**, 6, 171.  
 [9] J. Cao, A. Emadi, *IEEE Trans. Power Electron.* **2012**, 27, 122.  
 [10] J. Ding, W. Hu, E. Paek, D. Mitlin, *Chem. Rev.* **2018**, 118, 6457.  
 [11] V. Aravindan, J. Gnanaraj, Y.-S. Lee, S. Madhavi, *Chem. Rev.* **2014**, 114, 11619.  
 [12] J. B. Goodenough, Y. Kim, *Chem. Mater.* **2010**, 22, 587.  
 [13] T. S. Mathis, N. Kurra, X. Wang, D. Pinto, P. Simon, Y. Gogotsi, *Adv. Energy Mater.* **2019**, 9, 1902007.  
 [14] M. Li, J. Lu, Z. Chen, K. Amine, *Adv. Mater.* **2018**, 30, 1800561.  
 [15] C. Liu, Z. G. Neale, G. Cao, *Mater. Today* **2016**, 19, 109.  
 [16] A. Noori, M. F. El-Kady, M. S. Rahmanifar, R. B. Kaner, M. F. Mousavi, *Chem. Soc. Rev.* **2019**, 48, 1272.  
 [17] Y. Gogotsi, R. M. Penner, *ACS Nano* **2018**, 12, 2081.  
 [18] V. Augustyn, J. Come, M. A. Lowe, J. W. Kim, P.-L. Taberna, S. H. Tolbert, H. D. Abruña, P. Simon, B. Dunn, *Nat. Mater.* **2013**, 12, 518.  
 [19] T. Brousse, D. Bélanger, J. W. Long, *J. Electrochem. Soc.* **2015**, 162, A5185.  
 [20] C. Choi, D. S. Ashby, D. M. Butts, R. H. DeBlock, Q. Wei, J. Lau, B. Dunn, *Nat. Rev. Mater.* **2020**, 5, 5.  
 [21] H.-L. Girard, B. Dunn, L. Pilon, *Electrochim. Acta* **2016**, 211, 420.  
 [22] B. E. Conway, *Electrochemical Supercapacitors: Scientific Fundamentals and Technological Applications*, Kluwer Academic Publishers/Plenum Press, New York **1999**.  
 [23] B. E. Conway, *Electrochim. Acta* **1993**, 38, 1249.  
 [24] E. Herrero, L. J. Buller, H. D. Abruña, *Chem. Rev.* **2001**, 101, 1897.  
 [25] M. R. Lukatskaya, B. Dunn, Y. Gogotsi, *Nat. Commun.* **2016**, 7, 12647.  
 [26] A. Balducci, D. Belanger, T. Brousse, J. W. Long, W. Sugimoto, *J. Electrochem. Soc.* **2017**, 164, A1487.  
 [27] J. Wang, J. Polleux, J. Lim, B. Dunn, *J. Phys. Chem. C* **2007**, 111, 14925.  
 [28] J. Come, V. Augustyn, J. W. Kim, P. Rozier, P.-L. Taberna, P. Gogotsi, J. W. Long, B. Dunn, P. Simon, *J. Electrochem. Soc.* **2014**, 161, A718.  
 [29] J. Liu, J. Wang, C. Xu, H. Jiang, C. Li, L. Zhang, J. Lin, Z. X. Shen, *Adv. Sci.* **2018**, 5, 1700322.  
 [30] M. Sathiya, A. S. Prakash, K. Ramesha, J. M. Tarascon, A. K. Shukla, *J. Am. Chem. Soc.* **2011**, 133, 16291.  
 [31] J. Come, P.-L. Taberna, S. Hamelet, C. Masquelier, P. Simon, *J. Electrochem. Soc.* **2011**, 158, A1090.  
 [32] H. Lindström, S. Södergren, A. Solbrand, H. Rensmo, J. Hjelm, A. Hagfeldt, S.-E. Lindquist, *J. Phys. Chem. B* **1997**, 101, 7717.  
 [33] V. Augustyn, P. Simon, B. Dunn, *Energy Environ. Sci.* **2014**, 7, 1597.  
 [34] B. Babu, M. M. Shaijumon, *Electrochim. Acta* **2020**, 345, 136208.  
 [35] M. Forghani, S. W. Donne, *J. Electrochem. Soc.* **2018**, 165, A664.  
 [36] H. Shao, Z. Lin, K. Xu, P.-L. Taberna, P. Simon, *Energy Storage Mater.* **2019**, 18, 456.  
 [37] F. Liu, S. Song, D. Xue, H. Zhang, *Nanoscale Res. Lett.* **2012**, 7, 149.  
 [38] M. R. Palacin, *Chem. Soc. Rev.* **2009**, 38, 2565.  
 [39] D. Linden, T. Reddy, *Handbook of Batteries*, McGraw-Hill Education, New York **2001**.  
 [40] M. S. Whittingham, *Chem. Rev.* **2004**, 104, 4271.  
 [41] A. S. Aricò, P. Bruce, B. Scrosati, J.-M. Tarascon, W. van Schalkwijk, *Nat. Mater.* **2005**, 4, 366.  
 [42] P. G. Bruce, B. Scrosati, J.-M. Tarascon, *Angew. Chem., Int. Ed.* **2008**, 47, 2930.  
 [43] N. Nitta, F. Wu, J. T. Lee, G. Yushin, *Mater. Today* **2015**, 18, 252.  
 [44] W. Zhang, F. Zhang, F. Ming, H. N. Alshareef, *EnergyChem* **2019**, 1, 100012.  
 [45] Y. Wang, R. Chen, T. Chen, H. Lv, G. Zhu, L. Ma, C. Wang, Z. Jin, J. Liu, *Energy Storage Mater.* **2016**, 4, 103.  
 [46] C. Vaalma, D. Buchholz, S. Passerini, *Curr. Opin. Electrochem.* **2018**, 9, 41.  
 [47] D. A. Scherson, A. Palencsár, *The Electrochemical Society Interface Spring* **2006**, 15.  
 [48] <https://education.jlab.org/itselemental/ele006.html> (accessed: May 2020).  
 [49] Y. Nishi, *Chem. Rec.* **2001**, 1, 406.  
 [50] J. R. Dahn, T. Zheng, Y. Liu, J. S. Xue, *Science* **1995**, 270, 590.  
 [51] R. Yazami, P. Touzain, *J. Power Sources* **1983**, 9, 365.  
 [52] F. Beguin, E. Franckowiak, *Carbons for Electrochemical Energy Storage and Conversion Systems*, CRC Press Taylor & Francis Group, Boca Raton, FL **2010**.  
 [53] M. Winter, J. O. Besenhard, M. E. Spahr, P. Novák, *Adv. Mater.* **1998**, 10, 725.  
 [54] B. Simon, S. Flandrois, K. Guerin, A. Fevrier-Bouvier, I. Teulat, P. Biensan, *J. Power Sources* **1999**, 81, 312.  
 [55] K. Dai, Z. Wang, G. Ai, H. Zhao, W. Yuan, X. Song, V. Battaglia, C. Sun, K. Wu, G. Liu, *J. Power Sources* **2015**, 298, 349.  
 [56] S. Goriparti, E. Miele, F. De Angelis, E. Di Fabrizio, R. P. Zaccaria, C. Capiglia, *J. Power Sources* **2014**, 257, 421.  
 [57] V. A. Agubra, J. W. Fergus, *J. Power Sources* **2014**, 268, 153.  
 [58] W. Martin, *Z. Physikalische Chemie* **2009**, 223, 1379.  
 [59] S. J. An, J. Li, C. Daniel, D. Mohanty, S. Nagpure, D. L. Wood, *Carbon* **2016**, 105, 52.  
 [60] L. F. Li, B. Xie, H. S. Lee, H. Li, X. Q. Yang, J. McBreen, X. J. Huang, *J. Power Sources* **2009**, 189, 539.  
 [61] P. Verma, P. Maire, P. Novák, *Electrochim. Acta* **2010**, 55, 6332.  
 [62] M. Nie, D. Chalasani, D. P. Abraham, Y. Chen, A. Bose, B. L. Lucht, *J. Phys. Chem. C* **2013**, 117, 1257.  
 [63] E. Peled, S. Menkin, *J. Electrochem. Soc.* **2017**, 164, A1703.  
 [64] H. Ye, S. Xin, Y.-X. Yin, J.-Y. Li, Y.-G. Guo, L.-J. Wan, *J. Am. Chem. Soc.* **2017**, 139, 5916.  
 [65] C. Uhlmann, J. Illig, M. Ender, R. Schuster, E. Ivers-Tiffée, *J. Power Sources* **2015**, 279, 428.

- [66] T. Deng, X. Zhou, *Mater. Lett.* **2016**, 176, 151.
- [67] H. Buqa, D. Goers, M. Holzapfel, M. E. Spahr, P. Novák, *J. Electrochem. Soc.* **2005**, 152, A474.
- [68] Z. Chen, Y. Liu, Y. Zhang, F. Shen, G. Yang, L. Wang, X. Zhang, Y. He, L. Luo, S. Deng, *Mater. Lett.* **2018**, 229, 134.
- [69] X. Zhou, F. Chen, T. Bai, B. Long, Q. Liao, Y. Ren, J. Yang, *Green Chem.* **2016**, 18, 2078.
- [70] N. A. Kaskhedikar, J. Maier, *Adv. Mater.* **2009**, 21, 2664.
- [71] W. Luo, Z. Jian, Z. Xing, W. Wang, C. Bommier, M. M. Lerner, X. Ji, *ACS Cent. Sci.* **2015**, 1, 516.
- [72] S. Flandrois, B. Simon, *Carbon* **1999**, 37, 165.
- [73] M. Schroeder, S. Menne, J. Ségalini, D. Saurel, M. Casas-Cabanas, S. Passerini, M. Winter, A. Balducci, *J. Power Sources* **2014**, 266, 250.
- [74] Q. Zhang, H. Sun, X. Wang, Z. Zhu, W. Liang, A. Li, S. Wen, W. Deng, *Energy Technol.* **2013**, 1, 721.
- [75] L. Wang, Z. Schnepf, M. M. Titirici, *J. Mater. Chem. A* **2013**, 1, 5269.
- [76] Q. Sun, X.-Q. Zhang, F. Han, W.-C. Li, A.-H. Lu, *J. Mater. Chem.* **2012**, 22, 17049.
- [77] S. Li, Y. Luo, W. Lv, W. Yu, S. Wu, P. Hou, Q. Yang, Q. Meng, C. Liu, H.-M. Cheng, *Adv. Energy Mater.* **2011**, 1, 486.
- [78] F.-D. Han, Y.-J. Bai, R. Liu, B. Yao, Y.-X. Qi, N. Lun, J.-X. Zhang, *Adv. Energy Mater.* **2011**, 1, 798.
- [79] B. Guo, X. Wang, P. F. Fulvio, M. Chi, S. M. Mahurin, X.-G. Sun, S. Dai, *Adv. Mater.* **2011**, 23, 4661.
- [80] D. P. Dubal, P. Gomez-Romero, *Mater. Today Energy* **2018**, 8, 109.
- [81] V. Subramanian, H. Zhu, B. Wei, *J. Phys. Chem. B* **2006**, 110, 7178.
- [82] T. Wang, S. Shi, Y. Li, M. Zhao, X. Chang, D. Wu, H. Wang, L. Peng, P. Wang, G. Yang, *ACS Appl. Mater. Interfaces* **2016**, 8, 33091.
- [83] X.-L. Wu, Q. Liu, Y.-G. Guo, W.-G. Song, *Electrochem. Commun.* **2009**, 11, 1468.
- [84] Q. Xia, H. Yang, M. Wang, M. Yang, Q. Guo, L. Wan, H. Xia, Y. Yu, *Adv. Energy Mater.* **2017**, 7, 1701336.
- [85] W. Lv, F. Wen, J. Xiang, J. Zhao, L. Li, L. Wang, Z. Liu, Y. Tian, *Electrochim. Acta* **2015**, 176, 533.
- [86] L. Qie, W.-M. Chen, Z.-H. Wang, Q.-G. Shao, X. Li, L.-X. Yuan, X.-L. Hu, W.-X. Zhang, Y.-H. Huang, *Adv. Mater.* **2012**, 24, 2047.
- [87] G.-N. Zhu, Y.-G. Wang, Y.-Y. Xia, *Energy Environ. Sci.* **2012**, 5, 6652.
- [88] Z. Chen, I. Belharouak, Y.-K. Sun, K. Amine, *Adv. Funct. Mater.* **2013**, 23, 959.
- [89] J. Liu, J. S. Chen, X. Wei, X. W. Lou, X.-W. Liu, *Adv. Mater.* **2011**, 23, 998.
- [90] V. Aravindan, Y.-S. Lee, R. Yazami, S. Madhavi, *Mater. Today* **2015**, 18, 345.
- [91] J. Li, Z. Tang, Z. Zhang, *Electrochem. Solid-State Lett.* **2005**, 8, A316.
- [92] R. van de Krol, A. Goossens, E. A. Meulenkamp, *J. Electrochem. Soc.* **1999**, 146, 3150.
- [93] P. S. Kumar, S. A. S. Nizar, J. Sundaramurthy, P. Ragupathy, V. Thavasi, S. G. Mhaisalkar, S. Ramakrishna, *J. Mater. Chem.* **2011**, 21, 9784.
- [94] M. Wagemaker, G. J. Kearley, A. A. van Well, H. Mutka, F. M. Mulder, *J. Am. Chem. Soc.* **2003**, 125, 840.
- [95] L. Kavan, M. Kalbáč, M. Zúkalová, I. Exnar, V. Lorenzen, R. Nesper, M. Graetzel, *Chem. Mater.* **2004**, 16, 477.
- [96] M. Wagemaker, W. J. H. Borghols, F. M. Mulder, *J. Am. Chem. Soc.* **2007**, 129, 4323.
- [97] A. G. Dylla, G. Henkelman, K. J. Stevenson, *Acc. Chem. Res.* **2013**, 46, 1104.
- [98] H. Liu, Z. Bi, X.-G. Sun, R. R. Unocic, M. P. Paranthaman, S. Dai, G. M. Brown, *Adv. Mater.* **2011**, 23, 3450.
- [99] J.-Y. Shin, D. Samuelis, J. Maier, *Adv. Funct. Mater.* **2011**, 21, 3464.
- [100] M. Zúkalová, M. Kalbáč, L. Kavan, I. Exnar, M. Graetzel, *Chem. Mater.* **2005**, 17, 1248.
- [101] A. R. Armstrong, G. Armstrong, J. Canales, R. García, P. G. Bruce, *Adv. Mater.* **2005**, 17, 862.
- [102] A. R. Armstrong, G. Armstrong, J. Canales, P. G. Bruce, *Angew. Chem., Int. Ed.* **2004**, 43, 2286.
- [103] G. Armstrong, A. R. Armstrong, J. Canales, P. G. Bruce, *Electrochem. Solid-State Lett.* **2006**, 9, A139.
- [104] C. P. Sandhya, B. John, C. Gouri, *Ionics* **2014**, 20, 601.
- [105] I. Belharouak, Y.-K. Sun, W. Lu, K. Amine, *J. Electrochem. Soc.* **2007**, 154, A1083.
- [106] A. S. Prakash, P. Manikandan, K. Ramesha, M. Sathiya, J. M. Tarascon, A. K. Shukla, *Chem. Mater.* **2010**, 22, 2857.
- [107] L. Yu, H. B. Wu, X. W. Lou, *Adv. Mater.* **2013**, 25, 2296.
- [108] E. Zhao, C. Qin, H.-R. Jung, G. Berdichevsky, A. Nese, S. Marder, G. Yushin, *ACS Nano* **2016**, 10, 3977.
- [109] H. Kim, K.-Y. Park, M.-Y. Cho, M.-H. Kim, J. Hong, S.-K. Jung, K. C. Roh, K. Kang, *ChemElectroChem* **2014**, 1, 125.
- [110] H.-G. Jung, N. Venugopal, B. Scrosati, Y.-K. Sun, *J. Power Sources* **2013**, 221, 266.
- [111] H. Xu, X. Hu, Y. Sun, W. Luo, C. Chen, Y. Liu, Y. Huang, *Nano Energy* **2014**, 10, 163.
- [112] J. Kim, J. Cho, *Electrochem. Solid-State Lett.* **2007**, 10, A81.
- [113] K. Naoi, S. Ishimoto, Y. Isobe, S. Aoyagi, *J. Power Sources* **2010**, 195, 6250.
- [114] Y. Ma, B. Ding, G. Ji, J. Y. Lee, *ACS Nano* **2013**, 7, 10870.
- [115] L. Shen, H. Li, E. Uchaker, X. Zhang, G. Cao, *Nano Lett.* **2012**, 12, 5673.
- [116] J.-T. Han, Y.-H. Huang, J. B. Goodenough, *Chem. Mater.* **2011**, 23, 2027.
- [117] X. Lu, Z. Jian, Z. Fang, L. Gu, Y.-S. Hu, W. Chen, Z. Wang, L. Chen, *Energy Environ. Sci.* **2011**, 4, 2638.
- [118] K. Ise, S. Morimoto, Y. Harada, N. Takami, *Solid State Ionics* **2018**, 320, 7.
- [119] S. Lou, Y. Ma, X. Cheng, J. Gao, Y. Gao, P. Zuo, C. Du, G. Yin, *Chem. Commun.* **2015**, 51, 17293.
- [120] K. Tang, X. Mu, P. A. van Aken, Y. Yu, J. Maier, *Adv. Energy Mater.* **2013**, 3, 49.
- [121] C. Jo, Y. Kim, J. Hwang, J. Shim, J. Chun, J. Lee, *Chem. Mater.* **2014**, 26, 3508.
- [122] H. Li, L. Shen, J. Wang, S. Fang, Y. Zhang, H. Dou, X. Zhang, *J. Mater. Chem. A* **2015**, 3, 16785.
- [123] H. Park, D. H. Shin, T. Song, W. I. Park, U. Paik, *J. Mater. Chem. A* **2017**, 5, 6958.
- [124] S. Lou, X. Cheng, Y. Zhao, A. Lushington, J. Gao, Q. Li, P. Zuo, B. Wang, Y. Gao, Y. Ma, C. Du, G. Yin, X. Sun, *Nano Energy* **2017**, 34, 15.
- [125] Y. Ren, L. J. Hardwick, P. G. Bruce, *Angew. Chem., Int. Ed.* **2010**, 49, 2570.
- [126] H. Park, H. B. Wu, T. Song, X. W. Lou, U. Paik, *Adv. Energy Mater.* **2015**, 5, 1401945.
- [127] Q. Cheng, J. Liang, N. Lin, C. Guo, Y. Zhu, Y. Qian, *Electrochim. Acta* **2015**, 176, 456.
- [128] V. Aravindan, J. Sundaramurthy, A. Jain, P. S. Kumar, W. C. Ling, S. Ramakrishna, M. P. Srinivasan, S. Madhavi, *ChemSusChem* **2014**, 7, 1858.
- [129] A. G. Ashish, P. Arunkumar, B. Babu, P. Manikandan, S. Sarang, M. M. Shaijumon, *Electrochim. Acta* **2015**, 176, 285.
- [130] H. Noh, W. Choi, *J. Electrochem. Soc.* **2016**, 163, A1042.
- [131] X. Wang, G. Shen, *Nano Energy* **2015**, 15, 104.
- [132] Z. Chen, Y. Yuan, H. Zhou, X. Wang, Z. Gan, F. Wang, Y. Lu, *Adv. Mater.* **2014**, 26, 339.
- [133] R. Inada, T. Mori, R. Kumasaka, R. Ito, T. Tojo, Y. Sakurai, *Int. J. Appl. Ceram. Technol.* **2019**, 16, 264.
- [134] H. Song, Y.-T. Kim, *Chem. Commun.* **2015**, 51, 9849.
- [135] B. Guo, X. Yu, X.-G. Sun, M. Chi, Z.-A. Qiao, J. Liu, Y.-S. Hu, X.-Q. Yang, J. B. Goodenough, S. Dai, *Energy Environ. Sci.* **2014**, 7, 2220.
- [136] J. M. Tarascon, M. Armand, *Nature* **2001**, 414, 359.



- [137] K. Mizushima, P. C. Jones, P. J. Wiseman, J. B. Goodenough, *Mater. Res. Bull.* **1980**, *15*, 783.
- [138] C. M. Julien, A. Mauger, K. Zaghib, H. Groult, *Inorganics* **2014**, *2*, 132.
- [139] J. N. Reimers, J. R. Dahn, *J. Electrochem. Soc.* **1992**, *139*, 2091.
- [140] Q. Cao, H. P. Zhang, G. J. Wang, Q. Xia, Y. P. Wu, H. Q. Wu, *Electrochem. Commun.* **2007**, *9*, 1228.
- [141] J. Cho, Y. J. Kim, B. Park, *Chem. Mater.* **2000**, *12*, 3788.
- [142] J. Cho, Y. J. Kim, T.-J. Kim, B. Park, *Angew. Chem., Int. Ed.* **2001**, *40*, 3367.
- [143] M. Okubo, E. Hosono, J. Kim, M. Enomoto, N. Kojima, T. Kudo, H. Zhou, I. Honma, *J. Am. Chem. Soc.* **2007**, *129*, 7444.
- [144] Q. Wang, L. Zhang, P. Zhao, Z. Du, *Int. J. Electrochem. Sci.* **2018**, *13*, 10382.
- [145] N. Wu, H. Wu, W. Yuan, S. Liu, J. Liao, Y. Zhang, *J. Mater. Chem. A* **2015**, *3*, 13648.
- [146] H. Yang, P. Liu, Q. Chen, X. Liu, Y. Lu, S. Xie, L. Ni, X. Wu, M. Peng, Y. Chen, Y. Tang, Y. Chen, *RSC Adv.* **2014**, *4*, 35522.
- [147] Z. Wang, H. Liu, J. Wu, W.-M. Lau, J. Mei, H. Liu, G. Liu, *RSC Adv.* **2016**, *6*, 32365.
- [148] M.-J. Lee, S. Lee, P. Oh, Y. Kim, J. Cho, *Nano Lett.* **2014**, *14*, 993.
- [149] O. K. Park, Y. Cho, S. Lee, H.-C. Yoo, H.-K. Song, J. Cho, *Energy Environ. Sci.* **2011**, *4*, 1621.
- [150] B. K. Lesel, J. S. Ko, B. Dunn, S. H. Tolbert, *ACS Nano* **2016**, *10*, 7572.
- [151] R. Malik, D. Burch, M. Bazant, G. Ceder, *Nano Lett.* **2010**, *10*, 4123.
- [152] J. Wang, X. Sun, *Energy Environ. Sci.* **2012**, *5*, 5163.
- [153] K. Naoi, K. Kisu, E. Iwama, S. Nakashima, Y. Sakai, Y. Orikasa, P. Leone, N. Dupré, T. Brousse, P. Rozier, W. Naoi, P. Simon, *Energy Environ. Sci.* **2016**, *9*, 2143.
- [154] X. Rui, Q. Yan, M. Skyllas-Kazacos, T. M. Lim, *J. Power Sources* **2014**, *258*, 19.
- [155] H. Huang, S. C. Yin, T. Kerr, N. Taylor, L. F. Nazar, *Adv. Mater.* **2002**, *14*, 1525.
- [156] H. Liu, P. Gao, J. Fang, G. Yang, *Chem. Commun.* **2011**, *47*, 9110.
- [157] M. M. Ren, Z. Zhou, X. P. Gao, W. X. Peng, J. P. Wei, *J. Phys. Chem. C* **2008**, *112*, 5689.
- [158] A. R. Cho, J. N. Son, V. Aravindan, H. Kim, K. S. Kang, W. S. Yoon, W. S. Kim, Y. S. Lee, *J. Mater. Chem.* **2012**, *22*, 6556.
- [159] X. Zhang, R.-S. Kühnel, H. Hu, D. Eder, A. Balducci, *Nano Energy* **2015**, *12*, 207.
- [160] X. Xiao, L. Wang, D. Wang, X. He, Q. Peng, Y. Li, *Nano Res.* **2009**, *2*, 923.
- [161] K. Kang, Y. S. Meng, J. Bréger, C. P. Grey, G. Ceder, *Science* **2006**, *311*, 977.
- [162] S. Jayaraman, V. Aravindan, P. S. Kumar, W. C. Ling, S. Ramakrishna, S. Madhavi, *Chem. Commun.* **2013**, *49*, 6677.
- [163] N. Böckenfeld, A. Balducci, *J. Power Sources* **2013**, *235*, 265.
- [164] N. Yabuuchi, K. Kubota, M. Dahbi, S. Komaba, *Chem. Rev.* **2014**, *114*, 11636.
- [165] M. D. Slater, D. Kim, E. Lee, C. S. Johnson, *Adv. Funct. Mater.* **2013**, *23*, 947.
- [166] A. Bauer, J. Song, S. Vail, W. Pan, J. Barker, Y. Lu, *Adv. Energy Mater.* **2018**, *8*, 1702869.
- [167] Y. Huang, Y. Zheng, X. Li, F. Adams, W. Luo, Y. Huang, L. Hu, *ACS Energy Lett.* **2018**, *3*, 1604.
- [168] H. Kim, H. Kim, Z. Ding, M. H. Lee, K. Lim, G. Yoon, K. Kang, *Adv. Energy Mater.* **2016**, *6*, 1600943.
- [169] Y. Zhao, K. R. Adair, X. Sun, *Energy Environ. Sci.* **2018**, *11*, 2673.
- [170] P. Ge, M. Fouletier, *Solid State Ionics* **1988**, *28*, 1172.
- [171] D. A. Stevens, J. R. Dahn, *J. Electrochem. Soc.* **2001**, *148*, A803.
- [172] M. M. Doeff, Y. Ma, S. J. Visco, L. C. De Jonghe, *J. Electrochem. Soc.* **1993**, *140*, L169.
- [173] D. P. DiVincenzo, E. J. Mele, *Phys. Rev. B* **1985**, *32*, 2538.
- [174] G. Yoon, H. Kim, I. Park, K. Kang, *Adv. Energy Mater.* **2017**, *7*, 1601519.
- [175] K. Nobuhara, H. Nakayama, M. Nose, S. Nakanishi, H. Iba, *J. Power Sources* **2013**, *243*, 585.
- [176] Y. Liu, B. V. Merinov, W. A. Goddard, *Proc. Natl. Acad. Sci. USA* **2016**, *113*, 3735.
- [177] Z. Wang, S. M. Selbach, T. Grande, *RSC Adv.* **2014**, *4*, 4069.
- [178] B. Jache, P. Adelhelm, *Angew. Chem., Int. Ed.* **2014**, *53*, 10169.
- [179] H. Kim, J. Hong, Y.-U. Park, J. Kim, I. Hwang, K. Kang, *Adv. Funct. Mater.* **2015**, *25*, 534.
- [180] Y. Wen, K. He, Y. Zhu, F. Han, Y. Xu, I. Matsuda, Y. Ishii, J. Cumings, C. Wang, *Nat. Commun.* **2014**, *5*, 4033.
- [181] M. Wahid, D. Puthusseri, Y. Gawli, N. Sharma, S. Ogale, *ChemSusChem* **2018**, *11*, 506.
- [182] X. Dou, I. Hasa, D. Saurel, C. Vaalma, L. Wu, D. Buchholz, D. Bresser, S. Komaba, S. Passerini, *Mater. Today* **2019**, *23*, 87.
- [183] B. Xiao, T. Rojo, X. Li, *ChemSusChem* **2019**, *12*, 133.
- [184] N. Sun, Z. Guan, Y. Liu, Y. Cao, Q. Zhu, H. Liu, Z. Wang, P. Zhang, B. Xu, *Adv. Energy Mater.* **2019**, *9*, 1901351.
- [185] J. Ding, H. Wang, Z. Li, A. Kohandehghan, K. Cui, Z. Xu, B. Zahiri, X. Tan, E. M. Lotfabad, B. C. Olsen, D. Mitlin, *ACS Nano* **2013**, *7*, 11004.
- [186] E. M. Lotfabad, J. Ding, K. Cui, A. Kohandehghan, W. P. Kalisvaart, M. Hazelton, D. Mitlin, *ACS Nano* **2014**, *8*, 7115.
- [187] C. Bommier, T. W. Surta, M. Dolgos, X. Ji, *Nano Lett.* **2015**, *15*, 5888.
- [188] P. Bai, Y. He, X. Zou, X. Zhao, P. Xiong, Y. Xu, *Adv. Energy Mater.* **2018**, *8*, 1703217.
- [189] Y. Li, L. Zhang, X. Wang, X. Xia, D. Xie, C. Gu, J. Tu, *Research* **2019**, *2019*, 9.
- [190] K. Xu, Y. Li, J. Xiong, X. Ou, W. Su, G. Zhong, C. Yang, *Front. Chem.* **2018**, *6*, 366.
- [191] J. Ding, H. Wang, Z. Li, K. Cui, D. Karpuzov, X. Tan, A. Kohandehghan, D. Mitlin, *Energy Environ. Sci.* **2015**, *8*, 941.
- [192] L. Qie, W. Chen, X. Xiong, C. Hu, F. Zou, P. Hu, Y. Huang, *Adv. Sci.* **2015**, *2*, 1500195.
- [193] B. Cao, H. Liu, B. Xu, Y. Lei, X. Chen, H. Song, *J. Mater. Chem. A* **2016**, *4*, 6472.
- [194] Z. Jian, C. Bommier, L. Luo, Z. Li, W. Wang, C. Wang, P. A. Greaney, X. Ji, *Chem. Mater.* **2017**, *29*, 2314.
- [195] X. Yao, Y. Ke, W. Ren, X. Wang, F. Xiong, W. Yang, M. Qin, Q. Li, L. Mai, *Adv. Energy Mater.* **2019**, *9*, 1803260.
- [196] J. Li, J. Liu, Q. Sun, M. N. Banis, X. Sun, T.-K. Sham, *J. Phys. Chem. C* **2017**, *121*, 11773.
- [197] H. He, Q. Gan, H. Wang, G.-L. Xu, X. Zhang, D. Huang, F. Fu, Y. Tang, K. Amine, M. Shao, *Nano Energy* **2018**, *44*, 217.
- [198] T. Lan, T. Wang, W. Zhang, N.-L. Wu, M. Wei, *J. Alloys Compd.* **2017**, *699*, 455.
- [199] L. Wu, D. Bresser, D. Buchholz, S. Passerini, *J. Electrochem. Soc.* **2015**, *162*, A3052.
- [200] H. Xiong, M. D. Slater, M. Balasubramanian, C. S. Johnson, T. Rajh, *J. Phys. Chem. Lett.* **2011**, *2*, 2560.
- [201] R. Mogensen, D. Brandell, R. Younesi, *ACS Energy Lett.* **2016**, *1*, 1173.
- [202] M. B. Vazquez-Santos, P. Tartaj, E. Morales, J. M. Amarilla, *Chem. Rec.* **2018**, *18*, 1178.
- [203] F. Zhao, B. Wang, Y. Tang, H. Ge, Z. Huang, H. K. Liu, *J. Mater. Chem. A* **2015**, *3*, 22969.
- [204] M. N. Tahir, B. Oschmann, D. Buchholz, X. Dou, I. Lieberwirth, M. Panthöfer, W. Tremel, R. Zentel, S. Passerini, *Adv. Energy Mater.* **2016**, *6*, 1501489.
- [205] B. Babu, S. G. Ullattil, R. Prasannachandran, J. Kavil, P. Periyat, M. M. Shaijumon, *ACS Sustainable Chem. Eng.* **2018**, *6*, 5401.
- [206] Y. Xu, E. M. Lotfabad, H. Wang, B. Farbod, Z. Xu, A. Kohandehghan, D. Mitlin, *Chem. Commun.* **2013**, *49*, 8973.

- [207] L. Wu, D. Bresser, D. Buchholz, G. A. Giffin, C. R. Castro, A. Ochel, S. Passerini, *Adv. Energy Mater.* **2015**, *5*, 1401142.
- [208] C. Chen, Y. Wen, X. Hu, X. Ji, M. Yan, L. Mai, P. Hu, B. Shan, Y. Huang, *Nat. Commun.* **2015**, *6*, 6929.
- [209] Y. Yang, S. Liao, W. Shi, Y. Wu, R. Zhang, S. Leng, *RSC Adv.* **2017**, *7*, 10885.
- [210] M. Watanabe, Y. Bando, M. Tsutsumi, *J. Solid State Chem.* **1979**, *28*, 397.
- [211] J. Nava-Avendaño, A. Morales-García, A. Ponrouch, G. Rousse, C. Frontera, P. Senguttuvan, J. M. Tarascon, M. E. Arroyo-de Dompablo, M. R. Palacín, *J. Mater. Chem. A* **2015**, *3*, 22280.
- [212] G. Rousse, M. E. Arroyo-de Dompablo, P. Senguttuvan, A. Ponrouch, J.-M. Tarascon, M. R. Palacín, *Chem. Mater.* **2013**, *25*, 4946.
- [213] P. Senguttuvan, G. Rousse, V. Seznec, J.-M. Tarascon, M. R. Palacín, *Chem. Mater.* **2011**, *23*, 4109.
- [214] J. S. Ko, V. V. T. Doan-Nguyen, H.-S. Kim, G. A. Muller, A. C. Serino, P. S. Weiss, B. S. Dunn, *ACS Appl. Mater. Interfaces* **2017**, *9*, 1416.
- [215] H. Li, H. Fei, X. Liu, J. Yang, M. Wei, *Chem. Commun.* **2015**, *51*, 9298.
- [216] J. Xu, C. Ma, M. Balasubramanian, Y. S. Meng, *Chem. Commun.* **2014**, *50*, 12564.
- [217] K. Tang, L. Fu, R. J. White, L. Yu, M.-M. Titirici, M. Antonietti, J. Maier, *Adv. Energy Mater.* **2012**, *2*, 873.
- [218] K.-T. Kim, G. Ali, K. Y. Chung, C. S. Yoon, H. Yashiro, Y.-K. Sun, J. Lu, K. Amine, S.-T. Myung, *Nano Lett.* **2014**, *14*, 416.
- [219] Z. Le, F. Liu, P. Nie, X. Li, X. Liu, Z. Bian, G. Chen, H. B. Wu, Y. Lu, *ACS Nano* **2017**, *11*, 2952.
- [220] Y. Zhang, Y. Yang, H. Hou, X. Yang, J. Chen, M. Jing, X. Jia, X. Ji, *J. Mater. Chem. A* **2015**, *3*, 18944.
- [221] J. Chen, Z. Ding, C. Wang, H. Hou, Y. Zhang, C. Wang, G. Zou, X. Ji, *ACS Appl. Mater. Interfaces* **2016**, *8*, 9142.
- [222] Z. Hong, K. Zhou, J. Zhang, Z. Huang, M. Wei, *J. Mater. Chem. A* **2015**, *3*, 17412.
- [223] Y. Zhang, C. W. Foster, C. E. Banks, L. Shao, H. Hou, G. Zou, J. Chen, Z. Huang, X. Ji, *Adv. Mater.* **2016**, *28*, 9391.
- [224] J. Ni, S. Fu, C. Wu, Y. Zhao, J. Maier, Y. Yu, L. Li, *Adv. Energy Mater.* **2016**, *6*, 1502568.
- [225] S. S. M. Bhat, B. Babu, M. Feyngenson, J. C. Neufeind, M. M. Shaijumon, *ACS Appl. Mater. Interfaces* **2018**, *10*, 437.
- [226] Z. Dai, U. Mani, H. T. Tan, Q. Yan, *Small Methods* **2017**, *1*, 1700098.
- [227] X. Pu, H. Wang, D. Zhao, H. Yang, X. Ai, S. Cao, Z. Chen, Y. Cao, *Small* **2019**, *15*, 1805427.
- [228] H. Wang, C. Zhu, D. Chao, Q. Yan, H. J. Fan, *Adv. Mater.* **2017**, *29*, 1702093.
- [229] Q. Liu, Z. Hu, M. Chen, C. Zou, H. Jin, S. Wang, S.-L. Chou, S.-X. Dou, *Small* **2019**, *15*, 1805381.
- [230] W. Wang, B. Jiang, L. Hu, Z. Lin, J. Hou, S. Jiao, *J. Power Sources* **2014**, *250*, 181.
- [231] M.-S. Balogun, Y. Luo, F. Lyu, F. Wang, H. Yang, H. Li, C. Liang, M. Huang, Y. Huang, Y. Tong, *ACS Appl. Mater. Interfaces* **2016**, *8*, 9733.
- [232] D. Chao, C. Zhu, X. Xia, J. Liu, X. Zhang, J. Wang, P. Liang, J. Lin, H. Zhang, Z. X. Shen, H. J. Fan, *Nano Lett.* **2015**, *15*, 565.
- [233] D. Su, G. Wang, *ACS Nano* **2013**, *7*, 11218.
- [234] S. Tepavcevic, H. Xiong, V. R. Stamenkovic, X. Zuo, M. Balasubramanian, V. B. Prakapenka, C. S. Johnson, T. Rajh, *ACS Nano* **2012**, *6*, 530.
- [235] V. Raju, J. Rains, C. Gates, W. Luo, X. Wang, W. F. Stickle, G. D. Stucky, X. Ji, *Nano Lett.* **2014**, *14*, 4119.
- [236] D. W. Su, S. X. Dou, G. X. Wang, *J. Mater. Chem. A* **2014**, *2*, 11185.
- [237] D. Zhang, W. Shi, Y. Yan, S. Xu, L. Chen, X. Wang, S. Liu, *Electrochim. Acta* **2017**, *258*, 1035.
- [238] H. Kim, D. J. Kim, D.-H. Seo, M. S. Yeom, K. Kang, D. K. Kim, Y. Jung, *Chem. Mater.* **2012**, *24*, 1205.
- [239] B. Fu, X. Zhou, Y. Wang, *J. Power Sources* **2016**, *310*, 102.
- [240] C. Luo, A. Langrock, X. Fan, Y. Liang, C. Wang, *J. Mater. Chem. A* **2017**, *5*, 18214.
- [241] Y. Fang, X.-Y. Yu, X. W. Lou, *Angew. Chem., Int. Ed.* **2017**, *56*, 5801.
- [242] Y. Liu, Y. Qiao, W. Zhang, Z. Li, X. Ji, L. Miao, L. Yuan, X. Hu, Y. Huang, *Nano Energy* **2015**, *12*, 386.
- [243] M. J. Piernas Muñoz, E. Castillo Martínez, in *Prussian Blue Based Batteries* (Eds: M. J. Piernas Muñoz, E. Castillo Martínez), Springer International Publishing, Cham, Switzerland **2018**, p. 9, [https://doi.org/10.1007/978-3-319-91488-6\\_2](https://doi.org/10.1007/978-3-319-91488-6_2).
- [244] B. Wang, Y. Han, X. Wang, N. Bahlawane, H. Pan, M. Yan, Y. Jiang, *iScience* **2018**, *3*, 110.
- [245] J. Qian, C. Wu, Y. Cao, Z. Ma, Y. Huang, X. Ai, H. Yang, *Adv. Energy Mater.* **2018**, *8*, 1702619.
- [246] Y. You, A. Manthiram, *Adv. Energy Mater.* **2018**, *8*, 1701785.
- [247] Q. Ni, Y. Bai, F. Wu, C. Wu, *Adv. Sci.* **2017**, *4*, 1600275.
- [248] A. K. Padhi, V. Manivannan, J. B. Goodenough, *J. Electrochem. Soc.* **1998**, *145*, 1518.
- [249] Y. Zhu, Y. Xu, Y. Liu, C. Luo, C. Wang, *Nanoscale* **2013**, *5*, 780.
- [250] Z. Li, W. Shen, C. Wang, Q. Xu, H. Liu, Y. Wang, Y. Xia, *J. Mater. Chem. A* **2016**, *4*, 17111.
- [251] Y. You, X.-L. Wu, Y.-X. Yin, Y.-G. Guo, *Energy Environ. Sci.* **2014**, *7*, 1643.
- [252] L. Wang, Y. Lu, J. Liu, M. Xu, J. Cheng, D. Zhang, J. B. Goodenough, *Angew. Chem., Int. Ed.* **2013**, *52*, 1964.
- [253] X. Wu, D. P. Leonard, X. Ji, *Chem. Mater.* **2017**, *29*, 5031.
- [254] W. Zhang, Y. Liu, Z. Guo, *Sci. Adv.* **2019**, *5*, eaav7412.
- [255] V. Gabaudan, L. Monconduit, L. Stievano, R. Berthelot, *Front. Energy Res.* **2019**, *7*, 46.
- [256] Y.-S. Xu, S.-Y. Duan, Y.-G. Sun, D.-S. Bin, X.-S. Tao, D. Zhang, Y. Liu, A.-M. Cao, L.-J. Wan, *J. Mater. Chem. A* **2019**, *7*, 4334.
- [257] K. Kubota, M. Dahbi, T. Hosaka, S. Kumakura, S. Komaba, *Chem. Rec.* **2018**, *18*, 459.
- [258] Y. Liu, Z. Tai, J. Zhang, W. K. Pang, Q. Zhang, H. Feng, K. Konstantinov, Z. Guo, H. K. Liu, *Nat. Commun.* **2018**, *9*, 3645.
- [259] Z. Jian, W. Luo, X. Ji, *J. Am. Chem. Soc.* **2015**, *137*, 11566.
- [260] W. Zhang, W. K. Pang, V. Sencadas, Z. Guo, *Joule* **2018**, *2*, 1534.
- [261] Z. Xing, Y. Qi, Z. Jian, X. Ji, *ACS Appl. Mater. Interfaces* **2017**, *9*, 4343.
- [262] K. Share, A. P. Cohn, R. Carter, B. Rogers, C. L. Pint, *ACS Nano* **2016**, *10*, 9738.
- [263] W. Zhang, Z. Wu, J. Zhang, G. Liu, N.-H. Yang, R.-S. Liu, W. K. Pang, W. Li, Z. Guo, *Nano Energy* **2018**, *53*, 967.
- [264] Y.-H. Zhu, X. Yang, D. Bao, X.-F. Bie, T. Sun, S. Wang, Y.-S. Jiang, X.-B. Zhang, J.-M. Yan, Q. Jiang, *Joule* **2018**, *2*, 736.
- [265] Y. Okamoto, *J. Phys. Chem. C* **2014**, *118*, 16.
- [266] D. E. Nixon, G. S. Parry, *J. Phys. D: Appl. Phys.* **1968**, *1*, 291.
- [267] K. Beltróp, S. Beuker, A. Heckmann, M. Winter, T. Placke, *Energy Environ. Sci.* **2017**, *10*, 2090.
- [268] Y. An, H. Fei, G. Zeng, L. Ci, B. Xi, S. Xiong, J. Feng, *J. Power Sources* **2018**, *378*, 66.
- [269] B. Cao, Q. Zhang, H. Liu, B. Xu, S. Zhang, T. Zhou, J. Mao, W. K. Pang, Z. Guo, A. Li, J. Zhou, X. Chen, H. Song, *Adv. Energy Mater.* **2018**, *8*, 1801149.
- [270] Z. Jian, Z. Xing, C. Bommier, Z. Li, X. Ji, *Adv. Energy Mater.* **2016**, *6*, 1501874.
- [271] Z. Jian, S. Hwang, Z. Li, A. S. Hernandez, X. Wang, Z. Xing, D. Su, X. Ji, *Adv. Funct. Mater.* **2017**, *27*, 1700324.
- [272] Y. Xu, C. Zhang, M. Zhou, Q. Fu, C. Zhao, M. Wu, Y. Lei, *Nat. Commun.* **2018**, *9*, 1720.
- [273] B. Kishore, V. G. N. Munichandraiah, *J. Electrochem. Soc.* **2016**, *163*, A2551.
- [274] S. Dong, Z. Li, Z. Xing, X. Wu, X. Ji, X. Zhang, *ACS Appl. Mater. Interfaces* **2018**, *10*, 15542.
- [275] J. Han, M. Xu, Y. Niu, G.-N. Li, M. Wang, Y. Zhang, M. Jia, C. m. Li, *Chem. Commun.* **2016**, *52*, 11274.

- [276] Y. Dong, Z.-S. Wu, S. Zheng, X. Wang, J. Qin, S. Wang, X. Shi, X. Bao, *ACS Nano* **2017**, *11*, 4792.
- [277] P. Xiong, X. Zhao, Y. Xu, *ChemSusChem* **2018**, *11*, 202.
- [278] N. Naveen, W. B. Park, S. C. Han, S. P. Singh, Y. H. Jung, D. Ahn, K.-S. Sohn, M. Pyo, *Chem. Mater.* **2018**, *30*, 2049.
- [279] C. Delmas, C. Fouassier, P. Hagenmuller, *Physica B+C* **1980**, *99*, 81.
- [280] C. Vaalma, G. A. Giffin, D. Buchholz, S. Passerini, *J. Electrochem. Soc.* **2016**, *163*, A1295.
- [281] X. Wang, X. Xu, C. Niu, J. Meng, M. Huang, X. Liu, Z. Liu, L. Mai, *Nano Lett.* **2017**, *17*, 544.
- [282] H. Kim, J. C. Kim, M. Bianchini, D.-H. Seo, J. Rodriguez-Garcia, G. Ceder, *Adv. Energy Mater.* **2018**, *8*, 1702384.
- [283] Z. Shadik, D.-R. Shi, W. Tian, M.-H. Cao, S.-F. Yang, J. Chen, Z.-W. Fu, *J. Mater. Chem. A* **2017**, *5*, 6393.
- [284] A. Eftekhari, *J. Power Sources* **2004**, *126*, 221.
- [285] X. Bie, K. Kubota, T. Hosaka, K. Chihara, S. Komaba, *J. Mater. Chem. A* **2017**, *5*, 4325.
- [286] H. Kim, H. Ji, J. Wang, G. Ceder, *TrendsChem.* **2019**, *1*, 682.
- [287] N. Recham, G. Rousse, M. T. Sougrati, J.-N. Chotard, C. Frayret, S. Mariyappan, B. C. Melot, J.-C. Jumas, J.-M. Tarascon, *Chem. Mater.* **2012**, *24*, 4363.
- [288] T. Hosaka, T. Shimamura, K. Kubota, S. Komaba, *Chem. Rec.* **2019**, *19*, 735.
- [289] X. Lin, J. Huang, H. Tan, J. Huang, B. Zhang, *Energy Storage Mater.* **2019**, *16*, 97.
- [290] Z. Xing, Z. Jian, W. Luo, Y. Qi, C. Bommier, E. S. Chong, Z. Li, L. Hu, X. Ji, *Energy Storage Mater.* **2016**, *2*, 63.
- [291] H. Kim, J. C. Kim, S.-H. Bo, T. Shi, D.-H. Kwon, G. Ceder, *Adv. Energy Mater.* **2017**, *7*, 1700098.
- [292] C. Zhang, Y. Xu, M. Zhou, L. Liang, H. Dong, M. Wu, Y. Yang, Y. Lei, *Adv. Funct. Mater.* **2017**, *27*, 1604307.
- [293] J. Han, G.-N. Li, F. Liu, M. Wang, Y. Zhang, L. Hu, C. Dai, M. Xu, *Chem. Commun.* **2017**, *53*, 1805.
- [294] Z. Lin, E. Goikolea, A. Balducci, K. Naoi, P. L. Taberna, M. Salanne, G. Yushin, P. Simon, *Mater. Today* **2018**, *21*, 419.
- [295] F. Béguin, V. Presser, A. Balducci, E. Frackowiak, *Adv. Mater.* **2014**, *26*, 2219.
- [296] A. Krause, P. Kossyrev, M. Oljaca, S. Passerini, M. Winter, A. Balducci, *J. Power Sources* **2011**, *196*, 8836.
- [297] M. Yu, L. Zhang, X. He, H. Yu, J. Han, M. Wu, *Mater. Lett.* **2016**, *172*, 81.
- [298] Z. Zhao, Y. Wang, M. Li, R. Yang, *RSC Adv.* **2015**, *5*, 34803.
- [299] L.-F. Chen, X.-D. Zhang, H.-W. Liang, M. Kong, Q.-F. Guan, P. Chen, Z.-Y. Wu, S.-H. Yu, *ACS Nano* **2012**, *6*, 7092.
- [300] W. Huang, H. Zhang, Y. Huang, W. Wang, S. Wei, *Carbon* **2011**, *49*, 838.
- [301] Y. S. Yun, G. Yoon, K. Kang, H.-J. Jin, *Carbon* **2014**, *80*, 246.
- [302] R. Gokhale, V. Aravindan, P. Yadav, S. Jain, D. Phase, S. Madhavi, S. Ogale, *Carbon* **2014**, *80*, 462.
- [303] S. Trasatti, G. Buzzanca, *J. Electroanal. Chem. Interfacial Electrochem.* **1971**, *29*, A1.
- [304] T. Brezesinski, J. Wang, S. H. Tolbert, B. Dunn, *Nat. Mater.* **2010**, *9*, 146.
- [305] J. Duay, S. A. Sherrill, Z. Gui, E. Gillette, S. B. Lee, *ACS Nano* **2013**, *7*, 1200.
- [306] P. Yu, C. Li, X. Guo, *J. Phys. Chem. C* **2014**, *118*, 10616.
- [307] J. S. Ko, M. B. Sassin, J. F. Parker, D. R. Rolison, J. W. Long, *Sustainable Energy Fuels* **2018**, *2*, 626.
- [308] Q. Mahmood, S. K. Park, K. D. Kwon, S.-J. Chang, J.-Y. Hong, G. Shen, Y. M. Jung, T. J. Park, S. W. Khang, W. S. Kim, J. Kong, H. S. Park, *Adv. Energy Mater.* **2016**, *6*, 1501115.
- [309] H. Y. Lee, J. B. Goodenough, *J. Solid State Chem.* **1999**, *144*, 220.
- [310] M. Toupin, T. Brousse, D. Bélanger, *Chem. Mater.* **2004**, *16*, 3184.
- [311] T. Brousse, M. Toupin, D. Bélanger, *J. Electrochem. Soc.* **2004**, *151*, A614.
- [312] T. Brousse, D. Bélanger, *Electrochem. Solid-State Lett.* **2003**, *6*, A244.
- [313] M. Toupin, T. Brousse, D. Bélanger, *Chem. Mater.* **2002**, *14*, 3946.
- [314] M. Huang, F. Li, F. Dong, Y. X. Zhang, L. L. Zhang, *J. Mater. Chem. A* **2015**, *3*, 21380.
- [315] S. Devaraj, N. Munichandraiah, *J. Phys. Chem. C* **2008**, *112*, 4406.
- [316] X. Tang, Z. Liu, C. Zhang, Z. Yang, Z. Wang, *J. Power Sources* **2009**, *193*, 939.
- [317] Y. Hu, J. Wang, *J. Power Sources* **2015**, *286*, 394.
- [318] W. Li, K. Xu, B. Li, J. Sun, F. Jiang, Z. Yu, R. Zou, Z. Chen, J. Hu, *ChemSusChem* **2014**, *1*, 1003.
- [319] P. Yang, Y. Ding, Z. Lin, Z. Chen, Y. Li, P. Qiang, M. Ebrahimi, W. Mai, C. P. Wong, Z. L. Wang, *Nano Lett.* **2014**, *14*, 731.
- [320] K. Brezesinski, J. Wang, J. Haetge, C. Reitz, S. O. Steinmueller, S. H. Tolbert, B. M. Smarsly, B. Dunn, T. Brezesinski, *J. Am. Chem. Soc.* **2010**, *132*, 6982.
- [321] J. W. Kim, V. Augustyn, B. Dunn, *Adv. Energy Mater.* **2012**, *2*, 141.
- [322] K. J. Griffith, A. C. Forse, J. M. Griffin, C. P. Grey, *J. Am. Chem. Soc.* **2016**, *138*, 8888.
- [323] B. E. Conway, *J. Electrochem. Soc.* **1991**, *138*, 1539.
- [324] R. Kodama, Y. Terada, I. Nakai, S. Komaba, N. Kumagai, *J. Electrochem. Soc.* **2006**, *153*, A583.
- [325] H. Sun, L. Mei, J. Liang, Z. Zhao, C. Lee, H. Fei, M. Ding, J. Lau, M. Li, C. Wang, X. Xu, G. Hao, B. Papandrea, I. Shakir, B. Dunn, Y. Huang, X. Duan, *Science* **2017**, *356*, 599.
- [326] C.-H. Lai, D. Ashby, M. Moz, Y. Gogotsi, L. Pilon, B. Dunn, *Langmuir* **2017**, *33*, 9407.
- [327] E. Lim, H. Kim, C. Jo, J. Chun, K. Ku, S. Kim, H. I. Lee, I.-S. Nam, S. Yoon, K. Kang, J. Lee, *ACS Nano* **2014**, *8*, 8968.
- [328] M. Ghidui, M. R. Lukatskaya, M.-Q. Zhao, Y. Gogotsi, M. W. Barsoum, *Nature* **2014**, *516*, 78.
- [329] B. Anasori, Y. Xie, M. Beidaghi, J. Lu, B. C. Hosler, L. Hultman, P. R. C. Kent, Y. Gogotsi, M. W. Barsoum, *ACS Nano* **2015**, *9*, 9507.
- [330] M. Naguib, Y. Gogotsi, *Acc. Chem. Res.* **2015**, *48*, 128.
- [331] M. Naguib, V. N. Mochalin, M. W. Barsoum, Y. Gogotsi, *Adv. Mater.* **2014**, *26*, 992.
- [332] B. Anasori, M. R. Lukatskaya, Y. Gogotsi, *Nat. Rev. Mater.* **2017**, *2*, 16098.
- [333] M. Naguib, J. Come, B. Dyatkin, V. Presser, P.-L. Taberna, P. Simon, M. W. Barsoum, Y. Gogotsi, *Electrochem. Commun.* **2012**, *16*, 61.
- [334] M. Naguib, J. Halim, J. Lu, K. M. Cook, L. Hultman, Y. Gogotsi, M. W. Barsoum, *J. Am. Chem. Soc.* **2013**, *135*, 15966.
- [335] O. Mashtalir, M. R. Lukatskaya, M.-Q. Zhao, M. W. Barsoum, Y. Gogotsi, *Adv. Mater.* **2015**, *27*, 3501.
- [336] Z. Lin, D. Sun, Q. Huang, J. Yang, M. W. Barsoum, X. Yan, *J. Mater. Chem. A* **2015**, *3*, 14096.
- [337] X. Tang, X. Guo, W. Wu, G. Wang, *Adv. Energy Mater.* **2018**, *8*, 1801897.
- [338] Y. Dall'Agnese, P.-L. Taberna, Y. Gogotsi, P. Simon, *J. Phys. Chem. Lett.* **2015**, *6*, 2305.
- [339] X. Wang, S. Kajiyama, H. Iinuma, E. Hosono, S. Oro, I. Moriguchi, M. Okubo, A. Yamada, *Nat. Commun.* **2015**, *6*, 6544.
- [340] M. Hu, Z. Li, H. Zhang, T. Hu, C. Zhang, Z. Wu, X. Wang, *Chem. Commun.* **2015**, *51*, 13531.
- [341] R. Cheng, T. Hu, H. Zhang, C. Wang, M. Hu, J. Yang, C. Cui, T. Guang, C. Li, C. Shi, P. Hou, X. Wang, *J. Phys. Chem. C* **2019**, *123*, 1099.
- [342] D. Zuo, S. Song, C. An, L. Tang, Z. He, J. Zheng, *Nano Energy* **2019**, *62*, 401.
- [343] X. Liang, Y. Rangom, C. Y. Kwok, Q. Pang, L. F. Nazar, *Adv. Mater.* **2017**, *29*, 1603040.
- [344] M. R. Lukatskaya, O. Mashtalir, C. E. Ren, Y. Dall'Agnese, P. Rozier, P. L. Taberna, M. Naguib, P. Simon, M. W. Barsoum, Y. Gogotsi, *Science* **2013**, *341*, 1502.

- [345] M. R. Lukatskaya, S.-M. Bak, X. Yu, X.-Q. Yang, M. W. Barsoum, Y. Gogotsi, *Adv. Energy Mater.* **2015**, *5*, 1500589.
- [346] M. R. Lukatskaya, S. Kota, Z. Lin, M.-Q. Zhao, N. Shpigiel, M. D. Levi, J. Halim, P.-L. Taberna, M. W. Barsoum, P. Simon, Y. Gogotsi, *Nat. Energy* **2017**, *2*, 17105.
- [347] Y. Li, H. Shao, Z. Lin, J. Lu, L. Liu, B. Duployer, P. O. Å. Persson, P. Eklund, L. Hultman, M. Li, K. Chen, X.-H. Zha, S. Du, P. Rozier, Z. Chai, E. Raymundo-Piñero, P.-L. Taberna, P. Simon, Q. Huang, *Nat. Mater.* **2020**, <https://doi.org/10.1038/s41563-020-0657-0>.
- [348] M. Salanne, B. Rotenberg, K. Naoi, K. Kaneko, P. L. Taberna, C. P. Grey, B. Dunn, P. Simon, *Nat. Energy* **2016**, *1*, 16070.
- [349] E. Lim, C. Jo, H. Kim, M.-H. Kim, Y. Mun, J. Chun, Y. Ye, J. Hwang, K.-S. Ha, K. C. Roh, K. Kang, S. Yoon, J. Lee, *ACS Nano* **2015**, *9*, 7497.
- [350] X. Li, G. Wu, X. Liu, W. Li, M. Li, *Nano Energy* **2017**, *31*, 1.
- [351] M. Wei, K. Wei, M. Ichihara, H. Zhou, *Electrochem. Commun.* **2008**, *10*, 1164.
- [352] M. Ihsan, Q. Meng, L. Li, D. Li, H. Wang, K. H. Seng, Z. Chen, S. J. Kennedy, Z. Guo, H.-K. Liu, *Electrochim. Acta* **2015**, *173*, 172.
- [353] J. B. Cook, H.-S. Kim, T. C. Lin, C.-H. Lai, B. Dunn, S. H. Tolbert, *Adv. Energy Mater.* **2017**, *7*, 1601283.
- [354] H.-S. Kim, J. B. Cook, H. Lin, J. S. Ko, S. H. Tolbert, V. Ozolins, B. Dunn, *Nat. Mater.* **2017**, *16*, 454.
- [355] H. Ma, D. Kong, Y. Xu, X. Xie, Y. Tao, Z. Xiao, W. Lv, H. D. Jang, J. Huang, Q.-H. Yang, *Small* **2017**, *13*, 1701026.
- [356] N. Jabeen, Q. Xia, S. V. Savilov, S. M. Aldoshin, Y. Yu, H. Xia, *ACS Appl. Mater. Interfaces* **2016**, *8*, 33732.
- [357] L. Li, Z. A. Hu, N. An, Y. Y. Yang, Z. M. Li, H. Y. Wu, *J. Phys. Chem. C* **2014**, *118*, 22865.
- [358] E. Kayali, A. VahidMohammadi, J. Orangi, M. Beidaghi, *ACS Appl. Mater. Interfaces* **2018**, *10*, 25949.
- [359] J. T. Mefford, W. G. Hardin, S. Dai, K. P. Johnston, K. J. Stevenson, *Nat. Mater.* **2014**, *13*, 726.
- [360] K. Naoi, S. Ishimoto, J. Miyamoto, W. Naoi, *Energy Environ. Sci.* **2012**, *5*, 9363.
- [361] G. G. Amatucci, F. Badway, A. Du Pasquier, T. Zheng, *J. Electrochem. Soc.* **2001**, *148*, A930.
- [362] X. Wang, L. Liu, Z. Niu, *Mater. Chem. Front.* **2019**, *3*, 1265.
- [363] V. Khomenko, E. Raymundo-Piñero, F. Béguin, *J. Power Sources* **2008**, *177*, 643.
- [364] S. R. Sivakkumar, A. G. Pandolfo, *Electrochim. Acta* **2012**, *65*, 280.
- [365] W. J. Cao, J. P. Zheng, *J. Power Sources* **2012**, *213*, 180.
- [366] M. Schroeder, M. Winter, S. Passerini, A. Balducci, *J. Power Sources* **2013**, *238*, 388.
- [367] J. H. Lee, W. H. Shin, M.-H. Ryou, J. K. Jin, J. Kim, J. W. Choi, *ChemSusChem* **2012**, *5*, 2328.
- [368] R. Wang, Q. Zhao, W. Zheng, Z. Ren, X. Hu, J. Li, L. Lu, N. Hu, J. Molenda, X. Liu, C. Xu, *J. Mater. Chem. A* **2019**, *7*, 19909.
- [369] H. Wang, C. Guan, X. Wang, H. J. Fan, *Small* **2015**, *11*, 1470.
- [370] Y. Cai, B. Zhao, J. Wang, Z. Shao, *J. Power Sources* **2014**, *253*, 80.
- [371] B. Babu, P. G. Lashmi, M. M. Shaijumon, *Electrochim. Acta* **2016**, *211*, 289.
- [372] K. Naoi, *Fuel Cells* **2010**, *10*, 825.
- [373] K. Naoi, W. Naoi, S. Aoyagi, J. Miyamoto, T. Kamino, *Acc. Chem. Res.* **2013**, *46*, 1075.
- [374] Z. Chen, V. Augustyn, J. Wen, Y. Zhang, M. Shen, B. Dunn, Y. Lu, *Adv. Mater.* **2011**, *23*, 791.
- [375] S.-B. Ma, K.-W. Nam, W.-S. Yoon, X.-Q. Yang, K.-Y. Ahn, K.-H. Oh, K.-B. Kim, *Electrochem. Commun.* **2007**, *9*, 2807.
- [376] D. Cericola, P. Novák, A. Wokaun, R. Kötz, *J. Power Sources* **2011**, *196*, 10305.
- [377] R. Satish, V. Aravindan, W. C. Ling, S. Madhavi, *J. Power Sources* **2015**, *281*, 310.
- [378] J. Yin, L. Qi, H. Wang, *ACS Appl. Mater. Interfaces* **2012**, *4*, 2762.
- [379] K. Kuratani, M. Yao, H. Senoh, N. Takeichi, T. Sakai, T. Kiyobayashi, *Electrochim. Acta* **2012**, *76*, 320.
- [380] F. Wang, X. Wang, Z. Chang, X. Wu, X. Liu, L. Fu, Y. Zhu, Y. Wu, W. Huang, *Adv. Mater.* **2015**, *27*, 6962.
- [381] J. Ajuria, E. Redondo, M. Arnaiz, R. Mysyk, T. Rojo, E. Goikolea, *J. Power Sources* **2017**, *359*, 17.
- [382] P. Han, X. Han, J. Yao, L. Zhang, X. Cao, C. Huang, G. Cui, *J. Power Sources* **2015**, *297*, 457.
- [383] B. Yang, J. Chen, S. Lei, R. Guo, H. Li, S. Shi, X. Yan, *Adv. Energy Mater.* **2018**, *8*, 1702409.
- [384] B. Babu, M. M. Shaijumon, *J. Power Sources* **2017**, *353*, 85.
- [385] W. Feng, R. R. Maça, V. Etacheri, *ACS Appl. Mater. Interfaces* **2020**, *12*, 4443.
- [386] K. Wasirski, P. Pórolniczak, M. Walkowiak, *Electrochim. Acta* **2018**, *259*, 850.
- [387] K. Kaliyappan, Z. Chen, *Nano Energy* **2018**, *48*, 107.
- [388] A. Le Comte, Y. Reynier, C. Vincens, C. Leys, P. Azaïs, *J. Power Sources* **2017**, *363*, 34.
- [389] J. Chen, B. Yang, H. Hou, H. Li, L. Liu, L. Zhang, X. Yan, *Adv. Energy Mater.* **2019**, *9*, 1803894.
- [390] B. Yang, J. Chen, L. Liu, P. Ma, B. Liu, J. Lang, Y. Tang, X. Yan, *Energy Storage Mater.* **2019**, *23*, 522.
- [391] Y. Luo, L. Liu, K. Lei, J. Shi, G. Xu, F. Li, J. Chen, *Chem. Sci.* **2019**, *10*, 2048.
- [392] H. V. Ramasamy, B. Senthilkumar, P. Barpanda, Y.-S. Lee, *Chem. Eng. J.* **2019**, *368*, 235.